BRITTON, EMILY R., Ph.D. New Strategies to Identify Bioactive Compounds from Complex Matrices to Combat Drug-Resistant Bacterial Infections. (2018)
Directed by Dr. Nadja B. Cech. 135 pp.

The use of plants as medicine for human health has been documented on 5000-year-old Sumerian clay slabs, which also serve as the first evidence of written language. From 1940 to 2014, 83 % of small molecule anti-cancer treatments and 67 % of small-molecule anti-infective drugs were discovered from or modeled after compounds found in nature. Furthermore, botanical medicines constitute a large portion of dietary supplements, with sales in the United States exceeding $7 billion in 2016. Natural product mixtures are chemically complex with multifaceted bioactivity, which further complicates the goal of understanding how these mixtures interact with specific biological systems. High resolving-power mass spectrometry coupled to ultra-high pressure liquid chromatography has played a significant role in making natural product research more efficient and reliable by improving the quality of biological measurements and by assisting in guiding isolation. The goals of this project were to: (1) develop a mass spectrometry-based assay that could be used to discover compounds that inhibit the spread of *Staphylococcus aureus* in the skin and to (2) use *Hydrastis canadensis* as a case study for investigating how biochemometrics, a methodology that combines chemical and biological data using multivariate statistics, can be best used to identify synergists and additives in complex mixtures.

The first goal was achieved by adapting a crude disk-diffusion assay where bacterial hyaluronidase degrades polymeric hyaluronan into disaccharide units, into a quenchable, small volume aqueous reaction in lo-binding tubes that could be directly

analyzed via LC-MS. This method was validated by screening a known inhibitor of *Streptococcus agalactiae* hyaluronidase, ascorbic acid 6-palmitate, resulting in values within the same order of magnitude as literature reports. Instrumental method validation was also performed by evaluating repeatability, and intermediate precision, and determining the limit of detection and limit of quantification. This assay was then used to identify two fungal metabolites, leotiomycene A and leotiomycene B as the most potent *Streptococcus agalactiae* hyaluronidase inhibitors to date, and leotiomycene B as the first reported inhibitor of *Staphylococcus aureus* hyaluronidase. The concentrations at which these compounds inhibited hyaluronidase were found to not have any antimicrobial effects, and are therefore potential candidates for the development of anti-hyaluronidase treatments for *Streptococcus agalactiae* and *Staphylococcus aureus* infections.

The second goal was achieved by creating a database of isolated *Hydrastis canadensis* constituents using LC-MS that included retention time, accurate mass in both polarities, and high mass accuracy fragmentation patterns in both polarities. The raw file for each pure compound was uploaded into the Global Natural Product Social Molecular Networking database for dereplication purposes and to facilitate open access data sharing. To evaluate the effectiveness of biochemometrics for identifying synergists and additives, an organic extract of aerial material from *H. canadensis* underwent various stages of fractionation. Each stage of resultant fractions was profiled using the previously described LC-MS method, and their ability to enhance the antimicrobial activity of berberine against *S. aureus* was evaluated. These data were uploaded into the program Sirius, where multivariate statistical analyses were applied to create selectivity ratio (SR)

plots. Retention time-mass pairs with low SR values indicate that a specific compound correlates with the observed biological activity, and should therefore guide isolation efforts. It was found that three stages of sample purification were needed to obtain SR plots that correctly predicted known additives and synergists. Interestingly, a *m/z* that was not yet known to *H. canadensis* was predicted to be responsible for bioactivity, and upon isolation, structure elucidation and confirmatory testing, it was shown that the new flavonoid 3,3′-dihydroxy-5,7,4′-trimethoxy-6,8-*C*-dimethylflavone was indeed a synergist, thus showing that this workflow can be useful for understanding the complex biological activities of botanical medicines.

# NEW STRATEGIES TO IDENTIFY BIOACTIVE COMPOUNDS FROM COMPLEX MATRICES TO COMBAT DRUG-RESISTANT BACTERIAL INFECTIONS

by

Emily R. Britton

A Dissertation Submitted to
the Faculty of The Graduate School at
The University of North Carolina at Greensboro
in Partial Fulfillment
of the Requirements for the Degree
Doctor of Philosophy

Greensboro
2018

Approved by

_____
Committee Chair

To everyone who believed in me…
your support made this dream a reality.

APPROVAL PAGE

This dissertation, written by EMILY R. BRITTON, has been approved by the following committee of the Faculty of The Graduate School at The University of North Carolina at Greensboro.

Committee Chair _____

Committee Members _____

_____

_____

_____
Date of Acceptance by Committee

_____
Date of Final Oral Examination

# ACKNOWLEDGMENTS

This research was supported by the National Center for Complimentary and Integrative Health (1R01 AT006860) and by the Ruth L. Kirschstein Predoctoral Individual National Research Service Award (F31 AT009164).

I would like to thank Drs. Nicholas Oberlies, Gregory Raner and Alexander Horswill for serving as my committee and for offering advice and guidance, Drs. Brandie Ehrmann and Daniel Todd for mass spectrometry training and advice, Drs. Martha Leyte-Lugo and Joshua Kellogg for training in isolation and data processing techniques, Dr. Jose Rivera-Chávez for training and assisting in structure elucidation, Dr. Huzefa Raja for providing fungi and mycological guidance, Tyler Graf for training in instrument maintenance and chromatography development, the entire Cech and Oberlies laboratory past and present for their support, and Dr. Nadja Cech for allowing me the opportunity to join her research group and to participate in rewarding research, and for being an inspiring and strong mentor, role model and friend.

TABLE OF CONTENTS

Page

LIST OF TABLES

Page

LIST OF FIGURES

Page

# CHAPTER I

# INTRODUCTION

## History of Plants Used for Human Health

Plants have been used as medicine for human health since ancient times, with the first recorded evidence of usage dating back at least 5000 years ago via Sumerian clay slabs (1). Nature has provided many useful cures for disease since then; for instance, taxol, which is used today to treat ovarian, breast and non-small cell lung cancers, was discovered from the bark of the pacific yew tree (*Taxus brevifolia*) (2). The discovery of artemisinin and dihydroartemisinin from *Artemisia annua*, which is used to treat malaria, was due in part to Dr. Youyou Tu, who investigated traditional Chinese medicine to determine how to best prepare extracts (3). These studies led to her receiving the Nobel Prize in Physiology or Medicine in 2015. In fact, 146 of 174 anticancer drugs on the market from 1981 til 2014 were either derived from or inspired by compounds found in nature. In addition, 148 of 221 small molecule drugs have come from or inspired by nature, some of which were found by investigating traditional medicine (4). Botanicals play an important role in dietary supplements, with sales exceeding $7 billion in 2016 in the United States, with an increase of $530 million from the previous year (5). *Hydrastis canadensis* L. (Ranunculaceae), or goldenseal, is a common ingredient in dietary supplements that boast enhanced immunity, with most recent reports indicating that supplements containing both goldenseal and *Echinacea* were responsible for $6.68

million in the US in 2014, while goldenseal-only supplements had a total of $1.31 million in sales (6, 7). Goldenseal is a perennial herb native to the Appalachian Mountains that grows best in shaded, deciduous forests. Goldenseal thrives in soil with good water drainage and is commonly found growing alongside white oak trees, hickory trees, ginseng and mayapple (8). It has been used to treat a variety of ailments throughout history, with Native American tribes having prepared tonics from root material to treat digestive irritability and infections of the eyes and skin (9, 10). The effects that natural product mixtures have on biological systems are often attributed to the most abundant constituents. In the case of goldenseal, the isoquinoline alkaloids berberine and ß-hydrastine, which account for 0.5-6 % and 1.5-4 % of plant material, respectively, were thought to be responsible for broad-spectrum bioactivity (6). Advances in chromatography, mass spectrometry and purification techniques have led to the discovery of not only more isoquinoline alkaloids and other biologically relevant compound classes within goldenseal, but has also allowed for the detection and identification of low-abundance constituents that in fact contribute to bioactivity. This has been demonstrated where aerial extracts of goldenseal had more antimicrobial activity against the Gram positive pathogen *Staphylococcus aureus* than predicted based upon the concentration of berberine present in the tested extract (9, 11). It was determined via synergy-directed fractionation and follow-up testing that the enhanced antimicrobial activity of goldenseal aerial extracts is due to the presence of low abundance flavonoids (9).

## The Problem of Antibiotic-resistant Infections & the Idea of Anti-virulence Targeting

The development of antibiotic resistance by bacterial pathogens remains a worldwide health threat. It is estimated that in United States, antibiotic-resistant infections are responsible for over 2,000,000 hospitalizations and 23,000 deaths annually, while the annual estimated worldwide death toll surpasses 700,000 (12, 13). As the rate of resistance development continues to increase, the number of effective treatments decreases, as fewer pharmaceutical companies are pursuing antibiotic research due to lowered profitability, and as antibiotic resistance often encompasses entire compound classes (14, 15). Furthermore, there have been no new antibiotic compound classes discovered since 1987, constituting an ongoing discovery void (16). Many institutions and groups have recognized the promise of complementary and alternative approaches to ameliorating the burden of resistance development (17-20). One methodology, termed the "anti-virulence" approach, consists of targeting the mechanism of pathogenicity, as opposed to outright killing or inhibiting the growth of bacteria. As this method does not target essential pathways and therefore does not put selective pressure on the bacteria, it is thought to be exempt from resistance development. Research has been done to identify chemical entities that limit bacterial pathogenicity and virulence, although none have yet made it to the stage of clinical development (21). One of the challenges in finding anti-virulence compounds is the lack of target-specific biological assays. As bacterial growth inhibition is not the target of anti-virulence treatments, other biological metrics must also be measured; for example, signaling, toxin production and spreading (22-25). These

specialized biological assays can involve the engineering of knock-out bacterial strains and the utilization of sensitive analytical techniques, one of being liquid chromatography coupled to mass spectrometry.

## Advantages of Mass Spectrometry to Facilitate Natural Product Research

Ultra high pressure liquid chromatography coupled to high resolving-power mass spectrometry (UPLC-MS) has improved dereplication, which is the identification of known constituents earlier in fractionation process to better save time and resources. Although this technique has been used for some time, the shortening of chromatographic methods along with the addition of high mass accuracy measurements and fragmentation patterns has greatly improved this methodology. The benefit of the inclusion of accurate mass measurements and fragmentation patterns is that it allows for the differentiation of structural isomers when they happen to co-elute. Another advantage lies in the rapid detection of known constituents in understudied specimens like fungi, whose chemical profiles may not be annotated in the scientific literature. This workflow was successfully applied fungal extracts that possessed cytotoxic activity, resulting in the exclusion of approximately half of the extracts due to the presence of known cytotoxic compounds (26). Later, mass defect filtering was added to this pipeline, which is a post-acquisition data mining technique filters spectra for a certain windows of the nonintegral portion of the *m/z* (known as mass defect) to identify tentative structural analogues. This technique is based upon that fact that every compound has a defined mass defect, and is leveraged by the capability of high resolving-power mass spectrometers to measure mass to the

1000ths place (27). As the scientific community shifts to open-source data sharing, the desire for cloud-based fragmentation databases has grown, resulting in the development of the Global Natural Product Social Molecular Networking system (GNPS). Users can upload fragmentation data into the GNPS database, and could then upload their raw files into the cloud based software, which would then screen their data against the user-curated GNPS database along with others professionally-curated databases such as those provided by the National Institutes of Health, Pacific Northwest National Lab and Massbank. The results of this process are networks of *m/z* values that are connected based upon a measure of similarity between fragmentation patterns, as well as tentative structure identifications. Although this methodology does not include orthogonal measurements such as retention time, it does allow for the tentative identification of potentially new, structurally similar molecules to those present in the databases (28, 29). These advances in dereplication are a direct result of the utilization of LC-MS/MS.

The quality of and confidence in biological measurements has increased since the inclusion of mass spectrometry. When working with natural product mixtures, it is often observed that interferences arise in spectrophotometric or optical density-based measurements. This was demonstrated by Brown et al. in an evaluation of bacterial efflux pump inhibition, where compounds with known activity were falsely negative in a fluorescence-based assay. A mass spectrometry-based bioassay was presented as a quantitative alternative, and resulted in the positive identification of known inhibitors what were seemingly inactive via the fluorescence assay (30). Further, the identification of quorum-sensing inhibitors in a quantitative manner was made possible by mass

spectrometry, where instead of using fluorescence methods which require engineered strains of bacteria and are prone to optical interferences. *Staphylococcus aureus* auto-inducing peptide, a marker of quorum-sensing, was directly measured in filtered spent broth to quantify. This method was validated by screening a known inhibitor, which resulted in an $IC_{50}$ value that matched with previous literature reports (23).

Lastly, the application of multivariate statistics into discovery workflows has enhanced the informative power of mass spectral measurements and the ability of researchers to efficiently prioritize leads. One challenge of using large mass spectrometry data sets is the propensity to only analyze positive data; for example, when an extract or fraction is determined to be of interest based upon a biological measurement, its chemical profile is often investigated, while the chemical profiles of inactive or less-active samples are ignored. The inclusion of "negative" data is advantageous in that it sheds light on which constituents are not relevant to biological activity. When multiple samples are profiles, sometimes in both polarities, the amount of data acquired can become overwhelming to the point where the individual evaluation of each piece of data becomes cumbersome and inefficient (31). The application of multivariate statistics to mass spectrometry datasets has enabled rapid identification of chemical signals that influence similarity and dissimilarity between samples, which can be used to pinpoint markers of disease or the instance of sample adulteration (32-34). Another challenge in managing these datasets comes from the incorporation of biological data measurements, which serve as an orthogonal measurement of similarity between samples. The application of multivariate statistics has proven successful in determining which constituents in

complex mixtures are important for certain applications, and has therefore been shown to be an advantageous addition to mass spectrometry-based research (32, 35-40).

## Research Goals

The studies herein have two differing but important foci; the creation and use of a mass spectrometry-based bioassay to discover compounds that limit bacterial virulence by inhibiting spreading, and the integration of mass spectrometry and biological measurements via multivariate statistics to identify additives and synergists in complex mixtures (*Hydrastis canadensis*). The common thread between both is the pursuance of knowledge via mass spectrometry as to how natural product medicines can be used to treat infections.

CHAPTER II

# A NEW MASS SPECTROMETRY BASED BIOASSAY FOR THE DIRECT ASSESSMENT OF HYALURONIDASE ACTIVITY AND INHIBITION

This chapter has been published in the Journal of Microbiological Methods and is presented in that style. Britton, E.R., Ibberson, C.B., Horswill, A.R., Cech, N.B. J. Microbiol Methods. 2015, 119, 163-167.

Britton, E.R. developed the hyaluronidase assay, collected all data and wrote the manuscript. Ibberson, C.B. provided preliminary data that prompted the development of the assay, isolated hyaluronidase from *Staphylococcus aureus*, described the procedure in the Materials and Methods section, and provided edits on the manuscript.
Horswill, A.H. made experimental suggestions, provided guidance and made edits on the manuscript. Cech, N.B. provided suggestions and edits throughout manuscript preparation.

## Introduction

The development of resistance by bacterial pathogens is a growing threat (12). The overuse of antibiotics accelerates resistance development, and there is an urgent need for alternative therapeutic strategies against bacterial infections (41). One potential alternative target is hyaluronidase, a virulence factor secreted by Gram-positive bacterial pathogens such as *Staphylococcus aureus* (42) and *Streptococcus agalactiae* (43, 44). Both of these pathogens are considered by the Centers for Disease Control to be of concerning and serious threat for resistance development (12). Hyaluronidase degrades hyaluronan, a polymer found in the skin and other tissues. The resulting disaccharide product serves as an energy source for the bacteria, enabling the infection to spread

through tissues (43, 45). Thus, anti-virulence therapeutic agents could be developed against bacterial infections by specifically targeting hyaluronidase (42, 43, 46).

Only a few studies have investigated the inhibition of hyaluronidase by chemical means. It has been shown that ascorbic acyl 6-palmitate and other vitamin C derivatives have low micromolar potency against *Streptococcus pneumoniae* and *Streptococcus agalactiae* hyaluronidases (47, 48). These studies show the potential of hyaluronidase inhibition as a therapeutic target. Further efforts towards the identification and development of more potent hyaluronidase inhibitors will require a robust screening assay that provides quantitative comparisons of inhibitor potency.

Several methods have been developed to measure the activity of the hyaluronidase enzymes. Qualitative measurements can be obtained using agar plate assays. These assays rely on measuring clearance zones in solid media containing hyaluronan after addition of the hyaluronidase enzyme (42, 49, 50). More quantitative measurements can be obtained using spectrophotometric approaches, which rely on a reaction between the disaccharide and a substrate that in turn produces a colored product (51). For example, the Morgan-Elson reaction employs the transformation of the N-acetyl glucosamine reducing end of the disaccharide to a series of products using varied pH and temperature environments. The final product is subsequently reacted with p-dimethylaminobenzaldehyde to produce a red complex that can be detected by monitoring absorbance at 585 nm (52). This method was improved upon by measuring fluorescent intensity after excitation at 545 nm, resulting in an increase in sensitivity (51). Finally, turbidimetric measurements can be utilized to assess hyaluronidase inhibition, in

which hyaluronidase is incubated with hyaluronan, and subsequently treated with cetylpyridinium to precipitate undigested hyaluronan. An increase in light transmittance correlates with increasing disaccharide concentration (50). The aforementioned assays have important utility. For example, agar based assays and turbidimetric measurements can serve as a simple preliminary screen to identify potential inhibitors, and spectrophotometric assays have demonstrated utility for measuring enzyme kinetics parameters (53). However, the inherent indirect nature of these assays means that they are time-consuming and subject to interference. Our laboratory has designed an assay that utilizes mass spectrometry to reproducibly measure the production of disaccharides by hyaluronidase enzymes. In contrast to spectrophotometric techniques, our design requires fewer steps. The new assay is also sensitive and robust, providing excellent repeatability from assay to assay, even across multiple days. Here we present the new methodology and show its applicability to measuring the activity of hyaluronidase inhibitors.

## Materials and Methods

### Purification of *S. aureus* hyaluronidase

To generate the hyaluronidase overexpression construct pCR03, the *hysA* gene without the encoded signal sequence was amplified from AH1263 genomic DNA using primers CBR41 (5'GTTGTTGCTAGCGATACGAATGTTCAAACGCCAG3') and CBR42 (5'GTTGTTCTCGAGGTGTCGAGATTTTCTTGCATT3'), which contain *Nhe*I and *Xho*I sites at their 5' ends, respectively (42). The resulting PCR product was ligated into pET28a linearized with *Nhe*I and *Xho*I and electroporated into *E. coli* strain ER2566 to generate strain AH2856. To purify hyaluronidase, AH2856 was grown overnight at

37°C in luria broth (LB) (Sigma, St. Louis, MO) containing kanamycin (50 μg/mL), and subcultured into 1 L of fresh LB at a ratio of 1:250. The culture was grown at 30°C to mid-logarithmic phase, IPTG was added to 1 mM final concentration, and the culture was allowed to grow for an additional 4 h. Cells were harvested by centrifugation, washed once with water, pelleted by centrifugation, and frozen at -20°C. Cells were mechanically lysed by two passages through a Microfluidics Microfluidizer model LV1 (Newton, MA) at 25,000 psi. Cell lysate was clarified by centrifugation for 20 min at 15,000 × *g* at 4 °C. Protein was purified in the presence of 1 mM Tris(hydroxypropyl)phosphine (THP) using Fractogel His-Bind Resin (EMD Millipore, Darmstadt, Germany) as per the manufacturer's instructions. The protein was dialyzed into phosphate buffered saline (PBS) containing 1 mM THP, concentrated using Millipore Centrifugal Filter Unit (Temecula, CA, 30,000 molecular weight cut-off), and brought to 10 mg/mL in 1X PBS containing 1 mM THP. The protein suspension was frozen in 20% glycerol at -20°C until use.

**Bioassay procedure**

Concentrated stock solutions of hyaluronidase from *S. agalactiae* (R & D Systems, Minneapolis, MN) and *S. aureus* (isolated as described in 2.1) were prepared with PBS with 10% glycerol and stored at -80°C in Lo-binding Eppendorf tubes. Aliquots were thawed at room temperature and diluted with PBS to a concentration of 1.25 μg/mL. A stock solution of hyaluronic acid sodium salt from *Streptococcus equi* (Sigma, St. Louis, MO) was prepared at 5 mg/mL with deionized water (EMD Millipore, Temecula, CA). To each Lo-binding Eppendorf tube, 1.25 μg/mL hyaluronidase and 1

mg/mL extract in dimethylsulfoxide (DMSO) were added and incubated at 37°C. After incubation, 5 mg/mL hyaluronan was added to each tube and thoroughly mixed before incubation at 37°C for 15 min. and shaking at 400 rpm. The final assay concentrations of hyaluronidase, extract and hyaluronan were 0.61 μg/mL, 24.4 μg/mL and 2.44 mg/mL, respectively. To quench the reaction, an aliquot from the reaction mixture was diluted 50-fold with acetonitrile (Fisher Scientific, Pittsburgh, PA) containing 0.1% formic acid (Fisher Scientific, Pittsburgh, PA). The diluted reaction was then submitted to ultraperformance liquid chromatography-mass spectrometry (UPLC-MS) analysis via a Waters Acquity UPLC with an Acquity UPLC column (BEH HILIC, 1.7 μm, 2.1 x 50 mm, Waters Corporation, Milford, MA) and a Thermo Quantum Access triple stage quadrupole (TSQ) mass spectrometer with electrospray ionization source (Thermo Fisher Scientific, MA, USA). Ascorbic acyl 6-palmitate (also referred to as ascorbic acid 6-palmitate) (Sigma, St. Louis, MO) served as the positive control. The identity of the disaccharide (3-(4-deoxy-β-D-gluc-4-enuronosyl)-N-acetyl-D-glucosamine, Figure 1) was confirmed by accurate mass measurements (Thermo LTQ Orbitrap, Thermo Fisher Scientific, MA, USA), its absence in assays with inactive enzyme, and by comparison with a standard (Carbosynth, UK). The Thermo LTQ Orbitrap was operated at the following settings: spray voltage, 4000 V; sheath gas, ion sweep gas, and auxiliary gas pressure, 30, 0, and 20, respectively; capillary temperature, 300°C; tube lens offset, 100 V.

**ESI-MS analysis**

Hyaluronan was degraded by *S. agalactiae* hyaluronidase and used to optimize MS settings. All solvents used in the present study were Optima LC-MS grade (Fisher Scientific, Pittsburgh, PA). Diluted reaction mixtures (3 µL) were eluted from the column at a flow rate of 0.2 mL/min using the following binary gradient with solvent A consisting of water with 0.1% formic acid additive and solvent B consisting of acetonitrile with 0.1% formic acid additive. The gradient initiated at an isocratic composition of 15:85 (A:B) for 1.5 min., increasing linearly to 100:0 (A:B) from 1.5 to 2.5 min., followed by an isocratic hold at 100:0 (A:B) from 2.5 to 4.4 min., gradient returned to starting conditions of 15:85 (A:B) from 4.4 to 4.5 min., and was held from 4.5 to 5 min. The Thermo Quantum Access triple stage quadrupole mass spectrometer was operated at the following settings: spray voltage, 4000 V; vaporizer temperature, 384°C; sheath gas, ion sweep gas, and auxiliary gas pressure, 60, 2.0, and 5, respectively; capillary temperature, 202°C; tube lens offset, 181 V.

Percent inhibitions were based on a comparison of relative peak areas associated with the protonated *m/z* of the disaccharide units. Standard error was calculated for each triplicate set of measurements, and $IC_{50}$ values were calculated using a four parameter logistic standard curve analysis function in SigmaPlot (v12.5).

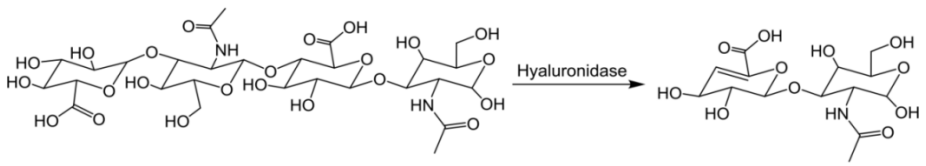


**Figure 1. Reaction Between Hyaluronan Polymer and Hyaluronidase.** 3-(4-deoxy-β-D-gluc-4-enuronosyl)-N-acetyl-D-glucosamine units are produced via β elimination of the 1→4 glycosidic bond.

**Method validation for the detection of 3-(4-deoxy-β-D-gluc-4-enuronosyl)-N-acetyl-D-glucosamine**

A stock solution of 3-(4-deoxy-β-D-gluc-4-enuronosyl)-N-acetyl-D-glucosamine (99% pure, Carbosynth, West Berkshire, UK) was serially diluted to make seven concentrations of 0.78, 1.6, 3.1, 6.2, 12.5, 25 and 50 µM. A calibration curve was generated using the UPLC-MS as described above, and the log of the peak areas of the selected ion chromatograms for 3-(4-deoxy-β-D-gluc-4-enuronosyl)-N-acetyl-D-glucosamine ions were plotted versus the log of the concentration.

Method validation was conducted according to the guidelines of the International Committee of Harmonisation (ICH) section Q2 (R1) (54) with external calibration curves. The linear dynamic range was determined by analyzing samples ranging in concentration from 0.39 to 500 µM. Repeatability was evaluated by analyzing the seven standards that fell within the linear range (0.78-50 µM) in triplicate and determining the standard deviation and relative standard deviation of the back-calculated 3-(4-deoxy-β-D-gluc-4-enuronosyl)-N-acetyl-D-glucosamine concentration for those analyses. Intermediate precision was evaluated by conducting the repeatability study three times on three different days. The standard deviation and relative standard deviation for the intermediate precision were calculated using the average back-calculated concentration for each of the three days for each standard concentration. Limit of detection (LOD) was defined as the lowest concentration of 3-(4-deoxy-β-D-gluc-4-enuronosyl)-N-acetyl-D-glucosamine that provided a signal-to-noise ratio of 3. Limit of quantitation (LOQ) was defined as the lowest concentration that provided a residual of less than 15%.

## Results

### Activity of *S.agalactiae* and *S. aureus* hyaluronidases

We first sought to confirm the ability to detect the disaccharide product ( Figure 1) produced by action of hyaluronidase on the hyaluronan polymer. LC-MS analysis of the reaction mixture in which *S. agalactiae* or *S. aureus* hyaluronidase enzymes were incubated with hyaluronan resulted in production of two slightly resolved ions detected with *m/z* 380.1192. The identity of the ions as products of hyaluronidase was supported by their observed loss after boiling the *S. aureus* and *S. agalactiae* reaction mixtures to deactivate the enzyme (Figure 2). Additional confirmation was provided by measurements with high resolving power mass spectrometry, in which the observed mass of the observed ions (380.1182) matched the calculated monoisotopic mass for protonated 3-(4-deoxy-β-D-gluc-4-enuronosyl)-N-acetyl-D-glucosamine (380.1192) to within 2.6 ppm. Finally, we monitored time-dependent production of the disaccharide products (Figure S1), and determined that disaccharide production increased over the range of 10 to 60 min. Thus, 15 min was chosen as the incubation time for the reactions.

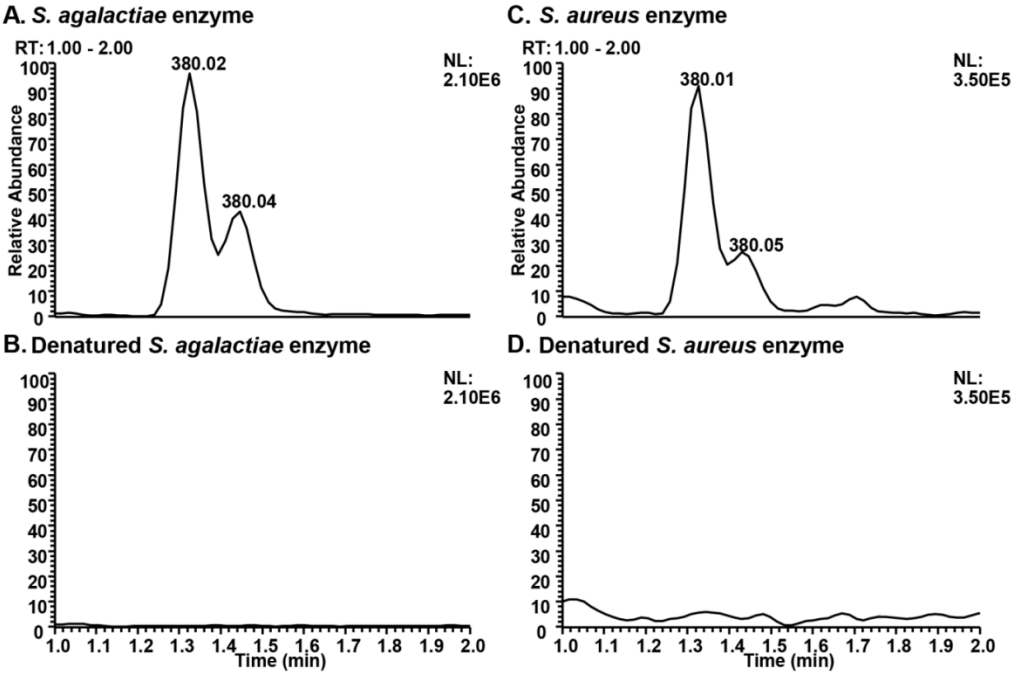


**Figure 2. Selected Ion Chromatograms Representing Two Parallel Hyaluronidase Bioassays.** A reaction performed with 0.61 µg/mL *S. agalactiae* hyaluronidase and 2.44 mg/mL hyaluronan is shown in panel (A), and another reaction with identical conditions except that the enzyme was boiled for 15 min. prior to incubation is shown in (B). The experiment performed under the same conditions using active and denatured *S. aureus* hyaluronidase is shown in panels C and D, respectively. Peaks for *m/z* 380.0 were observed at 1.3 min for the active enzyme (A, C), and not for the denatured hyaluronidase (D, E). The experiment was performed in triplicate and the same results in the representative chromatograms above were observed for all replicates. NL indicates the level of signal (counts detected by the mass spectrometer) used to normalize each chromatogram.

## Use of the HILIC-ESI-MS assay to evaluate inhibition

We also endeavored to evaluate the effectiveness of the method demonstrated in *Section 3.1* to monitor enzyme inhibition. Ascorbic acyl 6-palmitate (compound **1**, Figure 3), has a published $IC_{50}$ value of 4 µM against *S. agalactiae* hyaluronidase (47). This literature value is in agreement with the $IC_{50}$ value of 8.0 ± 1.0 µM that was measured for a dose-response study of hyaluronidase inhibition by ascorbic acyl 6-palmitate monitored with UPLC-MS detection (Figure 4A). On the basis of structural similarity to ascorbic acyl 6-palmitate, we predicted that n-cyclohexanecarbonylpentadecylamine (Cayman

Chemical, Ann Arbor, MI, compound **2**, Figure 3) would also act as a hyaluronidase inhibitor. This compound was also observed to inhibit the activity of hyaluronidase, although with somewhat less potency ($IC_{50}$ 30.4 ± 9.8 µM, Figure 4).

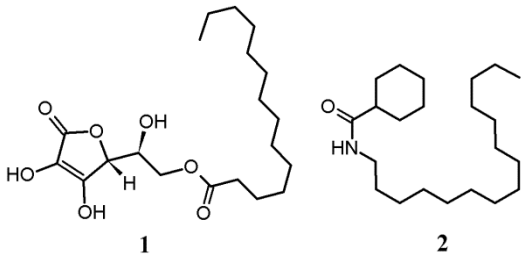


**Figure 3. Ascorbic acyl 6-palmitate (1) and n-cyclohexanecarbonylpentadecylamine (2).**

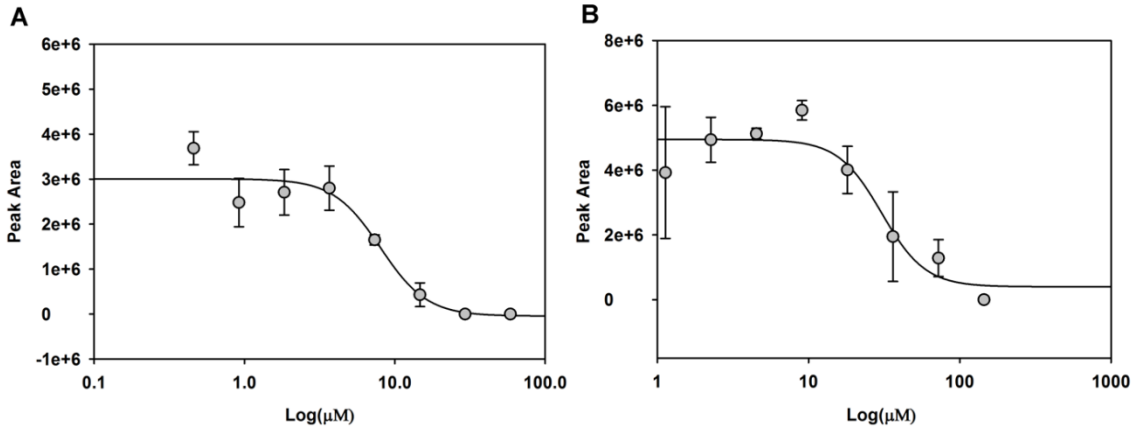


**Figure 4. Dose Response Curves of *Streptococcus agalactiae* Hyaluronidase Versus Compounds 1 (A) and 2 (B).** Panel A represents a dose response curve of *S. agalactiae* hyaluronidase versus ascorbic acyl 6-palmitate (conditions identical to Figure 2A). The measured $IC_{50}$ was 8.0 ± 1.0 µM. Panel B represents a dose response curve of *S. agalactiae* hyaluronidase versus n-cyclohexanecarbonylpentadecylamine, for which the $IC_{50}$ was 30.4 ± 9.8 µM. Each data point is an average of triplicate measurements of disaccharide peak area, with error bars corresponding to standard error.

## Method validation

A number of parameters were measured to validate the new method. From these validation studies, the linear dynamic range was determined to be from 0.78 to 50 µM 3-

(4-deoxy-β-D-gluc-4-enuronosyl)-N-acetyl-D-glucosamine (**Table 1**). A calibration curve generated over this concentration range had a correlation coefficient of 0.997. With the new method, the limit of detection (LOD) and limit of quantitation (LOQ) were 0.29 µM and 0.78 µM 3-(4-deoxy-β-D-gluc-4-enuronosyl)-N-acetyl-D-glucosamine, respectively. The LOD reported here lower than that reported by Reissig et al. using the Morgan-Elson colorimetric assay (1955). These investigators reported a limit of detection of $3 \times 10^{-10}$ moles of N-acetyl-D-glucosamine (the reducing end of the disaccharide product), which is equivalent to 1.32 µg/mL N-acetyl-D-glucosamine or 6.0 µM 3-(4-deoxy-β-D-gluc-4-enuronosyl)-N-acetyl-D-glucosamine. The LOD for the fluorometric version of the Morgan-Elson assay described by Takahashi et al. (2003) was 0.016 µg/mL N-acetyl-D-glucosamine, equivalent to 0.071 µM 3-(4-deoxy-β-D-gluc-4-enuronosyl)-N-acetyl-D-glucosamine. This limit of detection is approximately 4 times lower than the LOD reported here. Thus, the new mass spectrometric assay appears to be more sensitive than the published colorimetric assay, but less sensitive than the fluorometric assay.

As a measure of the accuracy of the new method, the back calculated concentrations of the standards (residuals) differed from their nominal concentrations by ≤ 11% across the linear dynamic range (**Table 2**). The new method also demonstrated excellent precision. As evidence of this, the relative standard deviation values for both repeatability (precision between injections) and intermediate precision (precision across multiple days) were less than or equal to 10% (**Table 2**).

**Table 1. Regression Parameters, Detection Limit, and Limit of Quantification for 3-(4-deoxy-β-D-gluc-4-enuronosyl)-N-acetyl-D-glucosamine**

| Validation parameter | Result[a] |
|---|---|
| Correlation coefficient | 0.997 |
| Standard error | 0.040 |
| *y*-Intercept | 5.886 ± 0.025 |
| Slope of regression line | 1.006 ± 0.025 |
| Number of data points | 21 |
| Limit of detection (LOD) | 0.29 μM[b] |
| Lower limit of quantitation (LLOQ) | 0.78 μM[c] |
| Upper limit of quantitation (ULOQ) | 50 μM |

[a] Calculations were based on triplicate analyses of seven standards of 3-(4-deoxy-β-D-gluc-4-enuronosyl)-N-acetyl-D-glucosamine using UPLC-MS.
[b] LOD was defined as the concentration that provided a signal to noise ratio of 3:1 with noise determined by injection of a solvent blank (acetonitrile with 0.1% formic acid).
[c] LOQ was defined as the lowest concentration of standard in the calibration curve that provided a residual of less than 15% (Table 2).

**Table 2. Precision Data for 3-(4-deoxy-β-D-gluc-4-enuronosyl)-N-acetyl-D-glucosamine**

| Theoretical concentration (μM) | Measured concentration[a] (μM) | Residuals[b] (%) | Repeatability[c] (%) | Intermediate precision[d] (%) |
|---|---|---|---|---|
| 0.78 | 0.82 | 5 | 2 | 10 |
| 1.6 | 1.4 | -11 | 7 | 6 |
| 3.1 | 3.2 | 1 | 2 | 4 |
| 6.2 | 6.2 | 0 | 2 | 10 |
| 12.5 | 13.8 | 10 | 3 | 4 |
| 25 | 27 | 7 | 5 | 5 |
| 50 | 46 | -7 | 5 | 7 |

[a] The measured concentration is an average of back calculated concentration of 3-(4-deoxy-β-D-gluc-4-enuronosyl)-N-acetyl-D-glucosamine obtained from triplicate analyses on three different days.
[b] (Measured concentration-theoretical concentration) / theoretical concentration x 100.
[c] Repeatability is expressed as the percentage relative standard deviation for triplicate analyses conducted on a single day.
[d] Intermediate precision is expressed as the percentage relative standard deviation of the three back-calculated 3-(4-deoxy-β-D-gluc-4-enuronosyl)-N-acetyl-D-glucosamine concentrations (each an average of triplicate measurements) determined on three separate days.

## Discussion

Mass spectrometric analysis of sugars in biological matrices has often been complicated by the high polarity of these compounds, which prevents their retention on the reversed phase C-18 columns that are commonly employed for LC-MS analyses (55).

With this study, we employed instead hydrophilic interaction liquid chromatography (HILIC), a chromatographic approach that has recently gained popularity for the analysis of polar species (55, 56). The application of HILIC enabled the disaccharide product to be retained effectively (1.4 min, Figure 2, panels A and C). This product was not retained with reverse phase chromatography (data not shown). Using HILIC coupled to mass spectrometry, it was possible to quantitatively monitor the activity of the hyaluronidase enzyme, and to replicate the published $IC_{50}$ value of a known hyaluronidase inhibitor. Unlike previously published spectrophotometric methods (50, 51), the new MS based assay directly measures the product of the enzyme. Another advantage of this approach is that it will not be subject to interference by compounds that absorb or scatter light. Thus, although it is somewhat less sensitive than the published fluorometric method, it could be a useful alternative approach for situations where interference is observed with fluorometric analyses.

The detection of two ions in the active enzyme cultures was unexpected. These ions were partially resolved chromatographically (Figure 2), which indicates that they are both present in the solution prior to analysis, and not an artifact of analysis by the mass spectrometer. Given that both of these ions match the predicted mass of the 3-(4-deoxy-β-D-gluc-4-enuronosyl)-N-acetyl-D-glucosamine product, it is presumed that they are isomers of the same molecule. The configuration of these isomers could not be confirmed with mass spectrometry, however, their presence and absence, respectively, in mixtures with and without active enzyme made them a useful product on which to base the biological assay.

Numerous pathogenic bacteria secrete hyaluronidase, including *Staphylococcus aureus*, *Streptococcus agalactiae*, *Streptococcus pyogenes*, *Streptococcus pneumoniae*, *Peptostreptococcus*, *Streptomyces*, *Clostridium*, and *Propionibacterium* (46). Hyaluronidases from *S. agalactiae*, *S. pneumoniae* and *S. aureus* have been found to have a high degree of homology, with greater than 35% amino acid identity across the entire enzyme and complete conservation of catalytic residues (46, 47). Thus, it is possible that a hyaluronidase inhibitor could have broad-spectrum activity against multiple pathogens that secrete hyaluronidase. Therapeutic agents targeting hyaluronidase would have the advantage of selectively targeting pathogenic bacteria, leaving beneficial bacterial flora intact (46). The bioassay developed here could enable screening for new hyaluronidase inhibitors against a range of bacteria pathogens, and, as such, could contribute importantly towards the development of new therapies based on hyaluronidase inhibition.

## Conclusion

This work demonstrates the effectiveness of a mass spectrometric method for monitoring activity and inhibition of hyaluronidase. Here we employed the assay to monitor activity of *S. aureus* and *S. agalactiae* hyaluronidases, and to identify a new hyaluronidase inhibitor (n-cyclohexanecarbonylpentadecylamine). Future studies could employ this mass spectrometric approach in more extensive screening efforts, or to study enzyme kinetics.

# CHAPTER III

# FUNGAL METABOLITE INHIBITORS OF HYALURONIDASE, THE STAPHYLOCOCCUS AUREUS SPREADING FACTOR

This chapter has been prepared for submission to the journal Antimicrobial Agents and Chemotherapy and is presented in that style. Britton, E.R., Stempin, J.J., Paguigan, N.D., Augustinovic, M., Raja, H.A., Horswill, A.H., Oberlies, N.H., Cech, N.B. Antimicrob. Agents Chemother. In preparation.

Britton, E.R. performed and interpreted all antimicrobial assay data, analyzed and prepared hyaluronidase assay data, created all of the figures and wrote the manuscript. Stempin, J.J. ran all of the hyaluronidase assays and provided organized data for interpretation. Paguigan, N.D. isolated the leotiomycene compounds and provided them for testing. Augustinovic, M. isolated and provided additional leotiomycene A and B for testing. Raja, H.A. grew the fungi from which the leotiomycenes were isolated. Horswill, A.H. and Oberlies, N.H. made experimental suggestions, provided guidance and made edits on the manuscript. Cech, N.B. provided suggestions and edits throughout manuscript preparation.

## Introduction

Approximately 700,000 people die each year from drug resistant infections worldwide, and it is predicted that the death toll will surpass 10 million by the year 2050, which exceeds the current number of annual deaths caused by cancer (13). An estimated 2 million people in the United States acquire antibiotic resistant infections annually, resulting in 23000 deaths (12). Methicillin-resistant *Staphylococcus aureus* infections, which are considered to pose a great risk to human health by the WHO, are the most

common of cause of these, accounting for almost 50% (12, 57). Few treatments are available to treat these problematic infections, and the pipeline for new antibiotics is lacking in leads, which could lead to an era where once-treatable infections will again become lethal (12). Therefore, it is of critical concern that alternative methods to treat drug resistant infections are explored.

One potential alternative approach is targeting bacterial virulence. Virulence factors are the toxins produced by bacteria that facilitate the spread and pathogenicity of infection. It is possible that blocking the pathogenicity of the bacteria could result in decreased severity of infection. Ambuic acid and ω-hydroxyemodin, both of which are secondary metabolites produced by fungi, have been shown to mediate pathogenicity by blocking the communication of bacteria via quorum sensing (58, 59). Both have demonstrated efficacy in the treatment of skin infections in mouse models (58, 59). Another potential anti-virulence therapeutic target is the spreading factor hyaluronidase, employed by some pathogenic Gram-positive bacteria to facilitate the spread of infection (42, 46, 60, 61). Hyaluronidase is an exo-enzyme that degrades hyaluronan, a large glycosaminoglycan found in the extracellular matrix of mammalian soft connective tissue, into disaccharide units. The degradation of hyaluronan allows for the penetration of host tissue while providing a source of carbon for the bacteria (25, 43, 45, 62). As hyaluronan plays a role in wound healing and tissue turnover, its degradation by bacterial hyaluronidase further complicates healing (61). Furthermore, bacterial hyaluronidases also break down host-created hyaluronan fragments into disaccharides that can no longer function as pro-inflammatory and immune-stimulatory activators of toll-like receptors,

thus aiding in evasion of the immune system (63). It has also been shown that bacteria secrete hyaluronidase within biofilms, and this is proposed to facilitate dispersion and dissemination of bacteria into surrounding tissue (64). The essential role of hyaluronidase in bacterial virulence supports the investigation of inhibitors of this enzyme as alternative therapeutics for the treatment of infections.

To date, several inhibitors of hyaluronidase from *Streptococcus agalactiae* have been identified. L-ascorbic acid was found to have modest levels of inhibition, and after molecular docking and synthetic studies, L-ascorbic acid 6-palmitate was shown to be more potent due to an increase in hydrogen bonding events within the binding site, resulting in an $IC_{50}$ of 4 μM (47, 65). Later synthetic studies identified that longer alkyl chains increased potency, resulting in the identification of ascorbic acid 6-*O*-octadecanoate as the most potent *Streptococcus agalactiae* hyaluronidase inhibitor to date, with an $IC_{50}$ of 0.9 μM (48). Benzimidazole and benzoxazole-2-thione derivatives were also identified to have inhibitory activity with $IC_{50}$ values as low as 5 μM (66). Carotenoids, flavonoids and triterpenes also have inhibitory activity, albeit much less potent than previously identified active compounds (67, 68). When using a new, mass spectrometry-based hyaluronidase screening assay, the activity of ascorbic acid 6-palmitate (**1**) was confirmed against *Streptococcus agalactiae* hyaluronidase ($IC_{50}$ of 8 μM) and n-cyclohexanecarbonylpentadecylamine was identified to have anti-hyaluronidase activity, with an $IC_{50}$ of 30.4 μM (24). To date, there are no published inhibitors of *Staphylococcus aureus* hyaluronidase, although the mass spectrometry based assay does have the capability to screen against this enzymatic target (24). With this

project, our goal was to identify small molecule fungal metabolites effective at inhibiting hyaluronidase from both *Streptococcus agalactiae* and *Staphylococcus aureus*.

## Results and Discussion

The fungal metabolites ω-hydroxyemodin (**3**) and leotiomycene A-C (**4-6**) were evaluated for activity, which have been previously identified as having anti-virulence activity via inhibition of quorum sensing in *Staphylococcus aureus* (69). Compounds **7-9**, synthetic modifications of **4**, were also evaluated for inhibition. Inhibition of hyaluronidase from both *Streptococcus agalactiae* and *Staphylococcus aureus* was evaluated for each compound (Figure 5) at high and low concentrations to prioritize hits. Ascorbic acid 6-palmitate (**1**) served as the positive control for experiments using hyaluronidase from *Streptococcus agalactiae*, as there are no published inhibitors of *Staphylococcus aureus* hyaluronidase.

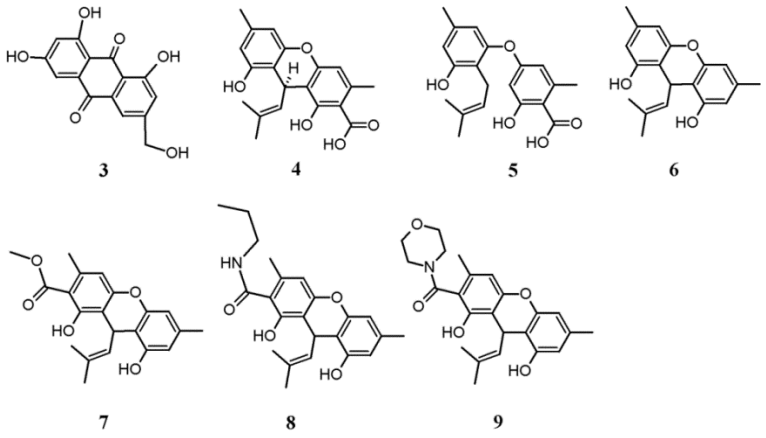


**Figure 5. Fungal Metabolites Tested Against Both *Streptococcus agalactiae* and *Staphylococcus aureus* Hyaluronidase.** Ascorbic acid 6-palmitate (**1**) inhibits hyaluronidase from *Streptococcus agalactiae* and served as a positive control. ω-hydroxyemodin (**3**) is a fungal metabolite that inhibits quorum sensing in *Staphylococcus aureus*. Leotiomycene A-C (**4-6**) are fungal metabolites isolated from *Leotiomycetes* sp. The last three compounds (**7-9**) are synthetic analogues made from **4**.

Leotiomycene A (**4**) and B (**5**) completely inhibited *Streptococcus agalactiae* hyaluronidase at both 60 and 6 μM, making them more potent than the positive control, which inhibited hyaluronidase by 84.1% at 6 μM, consistent with the literature (Figure 6). ω-hydroxyemodin (**3**) was less potent, and inhibited hyaluronidase by 60.1% at 60 μM and 18.7 % at 6 μM. Leotiomycene C (**6**) and the synthetic derivatives were inactive.

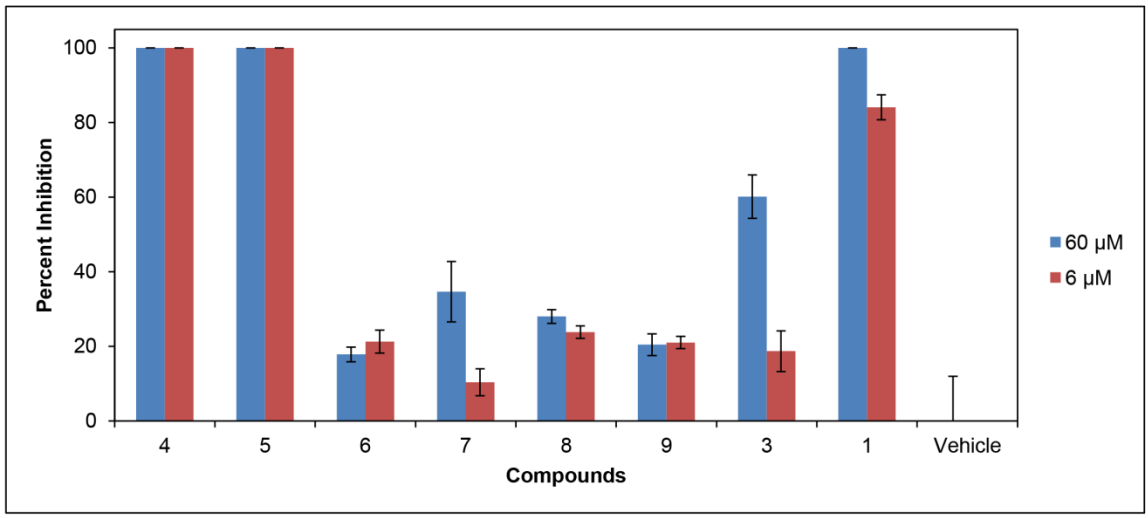


**Figure 6. Percent Inhibition of Hyaluronidase From *Streptococcus agalactiae* at 60 and 6 μM.** Ascorbic acid 6-palmitate served as the positive control, and the vehicle consisted of DMSO. Error bars represent the standard error of triplicate measurements.

The $IC_{50}$ of both compounds **4** and **5** against *Streptococcus agalactiae* hyaluronidase were determined to be 0.57 ± 0.12 μM and 0.686 ± 0.027 μM, respectively (Figure 7), making these the most potent inhibitors of *Streptococcus agalactiae* hyaluronidase to date.

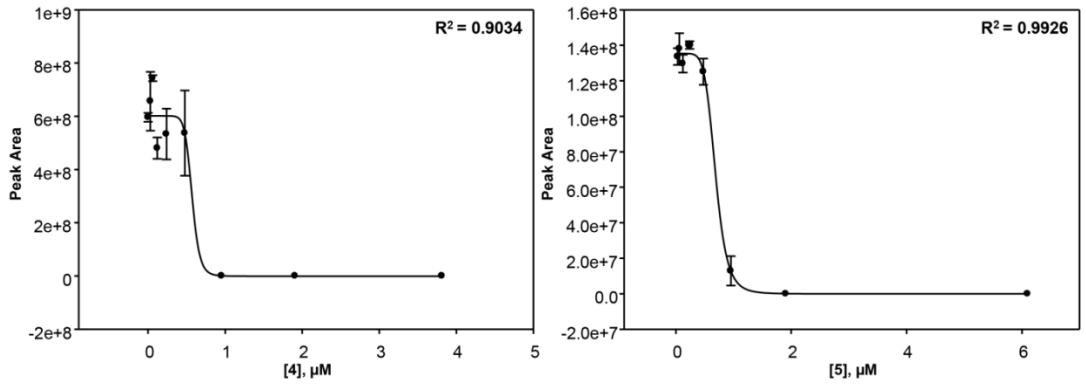


**Figure 7. Dose Response Curves of Leotiomycene A (4) and B (5) Against Hyaluronidase from *Streptococcus agalactiae.*** $IC_{50}$ and standard error was determined using a four-parameter logistic curve function in SigmaPlot (v 13).

Because the anti-virulence strategy consists of blocking bacterial pathogenesis instead of killing the bacteria, growth inhibition of both compounds **4** and **5** was evaluated against *Streptococcus agalactiae* (COH1). The minimum inhibitory concentration (MIC) of both was 5 µM, and there was no growth inhibition at the concentrations at which these compounds inhibited hyaluronidase (Figure 8).

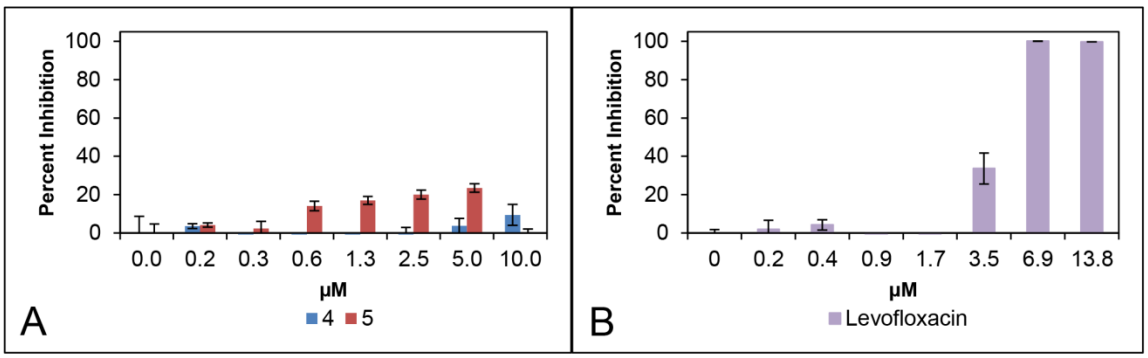


**Figure 8. Dose Response Curves of Compounds 4 and 5 Against *Streptococcus agalactiae* (Panel A).** Levofloxacin served as the positive control (Panel B), resulting in a MIC of 6.9 µM, consistent with literature reports.

When the same compounds were screened against *Staphylococcus aureus* hyaluronidase, compound **5** was the most potent, with 100 % and 53.9 % inhibition at 61 µM and 6 µM, respectively (Figure 9). Compound **4** was less potent, with 60.3 % and 29.7 % inhibition at 61 µM and 6.1 µM, respectively. The synthetic derivatives (**7**-**9**) had slightly higher potency, but not enough to warrant further studies, and compound **3** was inactive.

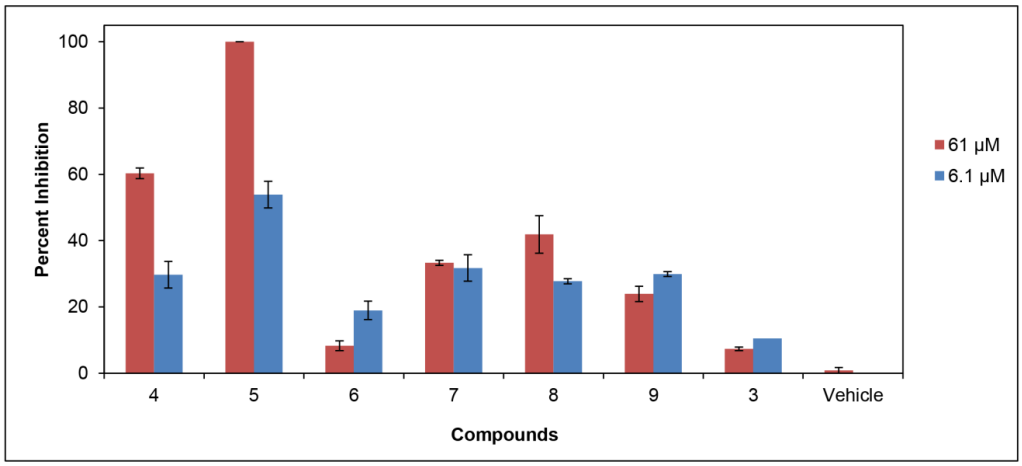


**Figure 9. Percent Inhibition of Hyaluronidase from *Staphylococcus aureus* at 61 and 6.1 µM.** No positive control was used, and the vehicle consisted of DMSO. Error bars represent the standard error of triplicate measurements.

Dose response curves were created to determine the $IC_{50}$ for both compounds **4** and **5**. Compound **4** did not achieve complete inhibition (data not shown), and compound **5** had an $IC_{50}$ of 8.93 ± 0.41 µM (FIG 6).

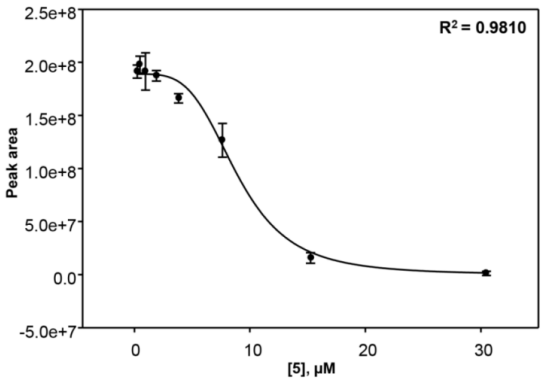


**Figure 10. Dose Response Curve of Compound 5 Against Hyaluronidase from *Staphylococcus aureus*.** $IC_{50}$ and standard error was determined using a four-parameter logistic curve function in SigmaPlot (v 13).

Compound **5** was evaluated and found to possess no antimicrobial activity against *Staphylococcus aureus* (MRSA, USA300 LAC strain AH1263) (70, 71). Therefore, compound **5** would not inhibit the growth of bacteria at the concentration required to inhibit spreading.

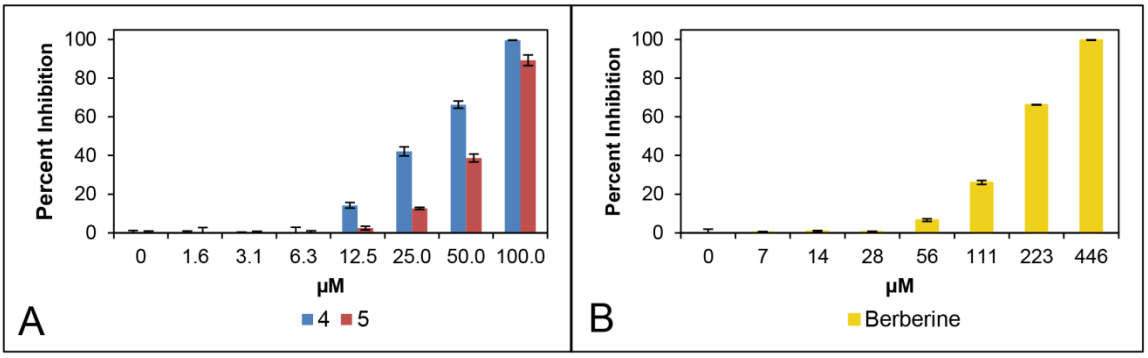


**Figure 11. Dose Response Curves of Compounds 4 and 5 Against *Staphylococcus aureus* (Panel A).** Berberine served as the positive control (Panel B), resulting in a MIC of 446 µM, consistent with literature reports (72).

Presumably, the carboxylic acid moiety found in compounds **4** and **5** is required for activity against *Streptococcus agalactiae* hyaluronidase, as compounds **3** and **7-9** did not have inhibitory activity and did not have a carboxylic acid group. Furthermore, the

activity of compound **5** against *Staphylococcus aureus* hyaluronidase may be due in part to the increased flexibility of the molecule, as the center ring is opened and rotatable, while the other tested compounds have a closed center ring. Further studies could include the preparation of derivatives of compound **5** to find more potent *Staphylococcus aureus* hyaluronidase inhibitors and to investigate structure/function relationships.

The discovery of leotiomycene A and B (**4** and **5**) as inhibitors of bacterial hyaluronidases opens the door for the discovery of more inhibitors. Compounds **4** and **5** show potent anti-hyaluronidase activity while exhibiting no antimicrobial activity against *Streptococcus agalactiae*, and could therefore serve as a launching point for *in vivo* studies, as they are the most potent inhibitors to date. Current reports state that *Streptococcus agalactiae* infections are routinely treated by penicillin, and that some isolates have been shown to be resistant to tetracycline, erythromycin, ciprofloxacin, chloramphenicol and clindamycin. This is problematic for patients that have penicillin allergies, as clindamycin is often used as a next-in-line treatment. It is possible that early development of alternative, anti-virulence-based therapeutics could prevent resistance from occurring as rapidly, which could be of use for patients with allergies that rely on the use of non-penicillin-based therapeutics (73).

Compound **5** has no *in vitro* antimicrobial activity against *Staphylococcus aureus* and is therefore an ideal candidate for further evaluation as an alternative therapeutic treatment. The basis of the anti-virulence approach is to limit pathogenicity and proliferation so that the host immune system can clear the infection on its own or in combination with existing antibiotics. There is evidence to support the phenomenon

where combination treatments are less likely to promote resistance development (74). Dual activity of compounds within one biological system indicate a lack of specificity which is required for relevant pharmaceutical drug leads (75). The activity of compound **5** against *Staphylococcus aureus* hyaluronidase serves as a starting point for synthetic derivatization and the pursuit of hyaluronidase inhibitors from fungal sources. It is well known that fungi and bacteria communicate and compete for resources in the environment using small molecules (76). This is apparent in the case of compounds **4**-**6**, which were isolated from fungi and possess anti-virulence activity against *Staphylococcus aureus* (58, 59, 69). Further support was shown here, with the anti-virulence activity of bacterial spreading being inhibited by compounds **4** and **5**. As many fungal species have yet to be investigated for their biological activity, they serve as a potentially rich source of hyaluronidase inhibitors. In conclusion, two new and potent inhibitors of *Streptococcus agalactiae* hyaluronidase have been identified and warrant further *in vivo* investigation. Also, the first inhibitor of *Staphylococcus aureus* hyaluronidase with modest potency has been identified, which can serve as a positive control for future studies as well as a starting place for structure-function and *in vivo* studies. As these compounds originated from fungi, future efforts to find anti-virulence compounds from fungi are justified.

## Materials and Methods

### Culture media and test compounds

Müeller Hinton broth, defibrinated sheep blood, laked horse blood, levofloxacin, berberine, ascorbic acid 6-palmitate (**1**) and PBS were provided by Sigma Aldrich, (St. Louis, MO). Agar and solvents were purchased from Fisher Scientific (Pittsburgh, PA).

### Bacterial strains

*Streptococcus agalactiae* (COH1) is a highly virulent serotype III clinical isolate (77). *Staphylococcus aureus* (AH1263) is a USA300 community-acquired MRSA strain with induced erythromycin susceptibility (70, 71).

### Purification of *S. aureus* hyaluronidase

The details of this purification can be found in Britton et al., 2015.

### Hyaluronidase assay procedure

This assay was performed as described in Britton et al., 2015, with some minor modifications. A stock solution of hyaluronic acid sodium salt from *Streptococcus equi* (Sigma, St. Louis, MO) was prepared at 5 mg/mL with PBS (EMD Millipore, Temecula, CA). An aliquot from the reaction mixture was diluted 20-fold with acetonitrile (Fisher Scientific, Pittsburgh, PA) containing 0.1% formic acid (Fisher Scientific, Pittsburgh, PA) in order to quench the reaction and prepare for LC-MS analysis. The diluted reaction was then submitted to ultraperformance liquid chromatography-mass spectrometry (UPLC-MS) analysis via a Waters Acquity UPLC with an Acquity UPLC column (BEH HILIC, 1.7 μm, 2.1 x 50 mm, Waters Corporation, Milford, MA) and a Thermo Q-Exactive Plus orbitrap mass spectrometer with electrospray ionization source (Thermo

Fisher Scientific, MA, USA). Ascorbic acid 6-palmitate (Sigma, St. Louis, MO) served as the positive control for experiments using hyaluronidase from *Streptococcus agalactiae*.

**Antimicrobial assay procedure**

MICs were determined as recommended by the Clinical Laboratory Standards Institute against clinically relevant strains of *Streptococcus agalactiae* (serotype III clinical isolate COH1) (77) and methicillin-resistant *Staphylococcus aureus* (MRSA, USA 300 LAC strain AH1263) (78). A single colony inoculum was grown to log phase in Müeller Hinton broth and adjusted to a final assay concentration of $1.0 \times 10^5$ CFU/mL based upon absorbance at 600 nm ($OD_{600}$). The negative control (vehicle) consisted of 2% DMSO in broth, and the known antimicrobial compounds levofloxacin and berberine served as the positive controls for *Streptococcus agalactiae* and *Staphylococcus aureus*, respectively (79, 80). Wells were prepared in triplicate with all treatments and controls, and duplicate plates were made without bacteria for background absorbance subtraction. $OD_{600}$ was read after 24 h for *Streptococcus agalactiae* and 18 h for *Staphylococcus aureus*, both at 37 °C using a Synergy H1 microplate reader (Biotek, Winooski, VT, USA). The MIC was defined as the concentration at which no statistically significant difference was observed between the negative control and treated sample.

**LC-MS analysis**

All solvents used were Optima LC-MS grade (Fisher Scientific, Pittsburgh, PA). Diluted reaction mixtures (7 µL) were eluted from the column using the chromatographic method found in Britton et al., 2015. The Thermo Q-Exactive Plus orbitrap mass spectrometer was operated in the positive polarity with the following settings: spray

voltage, 3700 V; capillary temperature, 350°C; sheath gas, 25; auxiliary gas, 5; and S lens level, 50.

Percent inhibitions were based on a comparison of integrated peak areas associated with the protonated *m/z* of the disaccharide units. Standard error was calculated for each triplicate set of analyses. $IC_{50}$ values were calculated using a four parameter logistic standard curve analysis function in SigmaPlot (v 13).

# CHAPTER IV

# SECONDARY METABOLITES FROM THE LEAVES OF THE MEDICINAL PLANT GOLDENSEAL (HYDRASTIS CANADENSIS)

This chapter has been published in the journal Phytochemistry Letters and is presented in that style. Leyte-Lugo, M.[1], Britton, E.R.[1], Foil, D.H., Brown, A.R., Todd, D.A., Rivera-Chávez, J., Oberlies, N.H., Cech, N.B. Phytochem. Lett. 2017, 20, 54-60. [1]Authors contributed equally to this publication.

Britton, E.R. ran and collected all mass spectrometric fragmentation data, collected $\lambda_{max}$ data, guided biological assay data collections, wrote the discussion section and experimental section related to fragmentation data, and edited the introduction and remaining experimental section. Leyte-Lugo, M. isolated all of the compounds presented here and performed structure elucidation to confirm their identities, and wrote the introduction, experimental and results sections. Foil, D.H. performed the afflux pump assay and prepared the figure used to present the data, and wrote the experimental section for the efflux pump assay. Brown A.R. and Todd D.A. provided technical assistance and advice. Rivera-Chávez, J. assisted in structure elucidation. Oberlies, N.H. assisted in the preparation of NMR data and made minor edits on the manuscript. Cech, N.B. assisted in the development of the research project and provided edits and suggestions throughout manuscript preparation.

## Introduction

The medicinal plant *Hydrastis canadensis* L. (Ranunculaceae) has a long history of use for the treatment of infections. Native Americans, particularly the Cherokee, used goldenseal roots to treat skin and eye infections, while other populations have used goldenseal tonics to treat gastrointestinal irritation (81). *H. canadensis* roots have been extensively profiled (6, 82, 83), although only a few reports have described the

composition of *H. canadensis* leaves (9, 84). *H. canadensis* has been of recent interest due to its ability to inhibit the growth of pathogenic bacteria, including *Staphylococcus aureus* (72). This activity was originally attributed to the antimicrobial alkaloid berberine and to other alkaloids that the plant contains (85-87). Recently, it has been shown that the activity of *H. canadensis* leaves is more complex. Three flavonoids, sideroxylin, 6-desmethyl sideroxylin and 8-desmethyl sideroxylin (9) were shown to synergistically enhance the antimicrobial activity of goldenseal alkaloids. These flavonoids act as bacterial efflux pump inhibitors, facilitating accumulation of berberine within bacterial cells and thereby reducing the necessary quantity of berberine (or other alkaloids) to achieve antimicrobial activity (9).

Botanicals are chemically complex and contain many compounds that may possess diverse structures and biological activities. On the basis of the previously reported interesting biological activity of *H. canadensis* leaves, we endeavored to conduct more in-depth chemical profiling of this botanical. With these studies, we sought to identify efflux pump inhibitors from *H. canadensis*, and to generate a more comprehensive profile of chemical compounds in this botanical than has previously been published.

## Results and Discussion

### Structures of isolated compounds

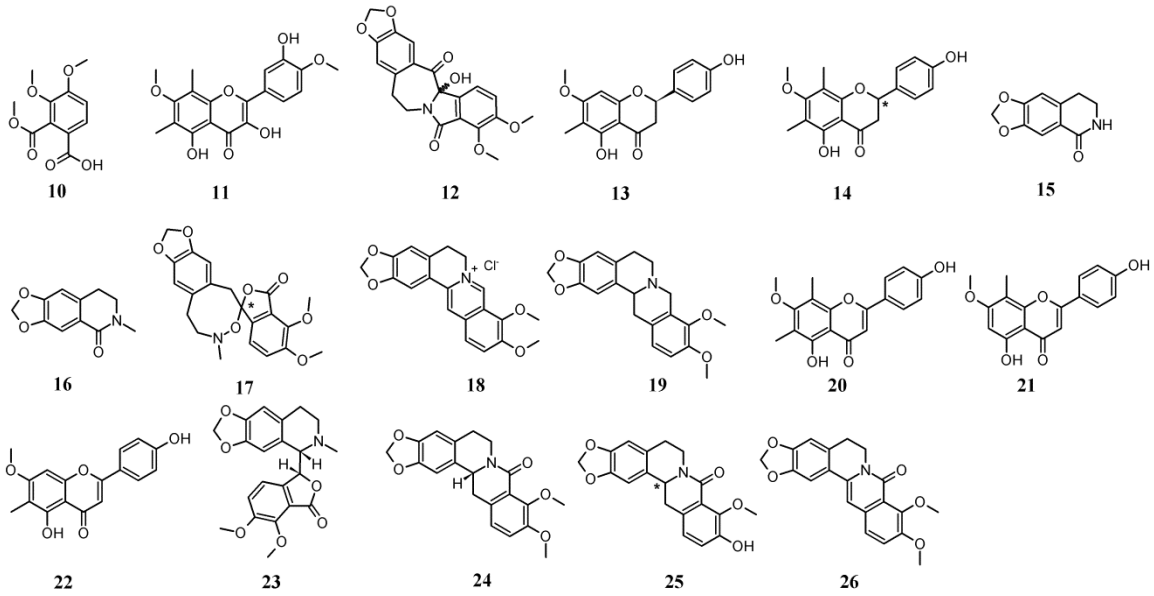


**Figure 12. Structures of Compounds, Some of Which Are Reported For The First Time In This Report As Constituents of Goldenseal (*Hydrastis canadensis*).** The configuration at locations with asterisks are unknown.

Investigation of *Hydrastis canadensis* leaves led to isolation of two new compounds, 3,4-dimethoxy-2-(methoxycarbonyl)benzoic acid (**10**) and 3,5,3´-trihydroxy-7,4´-dimethoxy-6,8-*C*-dimethyl-flavone (**11**), together with six additional compounds (**12-17**) that are known but new to *Hydrastis canadensis* (Figure 12). (±)-Chilenine (**12**), an isoindolobenzazepine alkaloid, was previously reported from *Berberis enpetrifolia* (88); flavonones (2*R*)-5,4´-dihydroxy-6-*C*-methyl-7-methoxy-flavanone (**13**) and 5,4´-dihydroxy-6,8-di-*C*-methyl-7-methoxy-flavanone (**14**) were isolated from leaf wax of *Callistemon coccineus* (89); and the isoquinolone derivatives noroxyhydrastinine (**15**) and oxyhydrastinine (**16**) were obtained from *Thalictrum minus* and *Hypecoum erectum*,

respectively (90, 91). Compound **17**, 4´,5´-dimethoxy-4-methyl-3´-oxo-(1,2,5,6-tetrahydro-4*H*-1,3-dioxolo-[4´,5´:4,5]-benzo[1,2-*e*]-1,2-oxazocin)-2-spiro-1´-phtalan, was reported previously as a product of ß-hydrastine-N-oxide under reflux conditions (92). Given that ß-hydrastine is an abundant constituent of *H. canadensis* (83), it is possible that compound **17** is an isolation artifact and not a constituent of *H. canadensis*. Additionally, nine compounds known to be constituents of *H. canadensis* were also isolated. These include berberine (**18**) (93), (-)-canadine (**19**) (94), sideroxylin (**20**), 6-desmethyl-sideroxylin (**21**), 8-desmethyl-sideroxylin (**22**) (9), ß-hydrastine (**23**) (95), (-)-8-oxocanadine (**24**), 8-oxotetrahydrothalifendine (**25**) (96), and oxyberberine (**26**) (97). The structures of these known compounds were determined by comparing their spectroscopic data with those reported in the literature.

Compound **10** was obtained as white amorphous powder. High resolving power electrospray ionization mass spectrometry (HRESIMS) analysis indicated an ion peak at *m*/*z* 241.0702 $[M+H]^+$ (calcd for $C_{11}H_{13}O_6^+$, 241.0707), suggesting six degrees of unsaturation. The NMR spectral data (Table 3) allowed the assignment of two aromatic protons ($\delta_H$ = 6.98 and 7.87) and three methoxy groups ($\delta_H$ = 3.87, 3.94 and 3.95). The HMBC analysis allowed correlation of two of the methoxy groups, ($\delta_H$ = 3.87 and 3.95) with carbon C-3 and C-4 ($\delta_C$ = 145.9 and 157.4), respectively. Additionally, the correlation between H-5 ($\delta_H$ = 6.98) and the resonance at $\delta_C$ = 145.9 (C-3), and between H-6 ($\delta_H$ = 7.87) with $\delta_C$ = 157.4 (C-4) supported the placement of the methoxy groups. The HMBC correlations between H-5 ($\delta_H$ = 6.98) and $\delta_C$ = 118.7, and H-6 ($\delta_H$ = 7.87) with $\delta_C$ = 131.8 supported the assignment of the carboxylic group at C-1 and the

methoxycarbonyl group at C-2 (Figure 13). Therefore, the structure of **1** was established as 3,4-dimethoxy-2-(methoxycarbonyl)benzoic acid.

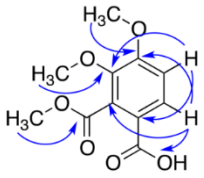


**Figure 13. HMBC Correlations of 10.**

Compound **11**, obtained as a yellow amorphous powder, showed in HRESIMS an ion peak at *m/z* 359.1129 $[M+H]^+$ (calcd for $C_{19}H_{19}O_7$, 359.1125). The UV maxima absorption bands at $\lambda_{max}$ 377, 346 and 258 nm were suggestive of a flavone skeleton, given that the absorbance maxima of flavonols are generally at longer wavelengths (350 –385 nm) (98). The $^1$H-NMR data (Table 4) indicated the presence of two aromatic methoxy groups ($\delta_H$ = 3.80 and 4.00), two C-methyls ($\delta_H$ = 2.41 and 2.23), and three aromatic protons ($\delta_H$ = 7.87, 7.82 and 7.00). Analysis of the $^{13}$C-NMR spectrum (Table 4) showed the presence of a α,β-unsaturated carbonyl ($\delta_C$ = 175.9) and a signal at $\delta_C$ = 136.2, which together with the proton signals of the aromatic rings corresponding to a flavonol skeleton. HMBC correlations of 7-$OCH_3$ ($\delta_H$ = 3.80), 6-$CH_3$ ($\delta_H$ = 2.23) and 8-$CH_3$ ($\delta_H$ = 2.41) methyl protons with C-7 ($\delta_C$ = 163.0) support the position of the substituents in ring A (Figure 14). In addition, the methoxy and hydroxy group in the B ring were assigned based on the correlation between 4´-$OCH_3$ ($\delta_H$ = 4.00) with the C-4´ ($\delta_C$ = 148.4), and the correlations between 5´-H ($\delta_H$ = 7.00) with C-1´ ($\delta_C$ = 124.6) and C-3´ ($\delta_C$ = 145.8) in the HMBC spectrum. Additionally, the HMBC correlations between

2´-H ($\delta_C$ = 7.82) and 6´-H ($\delta_H$ = 7.87) with C-2 ($\delta_C$ = 145.8) supported the connectivity of ring B to C-2 (ring C) (Figure S11). On the basis of this evidence, the compound was determined to be 3,5,3´-trihydroxy-7,4´-dimethoxy-6,8-*C*-dimethyl-flavone.

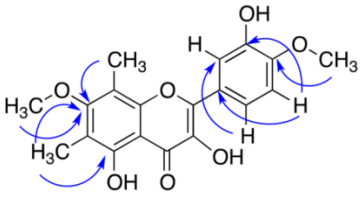


**Figure 14. HMBC Correlations of 11.**

**Table 3. $^1$H (400 MHz) and $^{13}$C (100 MHz) NMR Spectroscopic Data[a] for *3,4-dimethoxy-2-(methoxycarbonyl)benzoic acid* (10).**

| Position | $\delta_C$ | $\delta_H$, m (*J* in Hz) |
|---|---|---|
| 1 | 118.7 | |
| 2 | 131.8 | |
| 3 | 145.9 | |
| 4 | 157.4 | |
| 5 | 112.2 | 6.98, d (8.8) |
| 6 | 128.4 | 7.87, d (8.8) |
| 1a | 168.6 | |
| 2a | 167.5 | |
| 3-$OCH_3$ | 61.9 | 3.87, s |
| 4-$OCH_3$ | 56.3 | 3.95, s |
| 2a-$OCH_3$ | 53.0 | 3.94, s |

[a] $^1$H and $^{13}$C chemical shifts with reference to $CDCl_3$ ($\delta_H$ = 7.26 ppm) and $CDCl_3$ ($\delta_C$ = 77.16 ppm), respectively.
[b] HMBC correlations are from the proton stated to the indicated carbon.

**Table 4. $^{1}$H (400 MHz) and $^{13}$C (100 MHz) NMR Spectroscopic Data[a] for *3,5,3´-trihydroxy-7,4´-dimethoxy-6,8-C-dimethyl-flavone* (2).**

| Position | $\delta_C$ | $\delta_H$, m (*J* in Hz) | HMBC[b] |
|---|---|---|---|
| 2 | 146.8 | | |
| 3 | 133.9 | | |
| 4 | 174.3 | | |
| 5 | 155.9 | | |
| 6 | 113.4 | | |
| 7 | 163.9[c] | | |
| 8 | 109.7 | | |
| 9 | 151.6 | | |
| 10 | 106.8 | | |
| 1´ | 124.5 | | |
| 2´ | 113.7 | 7.82, d (2.4) | |
| 3´ | 145.7 | | |
| 4´ | 148.4 | | |
| 5´ | 110.6 | 7.00, d (8.4) | C-1´, C-3´ |
| 6´ | 121.1 | 7.88, dd (8.4, 2.4) | C-2´ |
| 6-$CH_3$ | 8.4 | 2.21, s | C-5, C-6, C-7 |
| 8-$CH_3$ | 8.7 | 2.39, s | C-7, C-8, C-9 |
| 7-$OCH_3$ | 60.8 | 3.79, s | C-7 |
| 4´-$OCH_3$ | 56.2 | 3.98, s | C-4´ |
| 3-OH | | 11.81 | |
| 3´-OH | | 5.73 | |
| 5-OH | | 6.66 | |

[a] $^{1}$H and $^{13}$C chemical shifts with reference to $CDCl_3$ ($\delta_H$ = 7.26 ppm) and $CDCl_3$ ($\delta_C$ = 77.16 ppm), respectively.
[b] HMBC correlations are from the proton stated to the indicated carbon.
[c] obtained from HMBC

Reisolation of known compounds from botanical extracts is a common problem when seeking to identify novel compounds from botanicals such as *H. canadensis*. To facilitate future identification of compounds **10**–**26** in botanical mixtures, tandem high resolving power electrospray ionization mass spectrometry (HRESIMS-MS) was employed to collect fragmentation spectra of all seventeen compounds in both the positive ion mode (Table S1) and the negative ion mode (Table S2). Notably, these fragmentation spectra were collected with high mass accuracy (<10 ppm), enabling the confirmation of molecular formulae of many of the fragments. An example of such a high resolution fragmentation spectrum is provided in Figure 4 for **11**. A fragmentation

spectrum of berberine (**18**), the most abundant alkaloid present in goldenseal (83) can be found as Supporting Information (Figure S27). High mass accuracy measurements of fragmentation data enable assignment of molecular formulae not just for the intact molecule, but also for its fragments (Figure 15). These data were uploaded into the Global Natural Product Social molecular networking library to facilitate identification of these compounds as well as structural analogues in other botanicals (28).

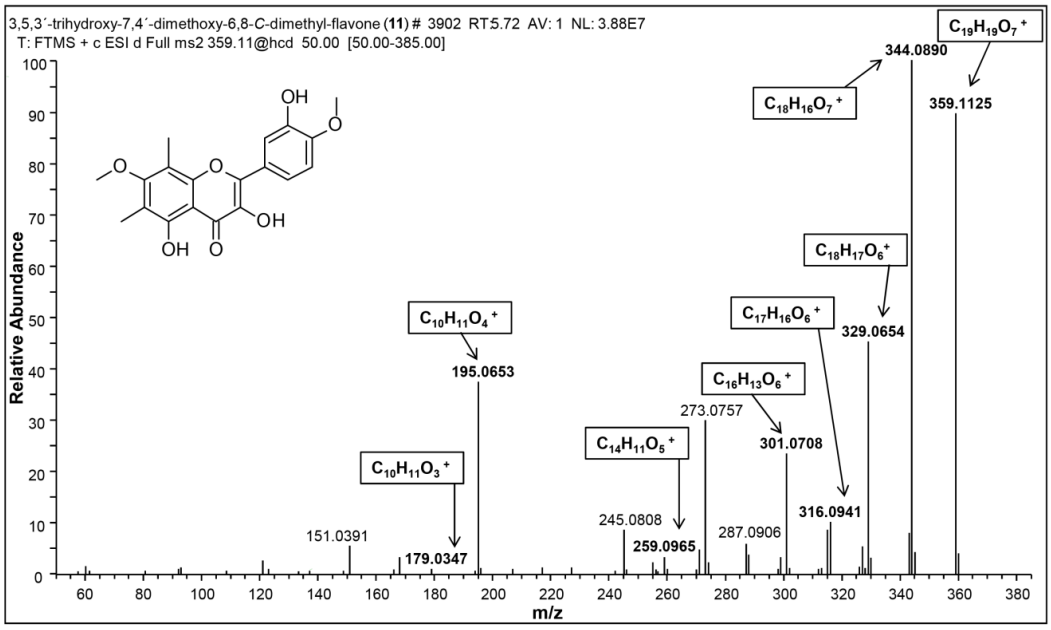


**Figure 15. Accurate Mass Fragmentation Spectrum of 3,5,3´-trihydroxy-7,4´-dimethoxy-6,8-*C*-dimethyl-flavone (11) In The Positive Polarity.** Fragments and molecular formulas were predicted using ACD MS fragmenter (Advanced Chemistry Development, Inc. Toronto, Canada) and compared to experimental data. Bold ions had a mass error within 10 ppm of the associated molecular formula.

## Efflux pump inhibitory activity of isolated compounds

The two new compounds isolated as part of this study [3,4-dimethoxy-2-(methoxycarbonyl)benzoic acid (**10**) and 3,5,3´-trihydroxy-7,4´-dimethoxy-6,8-*C*-dimethyl-flavone (**11**)], as well as the compounds **13** and **25** were tested for biological

activity. Specifically, a mass spectrometry based assay was employed to evaluate the ability of these compounds to inhibit efflux of an efflux pump substrate (ethidium bromide) from *Staphylococcus aureus* cells (30). The rationale for evaluating efflux pump inhibitory activity is that drug efflux constitutes a major form of antibiotic resistance in bacteria (99). Thus, compounds that prevent efflux of toxins from cells have the potential of contributing to antimicrobial activity. Efflux inhibitory activity against *Staphylococcus aureus* is particularly relevant given that this pathogen is responsible for approximately 50% of all skin infections, and *Hydrastis canadensis* is traditionally used in the treatment of such infections (100).

Compound **2** demonstrated moderate inhibitory activity of efflux from *Staphylococcus aureus* with an $IC_{50}$ value of 180 ± 6 μM. Compounds **10**, **13** and **25** were inactive. Figure 16 shows the raw experimental data evaluating the efflux pump inhibitory activities of compounds **10**, **11**, and the positive control, carbonyl cyanide *m*-chloro phenylhydrazone (CCCP), which had an $IC_{50}$ of 270 ± 50 μM. The data shown are relative quantities (as measured by mass spectrometric peak area) of ethidium ion in the spent bacterial media after exposure to an increasing amount of the test compound or control. As demonstrated for both CCCP and **11**, when efflux is blocked, the quantity of ethidium present in the media decreases (Figure 16). Ethidium concentration remains high regardless of concentration for the compound that does not possess efflux inhibitory activity (Compounds **10**, **13** & **25**).

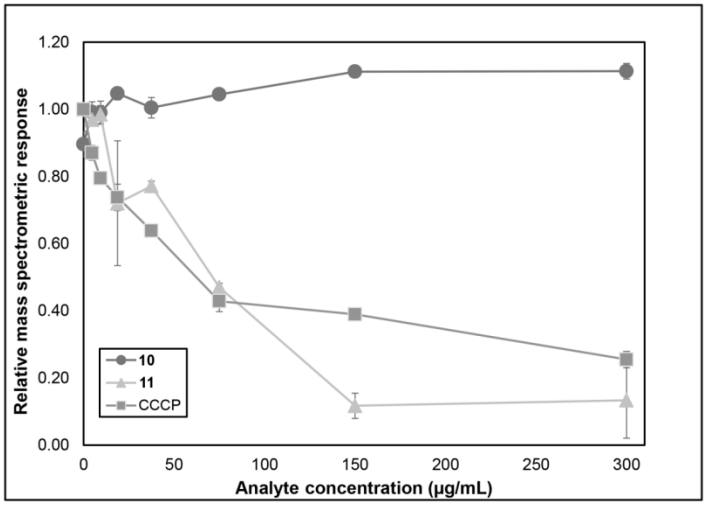


**Figure 16. Efflux Pump Inhibition Assay Data for 3,4-dimethoxy-2-(methoxycarbonyl) benzoic acid (10) and 3,5,30 -trihydroxy-7,40 -dimethoxy-6,8-C-dimethyl-flavone (11).** The positive control for this assay is carbonyl cyanide m-chloro-phenylhydrazone (CCCP), a compound that inhibits efflux by collapsing the proton motive force across the cell membrane (101). Each data point is the mean of triplicate measurements from separate bacterial cultures (biological replicates) and error bars represent standard error of the mean.

## Experimental

### General experimental procedures

Optical rotations at the sodium D-line wavelength of pure compounds were measured with a Rudolph Research Autopol (II) Polarimeter. 1D and 2D NMR spectra were recorded using a JEOL ECS-400 NMR spectrometer equipped with a high sensitivity JEOL Royal probe operating at 400 MHz for $^{1}$H and 100 MHz for $^{13}$C, or an Agilent 700 MHz NMR spectrometer (Agilent Technologies, Inc., Santa Clara, CA, USA) equipped with a cryoprobe, operating at 700 MHz for $^{1}$H and 175 MHz for $^{13}$C. Chemical shifts are reported as δ values (ppm), and coupling constants (*J*) were measured in Hz. HRESIMS was performed on a Thermo LTQ Orbitrap XL mass spectrometer equipped with an electrospray ionization source. HPLC was carried out using a Varian

ProStar HPLC system equipped with ProStar 210 pumps and a ProStar 335 photodiode array detector (PDA), with data collected and analyzed using Galaxie Chromatography Workstation software (version 1.9.3.2). For preparative HPLC, a Phenomenex Gemini-NX $C_{18}$ Column (5 µm; 250 × 21.2 mm) was used at a 21 mL/min flow rate. Flash chromatography was performed on a Teledyne ISCO CombiFlash®$R_f$ using 80 g or 120 g RediSep® RF Silica Column (35 – 70 µm particle size) and 12 g RediSep® $R_f$ Gold HP Silica Columns (20 – 40 µm particle size, Teledyne ISCO, Lincoln, NE, USA); and monitored by UV and evaporative light-scattering detectors. UV spectra were measured with a ProStar 335 photodiode array UV detector (PDA) and the reported λmax values were collected from the spectra for relevant compounds eluting from the HPLC. All other reagents and solvents were obtained from Fisher Scientific and were used without further purification.

**Plant material**

*Hydrastis canadensis* L. (Ranunculaceae) was collected in Hendersonville, North Carolina (NC, N 3524.2770, W 08220.9930, 702.4 m elevation), in July 2013. The plants were cultivated in their native environment, a hardwood forest understory. A voucher specimen (NCU583414) was deposited in the University of North Carolina Herbarium, Chapel Hill, NC and the identity was verified by herbarium director Dr. Alan S. Weakley.

**Extraction and isolation**

The isolation scheme is provided as Supporting Information (Figure S2). Batches of dried *H. canadensis* plant were pulverized into fine powder using a commercial coffee grinder (Kitchen Aid). *H. canadensis* powder was percolated in MeOH overnight, and the

MeOH extract was concentrated *in vacuo* and subjected to liquid-liquid partition, as described previously (9). This concentrated extract was defatted by partitioning between 10% aqueous MeOH and hexane (1:1), and the aqueous MeOH fraction was partitioned further between EtOAc:MeOH:$H_2O$ (4:1:5). The organic layer was washed with 1% saline solution to remove tannins.

The first stage of normal-phase flash chromatography (120 g silica gel column) was conducted with a Hex/$CHCl_3$/MeOH gradient, yielding 8 primary fractions (FI-FVIII). Fraction FII, FIII and FIV were subjected to a second stage of normal-phase flash chromatography (80 g silica gel column) with a Hex/EtOAc/MeOH gradient to give 5 (FII1-FII5), 3 (FIII1-FIII3) and 6 (FIV1-FIV6) subfractions, respectively.

The compounds were purified using reversed-phase preparative HPLC with a Phenomenex Gemini-NX $C_{18}$ column at a 21 mL/min flow rate. Fraction FII2 (32.5 mg) (eluents A: $H_2O$ 0.1% formic acid, B: $CH_3CN$, gradient: B 45% at time 0, B 75% at time 20 min, B 100% at time 25 min) yielded the compounds (2*R*)-5,4´-dihydroxy-6-*C*-methyl-7-methoxy-flavanone (**13**; 1.5 mg), 5,4´-dihydroxy-6,8-di-*C*-methyl-7-methoxy-flavanone (**14**; 0.7 mg), and *3,5,3´-trihydroxy-7,4´-dimethoxy-6,8-C-dimethyl-flavone* (**11**; 0.6 mg).

Fractions FII3 (30.1 mg), FII4 (7.3 mg) and FIII1 (26.9 mg) were purified (eluents A: $H_2O$ 0.1% formic acid, B: $CH_3CN$, gradient: B 35% at time 0, B 90% at time 27 min, B 100% at time 30 min) to obtain oxyhydrastinine (**16**; 2.0 mg), chilenine (**12**; 0.8 mg) for the first fraction, noroxyhydrastinine (**15**; 0.9 mg) for the second fraction, and (2*R*)-5,4´-dihydroxy-6-*C*-methyl-7-methoxy-flavanone (**13**; 0.5 mg) for the last fraction.

Fraction FIV3 (96.3 mg) (eluents A: $H_2O$ 0.1% formic acid, B: $CH_3CN$, gradient: B 30% at time 0, B 90% at time 20 min, B 100% at time 22 min) and fraction FIV5 (42.3 mg) (eluents A: $H_2O$ 0.1% formic acid, B: $CH_3CN$, gradient: B 30% at time 0, B 65% at time 20 min, B 100% at time 22 min) yielded chilenine (**12**; 1.0 mg) and 3,4-dimethoxy-2-(methoxycarbonyl) benzoic acid (**10**; 1.2 mg), respectively.

*3,4-dimethoxy-2-(methoxycarbonyl)benzoic acid* (**10**): white powder; UV $\lambda_{max}$ 208 and 259 nm; $^1$H (400 MHz) and $^{13}$C NMR (100 MHz) data see Table 1. HRESIMS *m*/*z* 241.07021 $[M+H]^+$ (calcd for $C_{11}H_{13}O_6$ 241.0707).

*3,5,3´-trihydroxy-7,4´-dimethoxy-6,8-C-dimethyl-flavone* (**11**): yellow powder; UV $\lambda_{max}$ 217, 258, 346 and 377 nm; $^1$H (700 MHz) and $^{13}$C NMR (175 MHz) data see Table 2. HRESIMS *m*/*z* 359.11287 $[M+H]^+$ (calcd for $C_{19}H_{19}O_7$ 359.1125).

*(±)-chilenine* (**12**): white powder; $[\alpha]_D^{25}$ = 0.0 (c 0.22, MeOH); UV $\lambda_{max}$ 215 and 318 nm; $^1$H-NMR (400 MHz, $CDCl_3$) $\delta$: 7.36 (1H, d, *J* = 8.4 Hz, H-11), 7.05 (1H, d, *J* = 8.4 Hz, H-12), 6.71 (1H, s, H-1), 6.66 (1H, s, H-4), 5.95 (2H, dd, *J* = 7.2, 1.2 Hz, $OCH_2O$), 4.26 (1H, m, H-6), 3.99 (3H, s, $OCH_3$-9), 3.87 (3H, s, $OCH_3$-10), 3.56 (1H, m, H-5), 3.30 (1H, m, H-6), 3.11 (1H, m, H-5); $^{13}$C-NMR (100 MHz, $CDCl_3$) $\delta$: 199.8 (C-14), 166.7 (C-8), 154.5 (C-10), 151.6 (C-3), 147.1 (C-2), 146.7 (C-9), 133.7 (C-4a), 131.7 (C-12a), 130.7 (C-14a), 124.1 (C-9a), 120.6 (C-12), 116.3 (C-11), 109.4 (C-4), 109.2 (C-1), 101.9 ($OCH_2O$), 94.9 (C-13), 62.6 ($OCH_3$-9), 56.6 ($OCH_3$-10), 38.9 (C-6), 30.7 (C-5); HRESIMS *m*/*z* 384.10751 $[M+H]^+$ (calcd for $C_{20}H_{18}NO_7$ 384.1078).

*(2R)-5,4´-dihydroxy-6-C-methyl-7-methoxy-flavanone* (**13**): yellow oil; $[\alpha]_D^{25}$ = -7.33 (c 0.3, MeOH); UV $\lambda_{max}$ 216, 291 and 338 nm; $^1$H-NMR (400 MHz, $CDCl_3$) $\delta$: 12.1

(OH-5), 7.35 (2H, d, *J* = 8.4 Hz, H-2´ and H-6´), 6.89 (1H, d, *J* = 8.4 Hz, H-3´ and H-5´), 6.07 (1H, s, H-8), 5.35 (1H, dd, *J* = 13.2, 2.8, H-2), 3.83 (3H, s, $OCH_3$-7), 3.09 (1H, dd, *J* = 17.2, 13.2 Hz, H-3), 2.77 (1H, dd, *J* = 17.2, 2.8 Hz, H-3), 2.01 (1H, s, $CH_3$-6); $^{13}$C-NMR (100 MHz, $CDCl_3$) *δ*: 196.2 (C-4), 165.8 (C-7), 161.3 (C-9), 160.5 (C-5), 156.2 (C-4´), 130.9 (C-1´), 128.1 (C-2´ and C-6´), 115.8 (C-3´ and C-5´), 106.1 (C-6), 102.9 (C-10), 90.9 (C-8), 79.2 (C-2), 55.9 ($OCH_3$-7), 43.5 (C-3), 7.0 ($CH_3$-6); HRESIMS *m*/*z* 301.10709 $[M+H]^+$ (calcd for $C_{17}H_{17}O_5$ 301.10780).

*5,4´-dihydroxy-6,8-di-C-methyl-7-methoxy-flavanone* (**14**): yellow oil; $[\alpha]_D^{25}$ = -6.86 (c 0.12, MeOH); UV $\lambda_{max}$ 192, 222, 282 and 361 nm; $^1$H-NMR (400 MHz, $CDCl_3$) *δ*: 12.0 (OH-5), 7.35 (2H, d, *J* = 8.4 Hz, H-2´ and H-6´), 6.89 (1H, d, *J* = 8.4 Hz, H-3´ and H-5´), 5.34 (1H, dd, *J* = 12.8, 2.8 Hz, H-2), 3.74 (3H, s, $OCH_3$-7), 3.06 (1H, dd, *J* = 17.2, 12.8 Hz, H-3), 2.83 (1H, dd, *J* = 17.2, 2.8 Hz, H-3), 2.10 (3H, s, $CH_3$-6), 2.07 (3H, s, $CH_3$-8); $^{13}$C-NMR (100 MHz, $CDCl_3$) *δ*: 197.7 (C-4), 162.5 (C-7), 160.2 (C-5), 158.1 (C-4´), 156.4 (C-9), 131.5 (C-1´), 127.8 (C-2´ and C-6´), 119.5 (C-8),116.2 (C-3´ and C-5´), 108.2 (C-6), 104.0 (C-10), 79.7 (C-2), 63.5 ($OCH_3$-7), 40.7 (C-3), 9.9 ($CH_3$-8), 9.3 ($CH_3$-6); HRESIMS *m*/*z* 315.12292 $[M+H]^+$ (calcd for $C_{18}H_{19}O_5$ 315.1227).

*Noroxyhydrastinine* (**15**): yellow powder; UV $\lambda_{max}$ 222, 261 and 306 nm; $^1$H-NMR (400 MHz, $CDCl_3$) *δ*: 7.50 (1H, s, H-8), 6.66 (1H, s, H-5), 6.01 (2H, s, $OCH_2O$), 3.53 (2H, t, *J* = 6.8, 6.4 Hz, H-3), 2.91 (1H, t, *J* = 6.8, 6.4 Hz, H-4); $^{13}$C-NMR (100 MHz, $CDCl_3$) *δ*: 166.5 (C-1), 151.5 (C-6), 147.2 (C-7), 135.0 (C-5a), 121.5 (C-8a), 108.0 (C-8), 107.5 (C-5), 101.8 ($OCH_2O$), 40.4 (C-3), 28.3 (C-4); HRESIMS *m*/*z* 192.06526 $[M+H]^+$ (calcd for $C_{10}H_{10}NO_3$ 192.0655).

*Oxyhydrastinine* (**16**): yellow pale powder; UV $\lambda_{max}$ 222, 264 and 304 nm; $^{1}$H-NMR (400 MHz, $CDCl_3$) $\delta$: 7.54 (1H, s, H-8), 6.61 (1H, s, H-5), 5.99 (2H, s, $OCH_2O$), 3.51 (2H, t, $J$ = 6.8, 6.8 Hz, H-3), 2.90 (1H, t, $J$ = 6.8, 6.8 Hz, H-4), 3.13 (3H, s, N-$CH_3$); $^{13}$C-NMR (100 MHz, $CDCl_3$) $\delta$: 164.7 (C-1), 150.4 (C-6), 146.9 (C-7), 133.6 (C-5a), 123.5 (C-8a), 108.3 (C-8), 107.0 (C-5), 101.6 ($OCH_2O$), 48.3 (C-3), 35.3 (N-$CH_3$), 28.1 (C-4); HRESIMS *m*/*z* 206.08127 $[M+H]^+$ (calcd for $C_{11}H_{12}NO_3$ 206.08117).

*4´,5´-dimethoxy-4-methyl-3´-oxo-(1,2,5,6-tetrahydro-4H-1,3-dioxolo-[4´,5´:4,5]-benzo[1,2-e]-1,2-oxazocin)-2-spiro-1´-phtalan* (**17**): yellow pale powder; $[\alpha]_D^{25}$ = + 4.8 (c 0.17, MeOH); UV $\lambda_{max}$ 218, 245 and 300 nm; $^{1}$H-NMR (400 MHz, $CDCl_3$) $\delta$: 7.04 (2H, d, $J$ = 8.4 Hz, H-6´), 6.75 (1H, s, H-7), 6.36 (1H, s, H-11), 6.33 (1H, d, $J$ = 8.4 Hz, H-7´), 6.00 and 5.94 (2H, s, $OCH_2O$), 4.28 (1H, m, H-1), 4.11 (3H, s, $OCH_3$-4´), 3.88 (3H, s, $OCH_3$-5´), 3.35 (1H, m, H-6), 3.07 (2H, m, H-5), 2.76 (3H, s, N-$CH_3$), 2.70 (2H, m, H-1 and H-6); $^{13}$C-NMR (100 MHz, $CDCl_3$) $\delta$: 165.8 (C-3´), 154.0 (C-5´), 148.1 (C-4´), 146.9 (C-8), 145.4 (C-10), 138.9 (C-7´a), 135.1 (C-7a), 126.9 (C-11a), 119.7 (C-7´), 119.1 (C-4´a), 118.0 (C-6´), 112.6 (C-11), 111.1 (C-7), 109.5 (C-2), 101.2 (C-9), 62.5 ($OCH_3$-4´), 62.1 (C-5), 56.8 ($OCH_3$-5´), 49.2 (N-$CH_3$), 40.6 (C-1), 36.6 (C-6); HRESIMS *m*/*z* 400.1375 $[M+H]^+$ (calcd for $C_{21}H_{22}NO_7$ 400.1391).

**Collection of HRESIMS fragmentation data**

Each of the 17 isolated compounds were suspended in MeOH at either 1 mg/mL or 0.1mg/mL and subjected to ultraperformance liquid chromatography tandem mass spectrometry (UPLC-MS/MS) analysis via a Waters Acquity UPLC with an Acquity UPLC column (BEH $C_{18}$, 1.7 μm, 2.1 x 50 mm), Waters Corporation, Milford, MA)

coupled to a Thermo Q Exactive Plus orbitrap mass spectrometer with heated electrospray ionization (Thermo Fisher Scientific, MA, USA). The compounds were eluted from the column at a flow rate of 0.3 mL/min using a binary solvent system with A consisting of water with 0.1% formic acid additive and solvent B consisting of acetonitrile with 0.1% formic acid additive. The gradient was as follows: 95:5 (A:B) from 0 to 1 min, increasing to 90:10 (A:B) from 1 to 2 min, 80:20 (A:B) from 2 to 3 min, 60:40 (A:B) from 3 to 4 min, 70:30 (A:B) from 4 to 5 min, 0:100 (A:B) from 5 to 6 min and held from 6 to 7 min, 95:5 (A:B) from 7 to 8 min and held from 8 to 9 min. Duplicate analyses of each sample were conducted in both positive and negative polarities using the following settings: spray voltage, 3.7 kV; capillary temperature, 350 °C; sheath gas, 25; auxiliary gas, 5; S-lens RF level, 50. Each compound was chosen for fragmentation via high energy collision-induced dissociation (HCD, normalized collision energy set to 50) from an inclusion list for both polarities. To determine the average mass accuracy of the product ions, the fragmentation spectra of **11** was compared to theoretical fragments produced by ACD MS fragmenter (Advanced Chemistry Development, Inc. Toronto, Canada). The resulting accurate mass of the predicted chemical formulas were matched with experimental data and were within 10 ppm mass error (Figure 15).

**Efflux pump inhibition assay**

Four of the isolated compounds (**10, 11, 13** and **25**) were of sufficient purity (91%, 98%, 95% and 100%, respectively, by LC-UV) and quantity for evaluation via an efflux pump inhibition assay, as previously described (30). The assay was modified from the previously reported method in the chromatographic gradient, in some of the mass

spectrometric conditions, and in the use *Staphyloccocus aureus* strain SA1199 (102). The gradient was as follows: 95:5 (A:B) from 0 to 1 min, increasing to 0:100 (A:B) from 1 to 3.5 min, held from 3.5 to 9.5 min, 95:5 (A:B) from 9.5 to 10 min. A divert valve was utilized, with the valve set to waste from 0 to 1.5 min and to inject from 1.5 to 10 min. The mass spectrometric analyses were conducted under the following conditions: spray voltage, 3 kV; capillary temperature, 250°C; vaporizer temperature, 40°C; sheath gas, 40; aux gas, 30; tube lens offset, -112. Mass spectral dose-response data were analyzed with SigmaPlot (Systat Software, San Jose, CA) to calculate $IC_{50}$ values for each of the active compounds.

**Acknowledgments**

This research was supported by the National Center for Complementary and Integrative Health (NCCIH), a component of the National Institute of Health (NIH), by grant numbers 1 R01 AT006860 and 1 F31 AT009164. We thank Bill Burch for supplying plant material and Noemi Paguigan, Vincent Sica, and Diana Kao for helpful suggestions related to the manuscript. Mass spectrometry data were collected in the Triad Mass Spectrometry facility.

# CHAPTER V

# BIOCHEMOMETRICS TO IDENTIFY SYNERGISTS AND ADDITIVES FROM BOTANICAL MEDICINES: A CASE STUDY WITH HYDRASTIS CANADENSIS (GOLDENSEAL)

This chapter has been published in the Journal of Natural Products and is presented in that style. Britton, E.R., Kellogg, J.J., Kvalheim, O.M., Cech, N.B. J. Nat. Prod. 2017, Epub ahead of print.

Britton, E.R. collected and processed all data and wrote the manuscript. Kellogg, J.J. provided training and guidance in performing data processing, and made minor edits on the manuscript. Kvalheim, O.M. created the software used in this manuscript (Sirius) and offered technical advice, and made minor edits. Cech, N.B. assisted in the development of the research project and provided edits and suggestions throughout manuscript preparation.

## Introduction

In traditional and modern alternative health care practices, botanical extracts are employed frequently for medicinal purposes as complex mixtures. The claim is often made that such mixtures are more effective than their constituents in isolation due to additive or synergistic interactions among compounds (103-106). However, the identification of the chemical constituents responsible for the observed activity of complex extracts remains a challenging pursuit.

The traditional approach to identify active compounds from botanical mixtures, bioassay-guided fractionation, is highly effective for studying natural product mixtures when the activity can be traced to single, highly potent active compounds. Unfortunately,

it is more difficult to effectively employ bioassay-guided fractionation when the activity of the mixture results from multiple compounds with low potency. Recently, a modification of the bioassay-guided fractionation approach designed to aid in the identification of multiple active compounds in a mixture, "synergy-directed fractionation" was developed (9). With synergy-directed fractionation, a botanical extract is fractionated and the resulting fractions are tested for activity in combination with a known active constituent of the original extract. This approach was shown to be effective for identifying synergists in [*Hydrastis canadensis* L. (Ranunculaceae)] (9). However, one of the limitations of synergy-directed fractionation is that this technique, like bioassay-guided fractionation, is inherently biased towards the compounds that are most easily isolated. Even though the methodology focuses on the most active fractions for isolation efforts, these fractions are often so complex that it is not possible to isolate every compound that they contain. Characteristics such as the abundance of a given compound and/or its ease of separation typically guide the isolation process in the latter steps, rather than true biological activity. As a result, the "active" compounds identified may represent only a subset of those responsible for the activity of the original mixture.

There has recently been a great deal of interest among the scientific community in the application of untargeted metabolomics to identify active mixture compounds (35-40, 107). With this approach, analytical methods (typically NMR or MS) are employed to detect as many of the small molecules in a mixture as possible (the "metabolome"), without bias towards which are chemically or biologically interesting. For metabolomics data to be employed for identification of active mixture components, it is necessary to

collect metabolite profiles and corresponding biological assay data for a series of mixtures. Statistical methods are then employed to correlate chemical profile to bioactivity, a process which has been termed "biochemometrics" (108).

In theory, biochemometrics has the potential to overcome some of the aforementioned limitations of bioassay-guided fractionation, and to provide a more comprehensive representation of which compounds are responsible for the activity of a botanical extract. However, the inherent complexity of botanical extracts makes the data analysis aspects of the biochemometrics challenging when employed for this purpose. Several data analysis approaches have been employed to address this challenge. Inui et al. applied Pearson correlation coefficients to 2D orthogonal chromatography and incorporated biological data to identify mass spectral ions for which variance positively correlated with biological activity (39). Pearson correlation coefficients are a univariate statistical approach to measure the strength of linear correlation between single pairs of variables (i.e., concentration and biological activity) in isolation. A limitation of this approach is that the Pearson correlation does not consider potential interactions between variables, and is easily skewed by such outliers (109). In contrast, Kulakowski et al. utilized unsupervised principal component analysis (PCA) and supervised orthogonal partial least-squares discriminatory analysis (OPLS-DA) to correlate bioactivity to LC-MS profiles (37). PCA can used to group samples based upon covariance, so fractions with similar profiles will be clustered while others will be in a different location in the PCA score plot. PCA is useful for describing chemical differences among samples, but does not provide insight into which of the constituents of these samples are biologically

active. OPLS-DA allows for the incorporation of biological data, which were in this case binary classifications, i.e., active/nonactive fractions (37). OPLS-DA plots appear similar to PCA plots, and an OPLS-DA model can represented as an S-plot, where each axis represents the covariance and correlation loading variables (110). Biomarkers with intensities that correlate and co-vary with the bioactivity appear the furthest from the origin (36, 37). An important limitation of this approach is that co-variance increases with increased concentration of a constituent, such that the approach is biased towards selection of abundant constituents at the expense of low-abundant compounds that may have high biological activity (35).

Selectivity ratio plots are derived from the ratio of explained and residual variance on a single univariate component that incorporates bioactivity information in the multivariate PLS model, and can thus be employed to identify mixture components that are most strongly associated with an observed biological effect independent of concentration (35). Selectivity ratios were first applied to identifying biomarkers of diseases from complex cerebrospinal fluid data sets (34). Recently, the applicability of this biochemometrics approach using selectivity ratios to identify biologically active compounds from fungal extracts was demonstrated (35). As of yet, this approach has not, however, been applied to botanical extracts. Compared to botanicals, fungi produce relatively simple mixtures of chemical compounds. Thus, it is expected that the application of this biochemometric approach to botanical extracts, which are more complex, would be more challenging. Furthermore, an added challenge with botanical

extracts is that their greater complexity means that synergistic, additive, or antagonistic interactions are likely to occur (111).

With the study presented herein, an approach combining biochemometrics with synergy-directed fractionation to identify active compounds and/or synergists from a botanical extract was developed. As a case study, the botanical *Hydrastis canadensis* was selected, which is used widely in alternative healthcare practices for the treatment of infections (10, 112). Activity against the common Gram-positive bacterium *Staphylococcus aureus* was evaluated, given that *H. canadensis* has previously been shown to possess activity against this pathogen (72).(113)(113)

Earlier studies with *H. canadensis* have identified several compounds that interact synergistically to effect antimicrobial activity; thus, this botanical serves as a useful test case for evaluating a new approach to identify synergists. Specifically, *H. canadensis* is known to contain a number of flavonoids (sideroxylin, 6-desmethyl-sideroxylin, 8-desmethyl-sideroxylin, 3,5,3´-trihydroxy-7,4´-dimethoxy-6,8-di-*C*-dimethylflavone, 5,4´-dihydroxy-6-*C*-methyl-7-methoxyflavone, 5,4´-dihydroxy-6,8-di-*C*-methyl-7-methoxyflavone, 6,8-di-*C*-methylluteolin-7-methyl ether, and 6-*C*-methylluteolin-7-methyl ether [**20-22, 11, 13, 14, 27, 28**, respectively]), alkaloids, and other compounds (berberine, oxyberberine, berberastine, tetrahydroberberastine, canadine, canadaline, canadinic acid, 8-oxocanadine, β-hydrastine, hydrastidine, hydrastinine, oxyhydrastinine, noroxyhydrastinine, chilenine, 4´,5´-dimethoxy-4-methyl-3´-oxo(1,2,5,6-tetrahydro-4*H*-1,3-dioxolo-[4´,5´:4,5]-benzo[1,2-e]-1,2-oxazocin)-2-spiro-1´-phtalan, 8-oxotetrahydrothalifendine, corypalmine, isocorypalmine, tetrahydropalmatine, and 3,4-

dimethoxycarbonylbenzoic acid [**18**, **29, 30, 19, 31, 32, 24, 23, 33, 34, 16, 15, 12, 17, 25, 35-37, 10**]) with diverse structures (87, 114). Recently, it was shown that the flavonoids from *H. canadensis* sideroxylin (**20**), 6-desmethyl-sideroxylin (**21**), and 8-desmethyl-sideroxylin (**22**) enhance synergistically the antimicrobial activity of the alkaloid berberine (**18**) against *S. aureus* by acting as bacterial efflux pump inhibitors (9). In a separate report, the flavonoid 3,5,3´-trihydroxy-7,4´-dimethoxy-6,8-*C*-dimethylflavone (**11**) was also shown to act as an efflux pump inhibitor (114). *H. canadensis* also contains several alkaloids that do not act as efflux pump inhibitors (**19**, **23**, **25**) or possess biologically relevant antimicrobial activity (**26**, **19, 31, 32**, **23**, **25**, **35**) (11, 86, 87, 96, 114-119). Finally, a number of compounds have also been identified from *H. canadensis* for which biological activity has not been evaluated (**14**, **29**, **30**, **24**, **33**, **34**, **17**, **37**) (6, 88, 89, 96, 114, 120-122). Relying on existing knowledge about the chemistry and biological activity of *H. canadensis*, the goal with this investigation was to apply synergy-directed fractionation combined with biochemometric data analysis to a *H. canadensis* extract. The ultimate objective of these studies was to evaluate the effectiveness of this methodology to identify known active constituents and/or identify new bioactive compounds from a botanical extract.

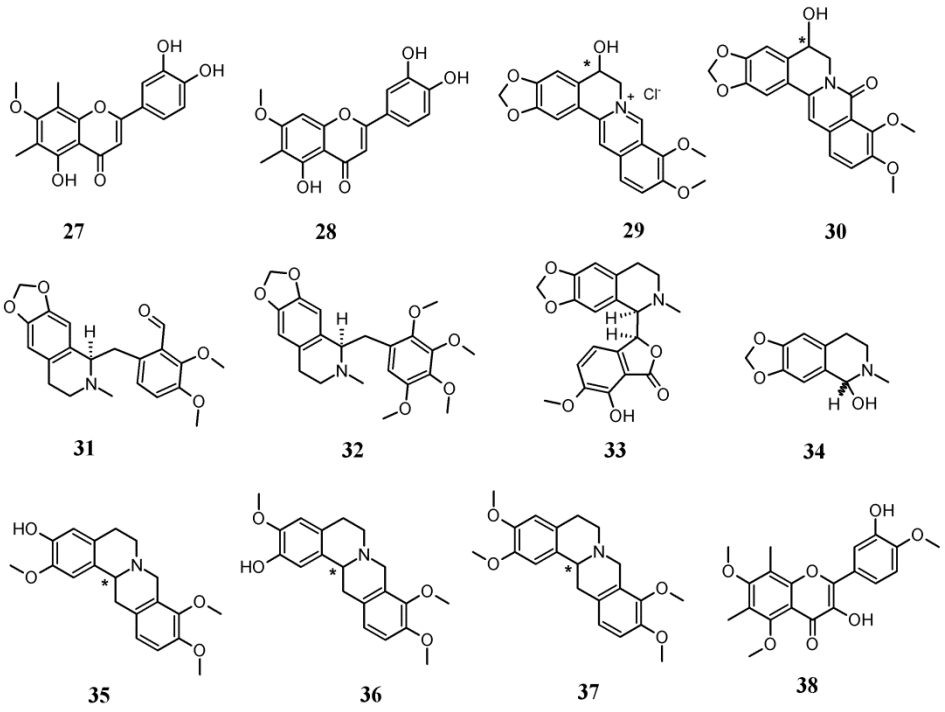


**Figure 17. Constituents of *Hydrastis canadensis*.** The configuration at locations with asterisks are unknown.

## Results and Discussion

For this study, a leaf extract was chosen for evaluation because *H. canadensis* leaves have a higher flavonoid content than the roots. Leaf material also tends to be highly complex, therefore, it was anticipated that reducing the complexity by fractionating a *H. canadensis* extract would be necessary to provide useful data for biochemometrics analysis. To determine how much fractionation would be necessary, the results of biochemometric analysis were compared on a sequential series of *H. canadensis* extract fractions and subfractions with decreasing complexity. Specifically, the original extract was subjected to liquid-liquid partitioning initially and then separated chromatographically in a series of four stages (Figure S1, Supporting Information). The

most active fraction from each stage was moved forward for further separation. To evaluate biological activity of the fractions produced by each stage of separation, *S. aureus* cultures were treated with varying concentrations of the alkaloid berberine (a known antimicrobial constituent of *H. canadensis*) in combination with constant concentrations of the *H. canadensis* fractions. The minimum concentration of berberine necessary to completely inhibit bacterial growth [minimum inhibitory concentration (MIC)] was compared in the presence of each *H. canadensis* fraction. With this approach, fractions containing compounds that enhance the antimicrobial activity of berberine (synergistically or additively) will lower the effective MIC of berberine against *S. aureus* (Figure 18). Metabolite profiles of the fractions from each stage of separation were collected using high resolving power mass spectrometry (Figure 19), as described in the Experimental Section, and biochemometric analyses (using selectivity ratio plots) were employed to integrate the metabolite profile data with the results of the bioassay data (Figure 20).

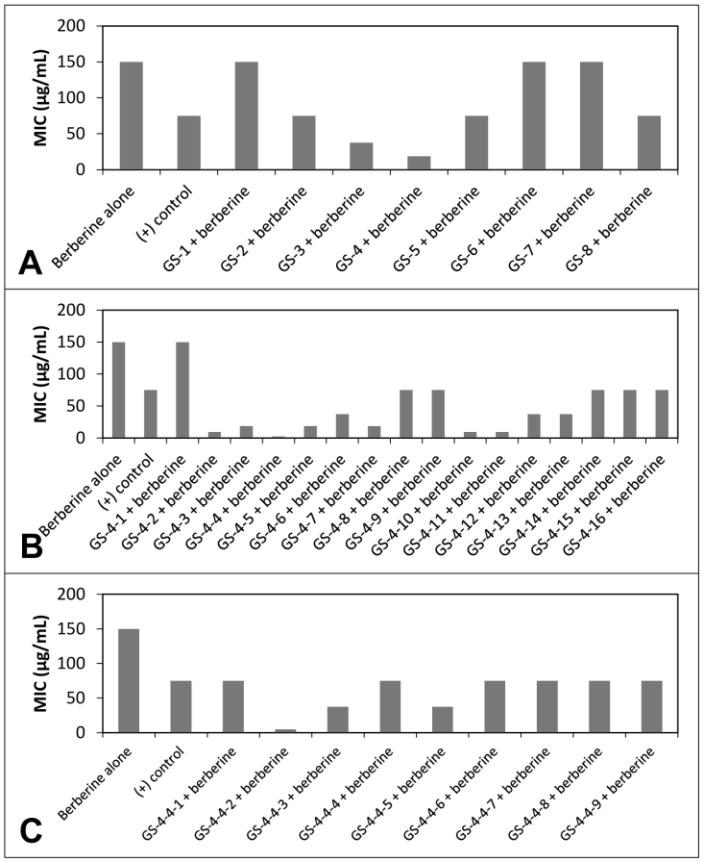


**Figure 18. Minimum Inhibitory Concentration (MIC) of Each Fraction + Berberine Against *Staphylococcus aureus*.** Berberine was tested alone, and berberine + piperine served as the positive control. Each fraction was combined at a constant concentration of fraction (75 µg/mL) with varying concentrations of berberine. See Figure S2 (Supporting Information) for MIC curves. (A) First stage normal phase fractions, where GS-4 lowered the MIC the greatest amount. (B) Secondary fractionation of GS-4 via normal phase chromatography yielded fractions GS-4-1 through 16, and the fractions therefrom were also tested in combination with berberine. (C) This process was repeated for stage 3 which was prepared using reversed phase chromatographic separation of GS-4-4.

## Biochemometrics to guide isolation

The *H. canadensis* extract and multiple fractions therefrom demonstrated the desired biological effect, an ability to enhance the antimicrobial activity of berberine (i.e., reduce its MIC value) against *S. aureus* (Figure 18; Figure S29). Importantly, the positive control, a known efflux pump inhibitor (123) (piperine) also reduced the MIC of berberine. From the first stage of fractionation, the strongest activity was observed for

fraction 4, which reduced the MIC of berberine from 150 to 18.8 μg/mL (Figure 18A). Thus, GS-4 was selected as starting material for subsequent fractionation, yielding a series of sub-fractions, from among which fraction GS-4-4 demonstrated the best activity (Figure 18B). This process was repeated to produce a subfraction set where GS-4-4-2 possessed the most potent activity in combination with berberine (Figure 18C) (see Figure S28 for fraction labeling scheme).

A necessary first step in the application of biochemometrics to identify active mixture components is that the compounds must be detectable by the analytical approach employed (in this case, LC-MS). Thus, the data resulting from LC-MS analysis of the *H. canadensis* extract (Figure 19A and 19F) were inspected to determine whether known *H. canadensis* constituents were detectable. Indeed, a number of flavonoids and alkaloids known to be present in *H. canadensis* were identifiable from the LC-MS data (Figure 19). Pursuit of the most biologically active fractions (Figure 18) throughout the isolation process resulted in selection of fractions with greater flavonoid abundance with each successive stage of isolation (Figure 19). This result is to be expected given that flavonoids are known to enhance the antimicrobial activity of alkaloids (106, 124-126), and the biological assay used as a basis for this study was enhancement of antimicrobial activity of the alkaloid berberine.

A known limitation of the application of mass spectrometric analysis to evaluate chemical composition of mixtures is the selectivity of the technique. Relative abundances in LC-MS chromatograms reflect what is most easily ionizable rather than what is truly present in the mixture at highest concentration. Inspection of the data resulting from

analysis of the *H. canadensis* extract evaluated herein illustrates this limitation. Alkaloids, which are easily protonatable, are highly amenable to analysis with electrospray ionization mass spectrometry in the positive-ion mode. Thus, positive-ion mode analysis of the *H. canadensis* resulted in chromatograms dominated by alkaloids (Figure 19A-D), at least in the earlier stages of fractionation before these alkaloids were separated into inactive fractions. Conversely, data collected in the negative-ion mode were dominated by flavonoids, which are more easily deprotonated (Figures 19E-H). It is important when conducting metabolomics profiling of a botanical extract to collect data in both ionization modes. Additionally, one must always be cognizant of the possibility that certain important mixture components may not be detected, and that the relative abundances in LC-MS chromatograms may not reflect the actual relative abundances in the mixture.

An advantage of LC-MS is that it enables the simultaneous detection of multiple constituents that have the same chromatographic retention time. This phenomenon is most apparent from Figure 19A, where eight goldenseal compounds were found within one chromatographic peak that eluted around 4.1 minutes. The peak shown represents the relative abundance of the most abundant ion during this time span, not the collective signal of all ions. For metabolomics analysis, these chromatograms are deconvoluted (using MZmine) to identify multiple retention time-mass pairs, even those that co-elute. Thus, all detectable ions (above a set noise threshold) are compared with bioactivity and correlations are determined, not just those that are apparent in the base peak chromatograms.

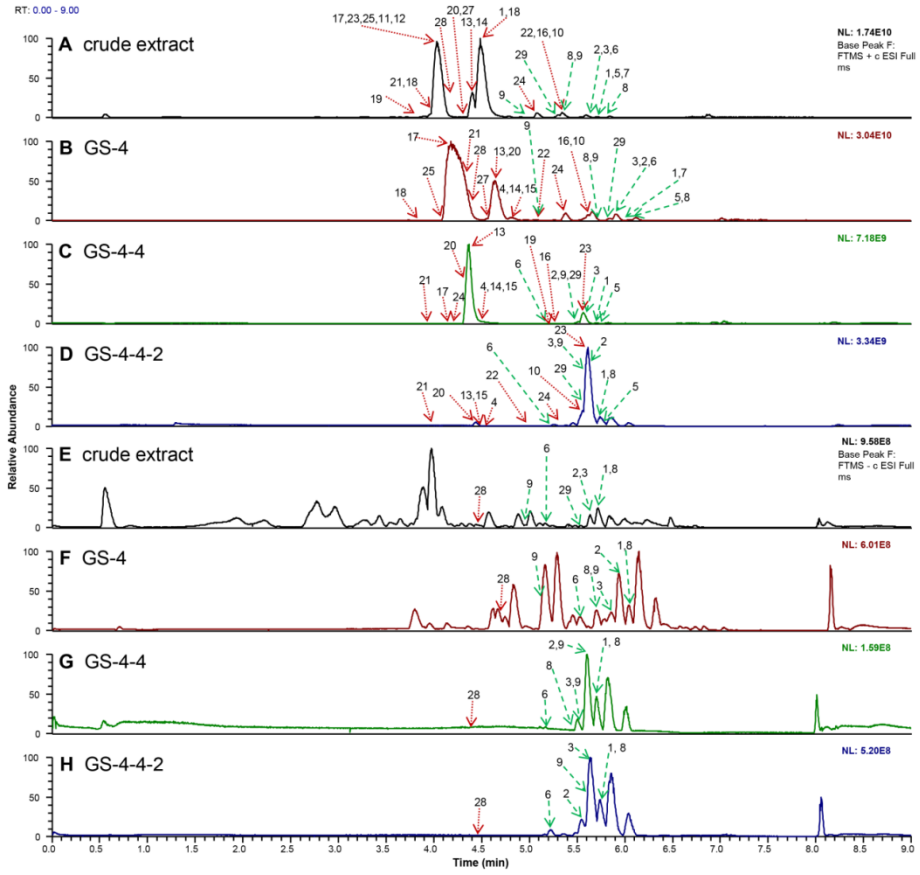


**Figure 19. LC-MS Chromatograms (Collected With Ultraperformance Liquid Chromatography Coupled to a Q-Exactive Orbitrap Mass Spectrometer) of a Series of *H. canadensis* Extract Fractions.** (A) Positive-ion electrospray mass spectrometry chromatogram of the crude extract after liquid-liquid partitioning. (B) The most active fraction (GS-4) of the crude extract shown in A after separation with flash chromatography over silica gel using a hexane/chloroform/methanol gradient (stage 1 separation). GS-4 was further fractionated using a second stage of flash chromatography over silica gel with a hexane/ethyl acetate/methanol gradient with GS-4-4 being the most active (C). GS-4-4-2 generated with stage 3 fractionation (using reversed phase preparative HPLC with a water:acetonitrile gradient) (D). (E-H) The same *H. canadensis* extract and fractions analyzed using LC-MS in the negative-ion mode. Arrows represent the region of the chromatogram in which a given ion corresponding to a known constituent of *H. canadensis* (indicated by compound numbers) could be detected. Compounds **20-22**, **11**, **12**, **13**, **14**, **18**, **26**, **19**, **23, 24**, **12**, **15-17, 25**, and **10** were identified by comparison of retention time and fragmentation with authenticated standards (72, 114), while compounds **27-37** were tentatively identified by comparison of accurate mass and molecular formula with literature reports (6, 87, 115, 118, 120, 122, 127). Red dotted arrows represent alkaloids and other compounds, while green dashed arrows represent flavonoids. In cases where a specific peak is not apparent in the chromatogram, the ion was identified based on mass spectrometric data.

The selectivity ratio plots shown in Figure 20 are the output of biochemometric analysis combining the data obtained from biological evaluation (Figure 18) and

chemical evaluation (Figure 19) of the *H. canadensis* extract and fractions. To generate these plots, a series of unique marker ions (*m/z*-retention time pairings) obtained from analysis of the LC-MS data were used from each stage of fractionation (595, 612, and 149 ions for stages one through three, respectively) Previous reports compounded mass spectrometric and biological data from previous stages of fractionation to increase statistical power.[11] Due to the chemical complexity of botanical data sets, the selectivity ratio plots produced from combining fractionation stages did not result in known synergists being predicted as bioactive (data not shown). The selectivity ratio plots represent the *m/z* of each ion detected on the x-axis, and the selectivity ratio (the ratio of explained variance to residual variance, which is derived from the PLS model) on the y-axis for each independent stage of fractionation. Since the biological assay data used for this analysis was growth inhibition, the ions with the most negative (pointing down in Figure 20) selectivity ratios represent those associated with the desired biological effect (antimicrobial activity). Ions with very small selectivity ratios or positive selectivity ratios (either no bar or pointing up, respectively, in Figure 20) are not expected to have synergistic or additive activity when combined with berberine.

Selectivity ratio plots (Figure 20) have the advantage over LC-MS or LC-UV chromatograms in that the size of bars is representative of constituents possessing the desired effect (biological activity) rather than unrelated effects such as high concentration, ionizability, or molar absorptivity. Thus, in theory, selectivity ratio plots should be extremely helpful for guiding the isolation of bioactive compounds. It is worth mentioning here that scientists engaged in bioassay-guided fractionation typically *do*

make decisions about which fractions to pursue for isolation based on which fractions possess the greatest biological activity. The challenge, of course, is in deciding which components of these fractions to isolate. Typically, a researcher would compare the chromatographic profile of active and inactive fractions to determine which peaks differ between them. However, when hundreds or thousands of components are present, and when more than one fraction is being compared, it becomes very difficult to do this with simple visual inspection. Also, visually one tends to be biased by the tallest peaks of those most distinctly separated from other peaks (even though these may be neither the most abundant nor the most active ions). The use of selectivity ratio plots improves the efficiency of the process by comparing all of the detected ions (both active *and* inactive) and corresponding peak areas of all fractions in a given stage of separation with their associated biological activity. The result is a quantitative value (the selectivity ratio) that describes how well each ion is associated with the observed biological activity independent of concentration bias (again, assuming that the ion is detected by the analytical method being employed).

**How much fractionation is necessary?**

It is important to recognize an inherent limitation of the biochemometric approach, in that associations between activity and chemical composition are correlative, rather than causal. It is always possible that ions identified as bioactive in a selectivity ratio plot may co-vary in fractions with active ions, but may not possess activity themselves. Such ions would represent false positives. The likelihood of observing such false positives increases as the chemical complexity of the fractions evaluated increases.

Conversely, it is also possible that particular bioactive mixture components might go undetected by the analytical approach used, or be at a concentration too low to register a biological effect (i.e., antimicrobial activity). Such a scenario would result in a false negative. Using *H. canadensis* as a test case, one of the goals of this study was to evaluate empirically the likelihood of occurrence of such false positives and false negatives by comparing the results of biochemometric analysis on three different stages of fractionation (Figure 20).

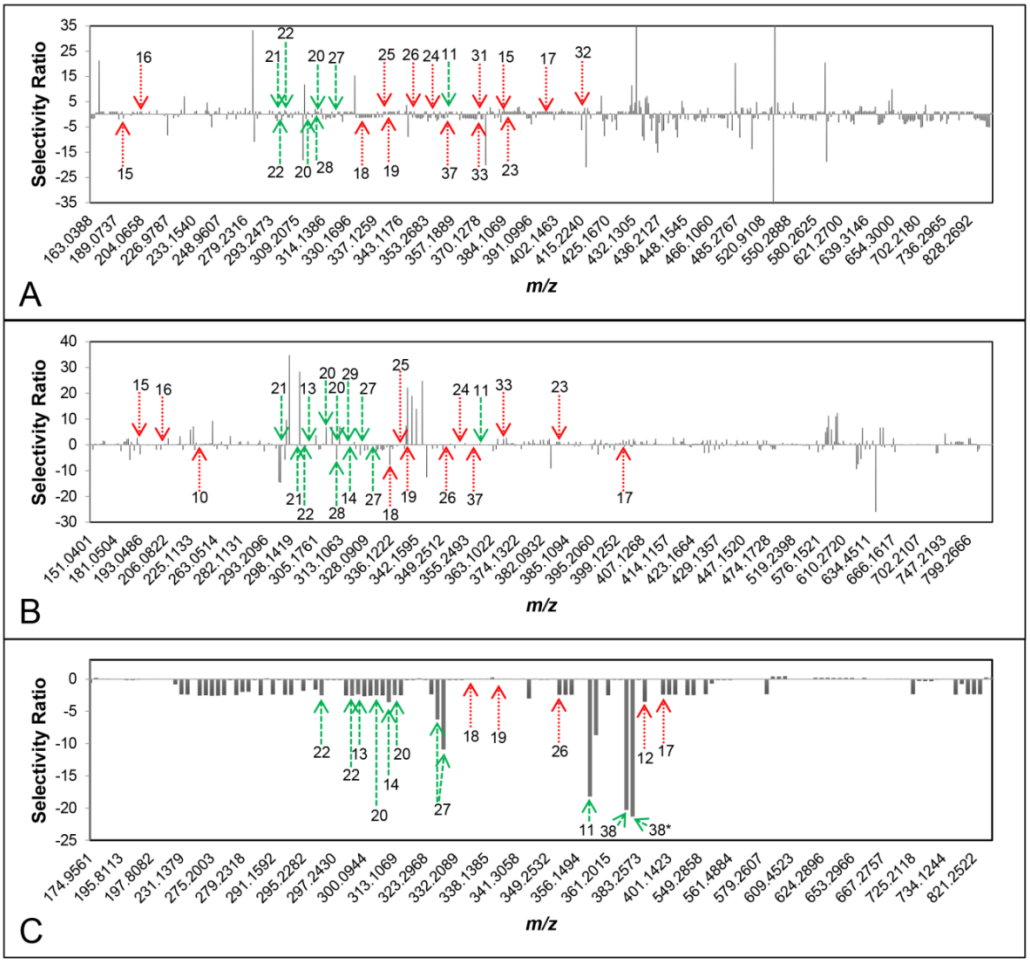


**Figure 20. Selectivity Ratio Plots for First, Second and Third Stages of Fractionation [(A), (B), and (C), Respectively] With Green Dashed Arrows Representing Flavonoids and Red Dotted Arrows Representing Alkaloids and Other Known Constituents of *H. canadensis*.** The signals of flavonoids and the alkaloid berberine, all known to be or predicted to be active in the assay being used, are not prominent in first stage fractionation (A) and second stage fractionation (B). (C) Third stage fractionation yielded seven flavonoids (**20-22**, **11**, **13**, **27**, **38**) and three alkaloids (**26**, **12**, **17**) with negative selectivity ratios (suggesting these compounds to contribute additively or synergistically to antimicrobial activity). The bar labeled **38*** represents the $^{13}C$ isotope of **38**. The identities and activities of compounds represented by other prominent peaks are not known.

Stage 1 fractions were subjected to subsequent biochemometric analysis, and multivariate partial least squares (PLS) modeling of the combined bioassay and spectral data matrix yielded the selectivity ratio plot shown in Figure 20A. The selectivity ratio plot based on the first stage of separation indicated several false negatives. Although four

confirmed active flavonoids (compounds **20**-**22** and **11**) and the alkaloid berberine (**18**) were detected among the ions from this first stage of fractionation (Figure 20A), none of these ions was highlighted as major active constituents in the selectivity plot (i.e., ions with large negative selectivity ratios). The flavonoids sideroxylin (**20**), 6-desmethyl-sideroxylin (**21**) and 8-desmethyl-sideroxylin (**22**) were detected in the most active fraction from the first stage of fractionation (GS-4, which lowered the MIC of berberine from 150 μg/mL to 18 μg/mL), but did not display the expected large, negative selectivity ratios. This failure to identify the active flavonoids among other mixture components can be explained by the high level of complexity of these fractions and inability to resolve active and inactive compounds. These findings demonstrate an inherent limitation of metabolomic studies in which investigators attempt to identify active compounds from mixtures without prior fractionation.

Notably, a number of ions were identified in this first stage fractionation with highly negative selectivity ratios (Figure 20A). It is unclear whether these ions (for which activity and structure are unknown) constitute a series of false positives, or whether they are truly active but hitherto unidentified constituents of *H. canadensis*. The data do suggest that at least one of the ions identified in Figure 20A is a false negative. The ion with the most negative SR (*m/z* 527.3156 $[M+H]^+$) was most abundant (relatively, based upon MS signal) in fraction GS-8, which did not prove to be an active fraction (Figure 18B). This highlights the potential for false positives when using this biochemometrics approach, and further supports the assertion that some fractionation is required to obtain useful selectivity ratio plots. In addition, ions that appear to be "active" in the stage 1

fractions are not present in later-stage selectivity ratio plots, which indicates that they are false positives and not true antimicrobials or antimicrobial synergists.

GS-4 was chosen for further purification based upon its lowering of the MIC of berberine from 150 μg/mL to 18 μg/mL (Figure 18A). The resulting 16 fractions, excluding GS-4-1, lowered the MIC of berberine to values ranging between 2.34 μg/mL and 75 μg/mL, and the resulting selectivity ratio plot is shown in Figure 3B. As with stage 1 fractions, the known flavonoid synergists (**20**-**22**) and the antimicrobial alkaloid berberine (**18**) were detected in these fractions. In this less complex series of stage 2 fractions, berberine (known to be active) displayed the expected negative selectivity ratio. However, the second stage of fractionation still failed to show activity for the known active flavonoids (**20**-**22**). Finally, as with the first stage fractionation, several ions of unknown identity displayed large negative selectivity ratios. The possible biological activity of these ions was not further pursued, but could be the subject of future investigations.

Fraction GS-4-4 was the most bioactive from the second stage of fractionation, decreasing the MIC of berberine from 150 μg/mL to 2.3 μg/mL (Figure 18B). The nine subfractions of GS-4-4 were subjected to biochemometric analysis, resulting in the selectivity ratio plot shown in Figure 20C. Compounds **11** (*m/z* 359.1121 and 359.1122 $[M+H]^+$) and **27** (*m/z* 329.1017 $[M+H]^+$ and 327.0879 $[M-H]^-$) had the second and third lowest selectivity ratios, with the lowest SR representing *m/z* 373.1279 $[M+H]^+$ and its $^{13}C$ isotope. This ion represented a compound not yet known to *H. canadensis*, and was targeted for isolation. Additionally, chilenine (**12**) and 4´,5´-dimethoxy-4-methyl-3´-

oxo(1,2,5,6-tetrahydro-4*H*-1,3-dioxolo-[4′,5′:4,5]-benzo[1,2-e]-1,2-oxazocin)-2-spiro-1′-phtalan (**17**) were identified as potential active components based on biochemometric analysis of the third stage fractions (Figure 20C). Chilenine has previously been reported as a constituent of *H. canadensis*, but its biological activity is unknown (114). The data presented here suggest that it might possess antimicrobial activity (alone or in combination with berberine), a possibility that could be investigated in a future study.

**Verification of activity for a compound predicted to be active based on biochemometrics**

Guided by the results of the biochemometric analysis (Figure 20C), **38** was isolated and identified as the new flavonoid 3,3′-dihydroxy- 5,7,4′-trimethoxy- 6,8-*C*-dimethylflavone (Figures S30-S34). The isolated mass (0.84 mg) was insufficient for completing a full synergy assessment, so **38** was tested at a constant concentration (75 μg/mL or 201.4 μM) in combination with concentrations of berberine ranging from 0 to 100 μg/mL (297.5 μM) (Figure 21). The known efflux pump inhibitor piperine (123) was also included in this assay (at a constant concentration of 200 μM) as a positive control.

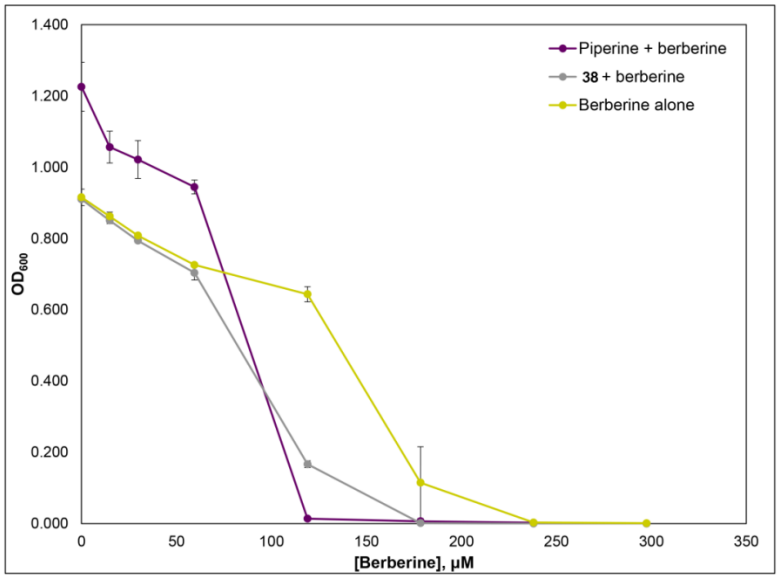


**Figure 21. Dose Response Curve of Berberine Ranging From 0 to 298 µM In Combination With Piperine (Positive Control, Fixed Concentration of 263 µM) and 38 (Fixed Concentration of 200 µM).** Error bars represent standard error (error bars are not visible for some datapoints because they are smaller than the point size). The expected shift to the left (increased potency) in the berberine dose-response curves in the presence of both piperine and **38** was observed. Notably, **38** did not have any antimicrobial effect when tested individually at 200 and 400 µM, which suggests that the increased potency of berberine in combination with this compound is due to synergy and not additivity.

Both piperine and **38** influenced the activity of berberine (Figure 21). The MIC of berberine alone was 238 µM, but in combination with piperine and **38**, the MIC was lowered to 119 µM and 179 µM, respectively. When tested in combination with **38**, the $IC_{50}$ of berberine was lowered from 132.2 ± 1.1 µM to 91.5 ± 1.1 µM. Piperine demonstrated a similar activity, resulting in a lowered berberine $IC_{50}$ of 72.3 ± 1.0 µM. These data suggest that **38** does, indeed enhance the antimicrobial activity of berberine. Importantly, **38** alone at 402.8 µM and 201.4 µM demonstrated no antimicrobial activity (data not shown), suggesting that the increased efficacy of berberine in combination with **38** is due to synergy, not additivity. Thus, **38**, which has no antimicrobial activity alone, potentiates the antimicrobial efficacy of berberine. The potency of **38** in combination

with berberine is not high as that of the precursor fraction (GS-4-4-2, which lowered the MIC of berberine from 150 μg/mL to 4.68 μg/mL), which further supports that the activity of fraction GS-4-4-2 is due to the presence of multiple constituents, including compounds **20-22**, **11**, and **13**.

**Did biochemometrics improve the synergy-directed fractionation process?**

Previous work using synergy-directed fractionation on *H. canadensis* (without biochemometrics) resulted in the identification of three flavonoids (**20-22**) that synergistically enhanced the antimicrobial activity of berberine (**18**) (9). The application of biochemometrics enabled the list of putative active compounds to be increased to be increased to nine compounds. Specifically, based on the biochemometrics data for the third stage of fractions (Figure 20C), the flavonoids **20**, **21**, **22**, **11**, **27**, and **38** and the alkaloids **26**, **12,** and **17** were all predicted to act as additives or synergists to the antimicrobial activity of berberine. How accurate were these predictions? Compounds **20-22**, and **11** are known efflux pump inhibitors, as demonstrated in several previous studies (9, 114). Compound **27** has not previously been evaluated for biological activity against *S. aureus*, but has been shown to have antimicrobial activity against *Streptococcus mutans* and *Fusobacterium nucleatum* (87). Based upon its structural similarity to **20**, which has one less hydroxy group at the C-3´ position, **27** is likely to be active as an efflux pump inhibitor. Compound **38** is a new compound, isolated as part of these studies, and demonstrated to increase synergistically the antimicrobial activity of berberine (Figure 21). It is likely that, like other flavonoids, the activity of **38** is due to bacterial efflux pump inhibition, although the efflux pump inhibitory activity of this

compound was not evaluated here. Alkaloid **26** was shown previously in the literature to not have antimicrobial activity against *S. aureus* when tested at 25.6 µg using a disk diffusion assay (119). Further studies would be needed to show if **26** is antimicrobial under other conditions and if it exhibits synergy in combination with berberine. Similarly, alkaloids **12** and **17** have no reported biological activity, and their activity as synergists or antimicrobials could be confirmed with further studies. As a side note, alkaloid **17** was found to be a product of β-hydrastine-*N*-oxide under reflux conditions and is likely present here as an isolation artifact (92, 114).

A major challenge faced by any investigator conducting bioassay-guided fractionation is to decide which mixture components to target for isolation. The magnitude of this challenge is illustrated by the sheer number of ions detectable with mass spectrometric analysis of a botanical extract. In this study, a total of 595, 612 and 149 features were detected (above the selected signal threshold) in the first, second, and third stage of *H. canadensis* fractionation, respectively. When addressing this challenge, the inclination of the investigator is to focus on the most detectable ions (which may or may not be the most abundant) in the most biologically active fraction. The application of biochemometrics to guide isolation helps reduce that inherent bias. Relevant to the study here, **38** was identified for isolation in this project because it has the lowest selectivity ratio in the third stage fractionation. *Notably, this compound was not the ion detected with highest abundance in the most active fraction (GS-4-4-2, Figure 19D and 19H).* Visual inspection of the data from that fraction would have led the observer to overlook **38** and instead focus on **20**, **21** and **22**, which appear to be highly abundant and have

already been isolated and identified as synergists as part of a previous study. Ultimately, isolation and subsequent NMR structure elucidation will always be needed to confirm absolute configuration and solve structures of unknown compounds. Furthermore, given the correlative rather than causal nature of activity predictions based on biochemometric data analysis, isolation and biological activity evaluation are very necessary as a means of validation. As demonstrated here, the use of biochemometrics to integrate bioassay data with mass spectrometric metabolite profiles can help guide the isolation process towards constituents that may possess relevant biological activity. Importantly, however, as was the case in this study, the complexity of botanical extracts may necessitate several stages of fractionation to simplify the mixture before biochemometric analysis yields useful results.

## Experimental

### General experimental procedures

Extracts were suspended in 1:1 MeOH-dioxane (LC/MS grade, Fisher Scientific, Hampton, NH, USA) at either 1 mg/mL or 0.1mg/mL and subjected to ultraperformance liquid chromatography tandem mass spectrometry (UPLC-MS/MS) analysis via a Waters Acquity UPLC with an Acquity UPLC column (BEH $C_{18}$, 1.7 µm, 2.1 x 50 mm, Waters Corporation, Milford, MA, USA) and a Thermo Q-Exactive Plus orbitrap mass spectrometer with heated electrospray ionization (Thermo Fisher Scientific, Milford, MA, USA). Analysis was performed at a flow rate of 0.3 mL/min using the following binary solvent system with A consisting of water with 0.1% formic acid additive and solvent B consisting of acetonitrile with 0.1% formic acid additive (LC/MS grade, Fisher

Scientific). The gradient was as follows: 95:5 (A:B) from 0 to 1 min, increasing to 90:10 (A:B) from 1 to 2 min, 80:20 (A:B) from 2 to 3 min, 60:40 (A:B) from 3 to 4 min, 70:30 (A:B) from 4 to 5 min, 0:100 (A:B) from 5 to 6 min and held from 6 to 7 min, 95:5 (A:B) from 7 to 8 min and held from 8 to 9 min. The Thermo Q-Exactive Plus was operated in both positive and negative polarities using the following settings: spray voltage, 3.7 kV; capillary temperature, 350°C; sheath gas, 25; auxiliary gas, 5; S-lens RF level, 50. Known constituents of goldenseal were listed in an inclusion list for fragmentation via high-energy collision-induced dissociation (HCD) and used for tentative identification based upon matching retention time, accurate mass, and accurate mass fragments with isolated standards (compounds **20-22**, **11**, **13**, **14**, **26**, **19**, **23**, **24**, **12**, **15-17**, **25**, and **10**) (72). Compounds without standards (**27-37**) were identified tentatively by comparison of accurate mass and molecular formula with literature reports (11, 86, 88, 89, 114, 117). Data were visualized using Xcalibur (v. 2.3.26, Thermo Fisher Scientific). Phenomenex Gemini-NX $C_{18}$ analytical (5 μm; 250 × 4.6 mm) and preparative (5 μm; 250 × 21.2 mm) and Phenomenex Luna PFP(2) 100A analytical (5 μm; 150 × 4.6 mm) and preparative (5 μm; 250 × 21.2 mm, Phenomenex, Torrance, CA, USA) columns were used on a Varian Prostar HPLC system equipped with Prostar 210 pumps and a Prostar 335 photodiode array detector (PDA) (Agilent Technologies, Santa Clara, CA, USA), with data collected and analyzed using Galaxie Chromatography Workstation software (version 1.9.3.2, Agilent Technologies). Flash chromatography was performed on a Teledyne ISCO CombiFlash ® $R_f$ 200 (Teledyne-Isco, Lincoln, NE, USA) using Silica Gold columns (330 g, 120 g, and 40 g columns) and monitored by UV and evaporative light-scattering

detectors. 1D and 2D NMR spectra were recorded using a JEOL ECA-500 NMR spectrometer operating at 400MHz for $^{1}H$ and 100 MHz for $^{13}C$ (JEOL, Peabody, MA, USA), or an Agilent 700 MHz NMR spectrometer (Agilent Technologies) equipped with a cryoprope, operating at 175 MHz for $^{13}C$. NMR data were visualized using MestReNova (v 11.0.4, Mestrelab Research, Santiago de Compostela, Spain). $IC_{50}$ values were calculated using a four parameter logistic standard curve analysis function in SigmaPlot (v.13, Systat Software, San Jose, CA, USA). All chemicals used unless otherwise stated were ACS grade and obtained from Fisher Scientific.

**Plant material**

*Hydrastis canadensis* bulk leaf material was collected in June 2014 from William Burch in Hendersonville, North Carolina (NC, N 35°24.277', W 082°20.993', 702.4 m elevation). The plants were cultivated in their natural environment, a hardwood forest understory, and were a year old at the time of harvest. A voucher specimen for this *H. canadensis* plot has been deposited at the Herbarium of the University of North Carolina at Chapel Hill (NCU583414) and authenticated by Dr. Alan S. Weakly. Samples were dried at room temperature until crisp before extraction.

**Extraction and isolation**

Dried aerial plant portions were ground mechanically using a Wiley Mill Standard Model No. 3 (Arthur H. Thomas Co., Philadelphia, PA, USA) with a 2 mm mesh size, and percolated in MeOH overnight three times. The MeOH extract was concentrated in vacuo before liquid-liquid extraction. The extract was defatted by partitioning between hexane and 10% aqueous MeOH (1:1). The dried aqueous MeOH was partitioned further

between 4:5:1 EtOAc-MeOH-$H_2O$, and the organic layer was washed with 1% saline solution to remove hydrosoluble tannins. The fractionation scheme is provided as Supporting Information. The first stage of normal-phase flash chromatography (330 g Gold silica gel column) was performed in two batches (58.49 g total) and conducted at a 200 mL/min flow rate with a 42.7 min hexane/$CHCl_3$/MeOH gradient. The most active fraction from the first stage separation (fraction 4, ~10 g) was subjected to a second stage of normal-phase flash chromatography (120 g Gold silica gel column and 40 g Gold silica gel column) and conducted at flow rates of 85 mL/min and 40 mL/min, respectively with 57.6 min and 33.4 min hexane/EtOAc/MeOH gradients, respectively. The most active fraction from the second-stage separation (subfraction 4, ~290 mg) was purified using reversed-phase HPLC with a Phenomenex Gemini-NX column at a 21.4 mL/min flow rate in three batches. A $CH_3CN/H_2O$ with 0.1% formic acid gradient was employed which held at 30:70 for five min, increased to 60:40 from five to ten min, increased to 0:100 from 10 to 25 min, and held at 100:0 from 25 to 40 min. It was determined that the ion of interest via biochemometric analysis of the third stage of fractionation, *m/z* 373.1279 $[M+H]^+$ had the greatest relative abundance in fraction GS-4-5 and was therefore used for isolation. GS-4-5 was subjected to reversed-phase HPLC with a preparative Luna PFP column at a 21.4 mL/min flow rate. A $CH_3CN/H_2O$ with 0.1% formic acid gradient was employed that increased from 35:65 to 50:50 over 8 min, held at 50:50 from 8 to 30 min, increased to 100:0 from 30 to 35 min, and then held at 100:0 from 35 to 55 min. Fractions 41 through 43 were recombined and subjected to reversed-phase HPLC with an analytical Luna PFP column at 1 mL/min. A MeOH/$H_2O$ with 0.1%

formic acid gradient was employed where the solvent composition increased from 72:28 to 76:24 over 30 min, and increased to 100:0 from 30 to 40 min. Fractions were collected manually into vials based upon UV absorption and LC-MS traces. One last stage of purification was performed to achieve 95.4% purity via UV (254 nm) using a Gemini analytical column with a $CH_3CN/H_2O$ with 0.1% formic acid solvent system at 1 mL/min where the gradient increased from 10:90 to 100:0 over 55 min, and held at 100:0 from 55 to 60 min. Compound **38** had a final yield of 0.84 mg (0.0014% of 58.49 g EtOAc extract).

*3,3´-Dihydroxy-5,7,4´-trimethoxy-6,8-C-dimethyl-flavone* (**38**): yellow solid; UV (MeOH) $\lambda_{max}$ (log $\varepsilon$) 254 (4.42) 363 (4.26) nm; $^1$H NMR (DMSO, 500 MHz, Figure S30) and $^{13}$C NMR (DMSO, 175 MHz, Figure S31), see Table 1; HRESIMS *m/z* 373.1279 $[M+H]^+$ (calcd for $C_{20}H_{21}O_7$, 373.1287). Because there were no HMBC correlations for the hydroxy protons attached to C-3 and C-3´, OH-3´ was assigned based upon literature precedent that hydroxy group protons attached to aromatic rings have sharper peaks than those that are not (128).

**Antimicrobial assays**

Minimum inhibitory concentrations (MIC values) were evaluated per the terms outlined by the Clinical Laboratory Standards Institute (78) against wild type *Staphylococcus aureus* (SA1199) (102).(129)(129) A single colony inoculum was grown to log phase in Müeller Hinton broth and adjusted to a final assay concentration of $1.0 \times 10^5$ CFU/mL based on absorbance at 600 nm ($OD_{600}$). The negative control consisted of 2% glycerol and 2% DMSO in broth (vehicle), and the known antimicrobial compound

berberine (80) served as the positive control. Triplicate wells were prepared with all treatments and controls. Duplicate plates were made without bacteria for background absorbance subtraction. $OD_{600}$ was read after 18 h at 37 °C using a Synergy H1 microplate reader (Biotek, Winooski, VT, USA). The MIC was defined as the concentration at which no statistically significant difference was observed between the negative control and treated sample.

**Combination assays**

Extracts were tested in combination with berberine over a concentration range of 2.3 to 150 µg/mL. Berberine alone served as a positive control, and demonstrated a MIC value between 75 and 150 µg/mL, consistent with the literature (9). The vehicle consisted of 2% glycerol and 2% DMSO in broth. A simplified version of the synergy assay was performed after each stage of fractionation to quickly assess those fractions possessing additive and/or synergistic behavior. This involved testing berberine at a range of concentrations (2.3 to 150 µg/mL) in combination with a constant concentration of each of the extract fractions (75 µg/mL) or purified compound **38** (200 µM). The known efflux pump inhibitor piperine (75 µg/mL or 240 µM) was used as the positive control for these experiments (123, 130). Fractions were classified as active if they enhanced the antimicrobial activity of berberine (lowered the MIC by 2-fold) and were advanced to the next stage of separation.

**Biochemometric analysis**

LC-MS data sets were collected in positive and negative polarities and were analyzed, aligned and filtered in independent batches using MZmine 2.17 software

(http://mzmine.sourceforge.net/) (131), as previously described by Kellogg et al (35). Briefly, raw data files were uploaded into MZmine for peak picking based upon mass spectral signals that were above the signal intensity of a mass spectrometric chromatogram of an injection of 1:1 MeOH:dioxane (solvent blank). Chromatograms were built based upon having a signal that lasted for longer than 0.01 min, minimum peak duration of 1.8 sec (0.03 min), *m/z* variation tolerance of 0.05 and a *m/z* intensity variation tolerance of 20%. Peak list filtering and retention time alignment were also performed, and the join align algorithm compiled the final peak list. The mass spectral data matrix was exported into Excel (Microsoft, Redmond, WA, USA) where ions in common between the samples and solvent blank was manually removed from the sample mass spectral profiles, positive and negative polarity data sets were combined and biological assay data was added in the form of MIC values of berberine in combination with certain fractions. Data matrices for each stage of fractionation were independently imported into Sirius version 10.0 (Pattern Recognition Systems AS, Bergen, Norway) (132). An internally cross-validated PLS model of 100 iterations with a significance threshold set to 0.05 was constructed and selectivity ratios were calculated using the Sirius software (32).

**Acknowledgements**

This work was supported by the National Center for Complimentary and Integrative Health, National Institutes of Health [grants 1R01 AT006860 (NBC) and F31 AT009164 (ERB)]. Mass spectrometry data were collected in the Triad Mass Spectrometry Facility. We thank D. Todd for technical assistance and J. Rivera-Chávez for assisting with structure elucidation.

**Table 5. NMR Spectroscopic Data (500 and 700 MHz, DMSO) for 3,3´-Dihydroxy- 5,7,4´ trimethoxy- 6,8-*C*-dimethylflavone (38).**

| position | $\delta_C$, type | $\delta_H$ (*J* in Hz) | HMBC[a] |
|---|---|---|---|
| 2 | 143.35, C | | |
| 3 | 138.49, C | | |
| 4 | 171.79, C | | |
| 5 | 155.28, C | | |
| 6 | 121.39, C | | |
| 7 | 160.96, C | | |
| 8 | 115.60, C | | |
| 9 | 153.47, C | | |
| 10 | 112.83, C | | |
| 1´ | 124.33, C | | |
| 2´ | 114.60, CH | 7.70, s | 2, 3´, 4´, 6´ |
| 3´ | 146.79, C | | |
| 4´ | 149.47, C | | |
| 5´ | 112.43, CH | 7.09, d (14) | 1´, 3´, 4´ |
| 6´ | 119.65, CH | 7.68, d (14) | 2, 2´, 4´ |
| OH-3 | | 9.43, s | |
| $OCH_3$-5 | 61.47, | 3.75, s | 5 |
| $CH_3$-6 | 9.17, | 2.18, s | 6, 5, 7 |
| $OCH_3$-7 | 60.83, | 3.74, s | 7 |
| $CH_3$-8 | 9.43, | 2.39, s | 7, 8 ,9 |
| OH-3´ | | 9.10, s | |
| $OCH_3$-4´ | 56.02, | 3.81, s | 4´ |

[a]HMBC correlations are from the proton(s) stated to the indicated carbon.

# CHAPTER VI

# CONCLUDING REMARKS

The studies described here demonstrate how the inclusion of liquid chromatography and mass spectrometry can improve the process of identifying bioactive constituents. Chapter II described the development of a mass spectrometry-based assay to identify inhibitor of the bacterial spreading factor hyaluronidase. This assay served as a direct, quantitative, accurate and precise alternative to existing methods that rely on turbidimetric or colorimetric measurements. Chapter III described the identification of two fungal metabolites, leotiomycene A and leotiomycene B, as the most potent inhibitors of *Streptococcus agalactiae* hyaluronidase to date. Leotiomycene B was also found to be the first ever reported inhibitor of hyaluronidase from *Staphylococcus aureus*. In addition, these compounds did not exhibit antimicrobial activity at the concentration in which they inhibit hyaluronidase, and thereby could serve as leads for the development of treatments to inhibit bacterial spreading.

Chapter IV described the isolation of two new compounds and six previously known compounds that were new to *Hydrastis canadensis*. One of the new compounds, 3,5,3´-trihydroxy-7,4´-dimethoxy-6,8-C-dimethyl-flavone, was found to inhibit efflux pumps in *Staphylococcus aureus*, which supports the supposed effectiveness of *H. canadensis* as a treatment for bacterial skin infections. In addition, high mass accuracy fragmentation spectra were obtained for all isolated constituents and were uploaded into

the Global Natural Products Social molecular networking database to facilitate identification in other botanical extracts. These methods and data were used in Chapter V, which involved using *H. canadensis* as a case study for the application of multivariate statistics to identify synergists and additives in complex matrices. Untargeted metabolomics profiles of *H. canadensis* extracts and fractions were combined with bioassay data (termed biochemometrics) to produce selectivity ratio plots, which indicate the variation of correlation that components have with bioactivity. The approach identified a new compound, 3,3′-dihydroxy-5,7,4′-trimethoxy-6,8-*C*-dimethylflavone, along with other active flavonoids. When tested in combination with berberine against *S. aureus*, it was confirmed that this new compound was indeed a synergist. This study demonstrated the importance of fractionation when using metabolomics to identify bioactive constituents from complex matrices, as well as the power of selectivity ratio plots to aid in interpreting combined complex chemical and biological data sets.

These studies clearly demonstrate the advantage of using mass spectrometry as a discovery tool in natural product research. The methods described here can be combined in order to find new inhibitors of bacterial spreading, or they can be applied to other botanicals or natural product mixtures with different biological effects. Based upon this work, continued improvement of these biological measurements, untargeted metabolomics experiments, and methods of complex data set combination is likely to result in even better ways to discover new treatments for disease.

REFERENCES


1. Petrovska BB. 2012. Historical review of medicinal plants' usage. Pharmacognosy Reviews 6:1-5.

2. Oberlies NH, Kroll DJ. 2004. Camptothecin and Taxol: Historic Achievements in Natural Products Research. Journal of Natural Products 67:129-135.

3. Tu Y. 2011. The discovery of artemisinin (qinghaosu) and gifts from Chinese medicine. Nature Medicine 17:1217.

4. Newman DJ, Cragg GM. 2016. Natural Products as Sources of New Drugs from 1981 to 2014. Journal of Natural Products 79:629-661.

5. Smith T, Kawa K, Eckl V, Morton C, Stredney R. 2017. Herbal Supplement Sales in US Increase 7.7% in 2016: Consumer preferences shifting toward ingredients with general wellness benefits, driving growth of adaptogens and digestive health products. Herbalgram.org.

6. Avula B, Wang Y-H, Khan IA. 2012. Quantitative determination of alkaloids from roots of *Hydrastis canadensis* L. and dietary supplements using ultra-performance liquid chromatography with UV detection. Journal of AOAC International 95:1398-405.

7. Tims M. 2016. Botanical Adulterants Bulletin on Adulteration of *Hydrastis canadensis* root and rhizome. American Botanical Council.

8. Davis J, Dressler A. 2013. Goldenseal (*Hydrastis canadensis* L.). Mountain Horticultural Crops Research & Extension Center, Extension.

9. Junio HA, Sy-Cordero AA, Ettefagh KA, Burns JT, Micko KT, Graf TN, Richter SJ, Cannon RE, Oberlies NH, Cech NB. 2011. Synergy-directed fractionation of botanical medicines: a case study with goldenseal (*Hydrastis canadensis*). Journal of Natural Products 74:1621-9.

10. Robbers JE, Tyler VE. 1999. Tyler's Herbs of Choice: The Therapeutic Use of Phytomedicinals. Haworth Herbal Press, Binghamptom, NY.

11. Ettefagh KA, Burns JT, Junio HA, Kaatz GW, Cech NB. 2011. Goldenseal (*Hydrastis canadensis* L.) extracts synergistically enhance the antibacterial activity of berberine via efflux pump inhibition. Planta Medica 77:835-40.

12. Anonymous. 2013. Antibiotic Resistance Threats in the United States, 2013. Centers for Disease Control and Prevention.

13. O'Neill J. 2016. Tackling Drug-Resistant Infections Globally: Final Report and Recommendations. Review on Antimicrobial Resistance.

14. Ventola CL. 2015. The Antibiotic Resistance Crisis: Part 1: Causes and Threats. Pharmacy and Therapeutics 40:277-283.

15. Munita JM, Arias CA. 2016. Mechanisms of Antibiotic Resistance. Microbiology Spectrum 4:1-24.

16. Silver LL. 2011. Challenges of Antibacterial Discovery. Clinical Microbiology Reviews 24:71-109.

17. Anonymous. 2016. A Scientific Roadmap for Antibiotic Discovery: A sustained and robust pipeline of new antibacterial drugs and therapies is critical to preserve public health. The Pew Charitable Trusts.

18. Czaplewski L, Bax R, Clokie M, Dawson M, Fairhead H, Fischetti VA, Foster S, Gilmore BF, Hancock REW, Harper D, Henderson IR, Hilpert K, Jones BV, Kadioglu A, Knowles D, Ólafsdóttir S, Payne D, Projan S, Shaunak S, Silverman J, Thomas CM, Trust TJ, Warn P, Rex JH. 2016. Alternatives to antibiotics—a pipeline portfolio review. The Lancet Infectious Diseases 16:239-251.

19. Escaich S. 2008. Antivirulence as a new antibacterial approach for chemotherapy. Current Opinion in Chemical Biology 12:400-408.

20. Totsika M. 2017. Disarming pathogens: benefits and challenges of antimicrobials that target bacterial virulence instead of growth and viability. Future Medicinal Chemistry 9:267-269.

21. Heras B, Scanlon MJ, Martin JL. 2015. Targeting virulence not viability in the search for future antibacterials. British Journal of Clinical Pharmacology 79:208-215.

22. Todd DA, Parlet CP, Crosby HA, Malone CL, Heilmann KP, Horswill AR, Cech NB. 2017. Signal Biosynthesis Inhibition with Ambuic Acid as a Strategy To Target Antibiotic-Resistant Infections. Antimicrobial Agents and Chemotherapy 61:e00263-17.

23. Todd DA, Zich DB, Ettefagh KA, Kavanaugh JS, Horswill AR, Cech NB. 2016. Hybrid Quadrupole-Orbitrap mass spectrometry for quantitative measurement of quorum sensing inhibition. Journal of Microbiological Methods 127:89-94.

24. Britton ER, Ibberson CB, Horswill AR, Cech NB. 2015. A new mass spectrometry based bioassay for the direct assessment of hyaluronidase activity and inhibition. Journal of Microbiological Methods 119:163-7.

25. Girish KS, Kemparaju K, Nagaraju S, Vishwanath BS. 2009. Hyaluronidase inhibitors: a biological and therapeutic perspective. Current Medicinal Chemistry 16:2261-88.

26. El-Elimat T, Figueroa M, Ehrmann BM, Cech NB, Pearce CJ, Oberlies NH. 2013. High-Resolution MS, MS/MS, and UV Database of Fungal Secondary Metabolites as a Dereplication Protocol for Bioactive Natural Products. Journal of Natural Products 76:1709-1716.

27. Paguigan ND, El-Elimat T, Kao D, Raja HA, Pearce CJ, Oberlies NH. 2017. Enhanced dereplication of fungal cultures via use of mass defect filtering. The Journal of Antibiotics 70:553-561.

28. Wang M, Carver JJ, Phelan VV, Sanchez LM, Garg N, Peng Y, Nguyen DD, Watrous J, Kapono CA, Luzzatto-Knaan T, Porto C, Bouslimani A, Melnik AV, Meehan MJ, Liu W-T, Crusemann M, Boudreau PD, Esquenazi E, Sandoval-Calderon M, Kersten RD, Pace LA, Quinn RA, Duncan KR, Hsu C-C, Floros DJ, Gavilan RG, Kleigrewe K, Northen T, Dutton RJ, Parrot D, Carlson EE, Aigle B, Michelsen CF, Jelsbak L, Sohlenkamp C, Pevzner P, Edlund A, McLean J, Piel J, Murphy BT, Gerwick L, Liaw C-C, Yang Y-L, Humpf H-U, Maansson M, Keyzers RA, Sims AC, Johnson AR, Sidebottom AM, Sedio BE, et al. 2016. Sharing and community curation of mass spectrometry data with Global Natural Products Social Molecular Networking. Nature Biotechnology 34:828-837.

29. Yang JY, Sanchez LM, Rath CM, Liu X, Boudreau PD, Bruns N, Glukhov E, Wodtke A, de Felicio R, Fenner A, Wong WR, Linington RG, Zhang L, Debonsi HM, Gerwick WH, Dorrestein PC. 2013. Molecular networking as a dereplication strategy. Journal of Natural Products 76:1686-99.

30. Brown AR, Ettefagh KA, Todd D, Cole PS, Egan JM, Foil DH, Graf TN, Schindler BD, Kaatz GW, Cech NB. 2015. A Mass Spectrometry-Based Assay for Improved Quantitative Measurements of Efflux Pump Inhibition. PLoS ONE 10:e0124814.

31. Sugimoto M, Kawakami M, Robert M, Soga T, Tomita M. 2012. Bioinformatics Tools for Mass Spectroscopy-Based Metabolomic Data Processing and Analysis. Current Bioinformatics 7:96-108.

32. Rajalahti T, Arneberg R, Berven FS, Myhr K-M, Ulvik RJ, Kvalheim OM. 2009. Biomarker discovery in mass spectral profiles by means of selectivity ratio plot. Chemometrics and Intelligent Laboratory Systems 95:35-48.

33. Rajalahti T, Arneberg R, Kroksveen AC, Berle M, Myhr K-M, Kvalheim OM. 2009. Discriminating variable test and selectivity ratio plot: quantitative tools for interpretation and variable (biomarker) selection in complex spectral or chromatographic profiles. Analytical Chemistry 81:2581-90.

34. Rajalahti T, Kroksveen AC, Arneberg R, Berven FS, Vedeler CA, Myhr K-M, Kvalheim OM. 2010. A multivariate approach to reveal biomarker signatures for disease classification: application to mass spectral profiles of cerebrospinal fluid from patients with multiple sclerosis. Journal of Proteome Research 9:3608-20.

35. Kellogg JJ, Todd DA, Egan JM, Raja HA, Oberlies NH, Kvalheim OM, Cech NB. 2016. Biochemometrics for Natural Products Research: Comparison of Data Analysis Approaches and Application to Identification of Bioactive Compounds. Journal of Natural Products 79:376-386.

36. Chan K-M, Yue GG-L, Li P, Wong EC-W, Lee JK-M, Kennelly EJ, Lau CB-S. 2017. Screening and analysis of potential anti-tumor components from the stipe of *Ganoderma sinense* using high-performance liquid chromatography/time-of-flight mass spectrometry with multivariate statistical tool. Journal of Chromatography A 1487:162-167.

37. Kulakowski DM, Wu S-B, Balick MJ, Kennelly EJ. 2014. Merging bioactivity with liquid chromatography-mass spectrometry-based chemometrics to identify minor immunomodulatory compounds from a Micronesian adaptogen, *Phaleria nisidai*. Journal of Chromatography A 1364:74-82.

38. Li P, AnandhiSenthilkumar H, Wu SB, Liu B, Guo ZY, Fata JE, Kennelly EJ, Long CL. 2016. Comparative UPLC-QTOF-MS-based metabolomics and bioactivities analyses of Garcinia oblongifolia. Journal of Chromatography B: Analytical Technologies in the Biomedical and Life Sciences 1011:179-195.

39. Inui T, Wang Y, Pro SM, Franzblau SG, Pauli GF. 2012. Unbiased evaluation of bioactive secondary metabolites in complex matrices. Fitoterapia 83:1218-25.

40. Qiu F, Cai G, Jaki BU, Lankin DC, Franzblau SG, Pauli GF. 2013. Quantitative purity-activity relationships of natural products: the case of anti-tuberculosis active triterpenes from Oplopanax horridus. Journal of Natural Products 76:413-9.

41. Aziz A-M. 2013. The role of healthcare strategies in controlling antibiotic resistance. British Journal of Nursing (Mark Allen Publishing) 22:1066-74.

42. Ibberson CB, Jones CL, Singh S, Wise MC, Hart ME, Zurawski DV, Horswill AR. 2014. *Staphylococcus aureus* hyaluronidase is a CodY-regulated virulence factor. Infection and Immunity 82:4253-64.

43. Wang Z, Guo C, Xu Y, Liu G, Lu C, Liu Y. 2014. Two novel functions of hyaluronidase from *Streptococcus agalactiae* are enhanced intracellular survival and inhibition of proinflammatory cytokine expression. Infection and Immunity 82:2615-25.

44. Li S, Jedrzejas MJ. 2001. Hyaluronan binding and degradation by *Streptococcus agalactiae* hyaluronate lyase. The Journal of Biological Chemistry 276:41407-16.

45. Starr CR, Engleberg NC. 2006. Role of hyaluronidase in subcutaneous spread and growth of group A streptococcus. Infection and Immunity 74:40-8.

46. Hynes WL, Walton SL. 2000. Hyaluronidases of Gram-positive bacteria. FEMS microbiology letters 183:201-7.

47. Botzki A, Rigden DJ, Braun S, Nukui M, Salmen S, Hoechstetter J, Bernhardt G, Dove S, Jedrzejas MJ, Buschauer A. 2004. L-Ascorbic acid 6-hexadecanoate, a potent hyaluronidase inhibitor. X-ray structure and molecular modeling of enzyme-inhibitor complexes. The Journal of Biological Chemistry 279:45990-7.

48. Spickenreither M, Braun S, Bernhardt G, Dove S, Buschauer A. 2006. Novel 6-O-acylated vitamin C derivatives as hyaluronidase inhibitors with selectivity for bacterial lyases. Bioorganic & Medicinal Chemistry Letters 16:5313-6.

49. Richman PG, Baer H. 1980. A convenient plate assay for the quantitation of hyaluronidase in Hymenoptera venoms. Analytical Biochemistry 109:376-81.

50. Tung JS, Mark GE, Hollis GF. 1994. A Microplate Assay for Hyaluronidase and Hyaluronidase Inhibitors. Analytical Biochemistry 223:149-152.

51. Takahashi T, Ikegami-Kawai M, Okuda R, Suzuki K. 2003. A fluorimetric Morgan–Elson assay method for hyaluronidase activity. Analytical Biochemistry 322:257-263.

52. Reissig JL, Storminger JL, Leloir LF. 1955. A modified colorimetric method for the estimation of N-acetylamino sugars. The Journal of Biological Chemistry 217:959-66.

53. Vercruysse KP, Lauwers AR, Demeester JM. 1995. Kinetic investigation of the action of hyaluronidase on hyaluronan using the Morgan-Elson and neocuproine assays. The Biochemical Journal 310 ( Pt 1):55-9.

54. Harmonisation ICo. 2005. Validation of analytical procedures: text and methodology Q2(R1).1-13.

55. Nguyen HP, Schug KA. 2008. The advantages of ESI-MS detection in conjunction with HILIC mode separations: Fundamentals and applications. Journal of Separation Science 31:1465-80.

56. Hemstrom P, Irgum K. 2006. Hydrophilic interaction chromatography. Journal of Separation Science 29:1784-821.

57. Anonymous. 2017. WHO publishes list of bacteria for which new antibiotics are urgently needed. World Health Organization.

58. Daly SM, Elmore BO, Kavanaugh JS, Triplett KD, Figueroa M, Raja HA, El-Elimat T, Crosby HA, Femling JK, Cech NB, Horswill AR, Oberlies NH, Hall PR. 2015. omega-Hydroxyemodin limits *Staphylococcus aureus* quorum sensing-mediated pathogenesis and inflammation. Antimicrobial Agents and Chemotherapy 59:2223-35.

59. Figueroa M, Jarmusch AK, Raja HA, El-Elimat T, Kavanaugh JS, Horswill AR, Cooks RG, Cech NB, Oberlies NH. 2014. Polyhydroxyanthraquinones as quorum sensing inhibitors from the guttates of *Penicillium restrictum* and their analysis by desorption electrospray ionization mass spectrometry. Journal of Natural Products 77:1351-8.

60. Larkin EA, Carman RJ, Krakauer T, Stiles BG. 2009. *Staphylococcus aureus*: the toxic presence of a pathogen extraordinaire. Current Medicinal Chemistry 16:4003-19.

61. Girish KS, Kemparaju K. 2007. The magic glue hyaluronan and its eraser hyaluronidase: a biological overview. Life Sciences 80:1921-43.

62. Pritchard DG, Lin B, Willingham TR, Baker JR. 1994. Characterization of the group B streptococcal hyaluronate lyase. Archives of Biochemistry and Biophysics 315:431-7.

63. Kolar SL, Kyme P, Tseng CW, Soliman A, Kaplan A, Liang J, Nizet V, Jiang D, Murali R, Arditi M, Underhill DM, Liu GY. 2015. Group B Streptococcus Evades Host Immunity by Degrading Hyaluronan. Cell Host & Microbe 18:694-704.

64. Ibberson CB, Parlet CP, Kwiecinski J, Crosby HA, Meyerholz DK, Horswill AR. 2016. Hyaluronan Modulation Impacts *Staphylococcus aureus* Biofilm Infection. Infection and Immunity 84:1917-29.

65. Li S, Taylor KB, Kelly SJ, Jedrzejas MJ. 2001. Vitamin C inhibits the enzymatic activity of *Streptococcus pneumoniae* hyaluronate lyase. The Journal of Biological Chemistry 276:15125-30.

66. Rigden DJ, Botzki A, Nukui M, Mewbourne RB, Lamani E, Braun S, von Angerer E, Bernhardt G, Dove S, Buschauer A, Jedrzejas MJ. 2006. Design of new benzoxazole-2-thione-derived inhibitors of *Streptococcus pneumoniae* hyaluronan lyase: structure of a complex with a 2-phenylindole. Glycobiology 16:757-65.

67. Wang N, Manabe Y, Sugawara T, Paul NA, Zhao J. 2018. Identification and biological activities of carotenoids from the freshwater alga *Oedogonium intermedium*. Food Chemistry 242:247-255.

68. Hertel W, Peschel G, Ozegowski J-H, Muller P-J. 2006. Inhibitory effects of triterpenes and flavonoids on the enzymatic activity of hyaluronic acid-splitting enzymes. Archiv der Pharmazie 339:313-8.

69. Paguigan ND, Rivera-Chávez J, Stempin J, Augustinovic M, Noras AI, Raja HA, Todd DA, Triplett KD, Day CS, Figueroa M, Hall PR, Cech NB, Oberlies NH. 2018. Prenylated Xanthenes Inhibit Bacterial Quorum Sensing In progress.

70. Tenover FC, McDougal LK, Goering RV, Killgore G, Projan SJ, Patel JB, Dunman PM. 2006. Characterization of a Strain of Community-Associated Methicillin-Resistant *Staphylococcus aureus* Widely Disseminated in the United States. Journal of Clinical Microbiology 44:108-118.

71. Boles BR, Thoendel M, Roth AJ, Horswill AR. 2010. Identification of genes involved in polysaccharide-independent *Staphylococcus aureus* biofilm formation. PloS One 5:e10146.

72. Cech NB, Junio HA, Ackermann LW, Kavanaugh JS, Horswill AR. 2012. Quorum quenching and antimicrobial activity of goldenseal (*Hydrastis canadensis*) against methicillin-resistant *Staphylococcus aureus* (MRSA). Planta Medica 78:1556-61.

73. Bolukaoto JY, Monyama CM, Chukwu MO, Lekala SM, Nchabeleng M, Maloba MRB, Mavenyengwa RT, Lebelo SL, Monokoane ST, Tshepuwane C, Moyo SR. 2015. Antibiotic resistance of *Streptococcus agalactiae* isolated from pregnant women in Garankuwa, South Africa. BMC Research Notes 8:364.

74. Fair RJ, Tor Y. 2014. Antibiotics and bacterial resistance in the 21st century. Perspectives in Medicinal Chemistry 6:25-64.

75. Faqi AS. 2017. Chapter 1 - Introduction, p 1-4, A Comprehensive Guide to Toxicology in Nonclinical Drug Development (Second Edition) doi:https://doi.org/10.1016/B978-0-12-803620-4.00001-3. Academic Press, Boston.

76. Frey-Klett P, Burlinson P, Deveau A, Barret M, Tarkka M, Sarniguet A. 2011. Bacterial-fungal interactions: hyphens between agricultural, clinical, environmental, and food microbiologists. Microbiology and Molecular Biology Reviews 75:583-609.

77. Wessels M, Benedi V-J, Kasper L, Heggen L, Rubens C. 1991. Type III capsule and virulence of group B streptococci. American Society for Microbiology, Washington, DC.

78. Anonymous. 2015. Methods for Dilution Antimicrobial Susceptibility Tests for Bacteria that Grow Aerobically—Tenth Edition: Approved Standard M7-A10. Clinical and Laboratory Standards Institute, Wayne, PA.

79. Montanari MP, Mingoia M, Marchetti F, Varaldo PE. 1999. In vitro activity of levofloxacin against gram-positive bacteria. Chemotherapy 45:411-7.

80. Amin AH, Subbaiah TV, Abbasi KM. 1969. Berberine sulfate: antimicrobial activity, bioassay, and mode of action. Canadian Journal of Microbiology 15:1067-76.

81. Foster S. 2000. The future of goldenseal. http://www.stevenfoster.com/education/monograph/goldenseal.html Accessed April.

82. McNamara CE, Perry NB, Follett JM, Parmenter GA, Douglas JA. 2004. A new glucosyl feruloyl quinic acid as a potential marker for roots and rhizomes of goldenseal, *Hydrastis canadensis*. Journal of Natural Products 67:1818-22.

83. Le PM, McCooeye M, Windust A. 2014. Application of UPLC-QTOF-MS in MS(E) mode for the rapid and precise identification of alkaloids in goldenseal (*Hydrastis canadensis*). Analytical and Bioanalytical Chemistry 406:1739-49.

84. Douglas JA, Follett JM, Parmenter GA, Sansom CE, Perry NB, Littler RA. 2010. Seasonal variation of biomass and bioactive alkaloid content of goldenseal, *Hydrastis canadensis*. Fitoterapia 81:925-8.

85. Knight SE. 1999. Goldenseal (*Hydrastis canadensis*) versus Penicillin: A Comparison of Effects on *Staphylococcus aureus*, *Streptococcus pyogenes*, and *Pseudomonas aeruginosa*. Bios 70:3-10.

86. Scazzocchio F, Cometa MF, Tomassini L, Palmery M. 2001. Antibacterial activity of *Hydrastis canadensis* extract and its major isolated alkaloids. Planta Medica 67:561-4.

87. Hwang BY, Roberts SK, Chadwick LR, Wu CD, Kinghorn AD. 2003. Antimicrobial constituents from goldenseal (the Rhizomes of *Hydrastis canadensis*) against selected oral pathogens. Planta Medica 69:623-7.

88. Fajardo V, Elango V, Cassels BK, Shamma M. 1982. Chilenine : an isoindolobenzazepine alkaloid. Tetrahedron Letters 23:39-42.

89. Wollenweber E, Wehde R, Dorr M, Lang G, Stevens JF. 2000. C-methyl-flavonoids from the leaf waxes of some Myrtaceae. Phytochemistry 55:965-70.

90. Doskotch RW, Schiff PL, Beal JL. 1969. Alkaloids of Thalictrum. X. Two new alkaloids from T. minus var. adiantifolium: noroxyhydrastinine and thalifoline. Tetrahedron 25:469-75.

91. Zhang G-L, Rücker G, Breitmaier E, Mayer R. 1995. Alkaloids from *Hypecoum leptocarpum* Phytochemistry 40:1813-1816.

92. Klötzer W, Oberhänsli WE. 1973. Die struktur des sogenannten anhydro-N-oxy-nornarcein. Helvetica Chimica Acta 56:223-224.

93. Qiu F, Zhu Z, Kang N, Piao S, Qin G, Yao X. 2008. Isolation and identification of urinary metabolites of berberine in rats and humans. Drug Metabolism and Disposition: The Biological Fate of Chemicals 36:2159-65.

94. Malhotra S, Taneja SC, Dhar KL. 1989. Minor alkaloid from *Coscinium fenestratum*. Phytochemistry 28:1998-1999.

95. Seger C, Sturm S, Strasser E-M, Ellmerer E, Stuppner H. 2004. 1H and 13C NMR signal assignment of benzylisoquinoline alkaloids from *Fumaria officinalis* L. (Papaveraceae). Magnetic Resonance in Chemistry 42:882-6.

96. Pinho PMM, Pinto MMM, Kijjoa A, Pharadai K, Diaz JG, Herz W. 1992. Protoberberine alkaloids from *Coscinium fenestratum*. Phytochemistry 31:1403-1407.

97. Singh S, Singh TD, Singh VP, Pandey VB. 2010. Quaternary alkaloids of *Argemone mexicana*. Pharmaceutical Biology 48:158-60.

98. Tsimogiannis D, Samiotaki M, Panayotou G, Oreopoulou V. 2007. Characterization of flavonoid subgroups and hydroxy substitution by HPLC-MS/MS. Molecules 12:593-606.

99. Kaatz GW. 2005. Bacterial efflux pump inhibition. Current Opinion in Investigational Drugs 6:191-8.

100. McCaig LF, McDonald LC, Mandal S, Jernigan DB. 2006. *Staphylococcus aureus*-associated skin and soft tissue infections in ambulatory care. Emerging Infectious Diseases 12:1715-23.

101. Hopfer U, Lehninger AL, Thompson TE. 1968. Protonic conductance across phospholipid bilayer membranes induced by uncoupling agents for oxidative phosphorylation. Proceedings of the National Academy of Sciences of the United States of America 59:484-90.

102. Kaatz GW, Seo SM. 1995. Inducible NorA-mediated multidrug resistance in *Staphylococcus aureus*. Antimicrobial Agents and Chemotherapy 39:2650-5.

103. Gilbert B, Alves LF. 2003. Synergy in plant medicines. Current Medicinal Chemistry 10:13-20.

104. Wagner H, Ulrich-Merzenich G. 2009. Synergy research: approaching a new generation of phytopharmaceuticals. Phytomedicine: International Journal of Phytotherapy and Phytopharmacology 16:97-110.

105. Rasoanaivo P, Wright CW, Willcox ML, Gilbert B. 2011. Whole plant extracts versus single compounds for the treatment of malaria: synergy and positive interactions. Malaria Journal 10 Suppl 1:S4.

106. Stermitz FR, Lorenz P, Tawara JN, Zenewicz LA, Lewis K. 2000. Synergy in a medicinal plant: antimicrobial action of berberine potentiated by 5'-methoxyhydnocarpin, a multidrug pump inhibitor. Proceedings of the National Academy of Sciences of the United States of America 97:1433-7.

107. Kurita KL, Glassey E, Linington RG. 2015. Integration of high-content screening and untargeted metabolomics for comprehensive functional annotation of natural product libraries. Proceedings of the National Academy of Sciences of the United States of America 112:11999-12004.

108. Martens H, Bruun SW, Adt I, Sockalingum GD, Kohler A. 2006. Pre-processing in biochemometrics: correction for path-length and temperature effects of water in FTIR bio-spectroscopy by EMSC. Journal of Chemometrics 20:402-417.

109. Wilcox RR. 2012. Introduction to Robust Estimation and Hypothesis Testing, Third Edition (Statistical Modeling and Decision Science). Academic Press.

110. Wiklund S, Johansson E, Sjostrom L, Mellerowicz EJ, Edlund U, Shockcor JP, Gottfries J, Moritz T, Trygg J. 2008. Visualization of GC/TOF-MS-based metabolomics data for identification of biochemically interesting compounds using OPLS class models. Analytical Chemistry 80:115-22.

111. van Vuuren S, Viljoen A. 2011. Plant-based antimicrobial studies--methods and approaches to study the interaction between natural products. Planta Medica 77:1168-82.

112. McGuffin M, Hobbs C, Upton R, Goldberg A. American Herbal Products Association's Botanical Safety Handbook. CRC Press, Boca Raton, FL.

113. Cech NB, Junio HA, Ackermann LW, Kavanaugh JS, Horswill AR. 2012. Quorum quenching and antimicrobial activity of goldenseal (Hydrastis canadensis) against methicillin-resistant Staphylococcus aureus (MRSA). Planta Med 78:1556-61.

114. Leyte-Lugo M, Britton ER, Foil DH, Brown AR, Todd DA, Rivera-Chávez J, Oberlies NH, Cech NB. 2017. Secondary metabolites from the leaves of the medicinal plant goldenseal (*Hydrastis canadensis*). Phytochemistry Letters 20:54-60.

115. Orhana I, Ozcelik B, Karaoglu T, Sener B. 2007. Antiviral and antimicrobial profiles of selected isoquinoline alkaloids from *Fumaria* and *Corydalis* species. Zeitschrift fur Naturforschung C, Journal of Biosciences 62:19-26.

116. Wu WN, Beal JL, Mitscher LA, Salman KN, Patil P. 1976. Alkaloids of Thalictrum. XV. Isolation and identification of the hypotensive alkaloids of the root of *Thalictrum lucidum*. Lloydia 39:204-12.

117. Gentry EJ, Jampani HB, Keshavarz-Shokri A, Morton MD, Velde DV, Telikepalli H, Mitscher LA, Shawar R, Humble D, Baker W. 1998. Antitubercular natural products: berberine from the roots of commercial *Hydrastis canadensis* powder. Isolation of inactive 8-oxotetrahydrothalifendine, canadine, beta-hydrastine, and two new quinic acid esters, hycandinic acid esters-1 and -2. Journal of Natural Products 61:1187-93.

118. Galeffi C, Cometa MF, Tomassini L, Nicoletti M. 1997. Canadinic acid: an alkaloid from *Hydrastis canadensis*. Planta Medica 63:194.

119. Wang L, Zhang SY, Chen L, Huang XJ, Zhang QW, Jiang RW, Yao F, Ye WC. 2014. New enantiomeric isoquinoline alkaloids from *Coptis chinensis*. Phytochemistry Letters 7:89-92.

120. Messana I, La Bua R, Galeffi C. 1981. The alkaloids of *Hydrastis canadensis* L. (Ranunculaceae). Two new alkaloids: hydrastidine and isohydrastidine. Gazzetta Chimica Italiana 110:539-543.

121. Rosa MC. 1939. Determination of hydrastin in extracts of *Hydrastis canadensis*. Revista da Associacao Brasileira de Farmaceuticos 20:191-196.

122. Weber HA, Zart MK, Hodges AE, White KD, Barnes SM, Moody LA, Clark AP, Harris RK, Overstreet JD, Smith CS. 2003. Method validation for determination of alkaloid content in goldenseal root powder. Journal of AOAC International 86:476-83.

123. Khan IA, Mirza ZM, Kumar A, Verma V, Qazi GN. 2006. Piperine, a phytochemical potentiator of ciprofloxacin against *Staphylococcus aureus*. Antimicrobial Agents and Chemotherapy 50:810-2.

124. Morel C, Stermitz FR, Tegos G, Lewis K. 2003. Isoflavones as potentiators of antibacterial activity. Journal of Agricultural and Food Chemistry 51:5677-9.

125. Guz NR, Stermitz FR, Johnson JB, Beeson TD, Willen S, Hsiang J, Lewis K. 2001. Flavonolignan and flavone inhibitors of a *Staphylococcus aureus* multidrug resistance pump: structure-activity relationships. Journal of Medicinal Chemistry 44:261-8.

126. Stermitz FR, Tawara-Matsuda J, Lorenz P, Mueller P, Zenewicz L, Lewis K. 2000. 5'-Methoxyhydnocarpin-D and pheophorbide A: Berberis species components that potentiate berberine growth inhibition of resistant *Staphylococcus aureus*. Journal of Natural Products 63:1146-9.

127. Costa EV, Marques FA, Pinheiro MLB, Vaz NP, Duarte MCT, Delarmelina C, Braga RM, Maia BHLNS. 2009. 7,7-Dimethylaporphine alkaloids from the stem of *Guatteriopsis friesiana*. Journal of Natural Products 72:1516-9.

128. Qiu Y, Yoshikawa M, Li Y, Dou D, Pei Y, Chen Y. 2000. A study on chemical constituents of the stems of *Opuntia dillenii* (Ker-Gawl.) Haw. Journal of Shenyang Pharmaceutical University 17:267-268.

129. Kaatz GW, Seo SM. 1995. Inducible NorA-mediated multidrug resistance in Staphylococcus aureus. Antimicrob Agents Chemother 39:2650-5.

130. Nargotra A, Koul S, Sharma S, Khan IA, Kumar A, Thota N, Koul JL, Taneja SC, Qazi GN. 2009. Quantitative structure-activity relationship (QSAR) of aryl alkenyl amides/imines for bacterial efflux pump inhibitors. European Journal of Medicinal Chemistry 44:229-38.

131. Pluskal T, Castillo S, Villar-Briones A, Oresic M. 2010. MZmine 2: modular framework for processing, visualizing, and analyzing mass spectrometry-based molecular profile data. BMC Bioinformatics 11:395.

132. Kvalheim OM, Chan H-y, Benzie IFF, Szeto Y-t, Tzang AH-c, Mok DK-w, Chau F-t. 2011. Chromatographic profiling and multivariate analysis for screening and quantifying the contributions from individual components to the bioactive signature in natural products. Chemometrics and Intelligent Laboratory Systems 107:98-105.

# APPENDIX A

## SUPPLEMENTARY TABLES

**Table S1. Mass spectral data for isolated compounds in the positive ion mode.**

**Table S2. Mass spectral data for isolated compounds in the negative ion mode.**

**Table S1. Mass spectral data for isolated compounds in the positive ion mode.**

| Compound | Molecular Formula | Retention Time | $[M+H]^+$ *m/z*[a] | Fragments[b] and Intensities |
|---|---|---|---|---|
| **10** | $C_{11}H_{12}O_6$ | 4.61 | 241.0702 | 209.0440(100) |
| **11** | $C_{19}H_{18}O_7$ | 5.95 | 359.1118 | 359.1116(84)<br>344.0882(100)<br>329.0648(47)<br>301.0700(26)<br>273.0750(28)<br>195.0648(42) |
| **12** | $C_{20}H_{17}NO_7$ | 5.06 | 384.1073 | 384.0964(20)<br>366.0964(48)<br>338.1014(54)<br>322.0703(25)<br>294.0754(30)<br>149.0595(100)<br>199.0490(60)<br>91.0541(63) |
| **13** | $C_{17}H_{16}O_5$ | 5.87 | 301.1069 | 301.1063(10)<br>181.0492(100)<br>147.0438(60)<br>119.0489(20) |
| **14** | $C_{18}H_{18}O_5$ | 5.92 | 315.1217 | 315.1206(8)<br>299.0858(7)<br>195.0648(100)<br>147.0437(50)<br>119.0541(16) |
| **15** | $C_{10}H_9NO_3$ | 4.31 | 192.0651 | 192.0650(100)<br>174.0546(17)<br>149.0594(90)<br>119.0489(27)<br>91.05423 (18) |
| **16** | $C_{11}H_{11}NO_3$ | 4.70 | 206.0809 | 206.0806(92)<br>149.0594(100)<br>119.0489(32)<br>91.05408(26) |
| **17** | $C_{21}H_{21}NO_7$ | 5.84 | 400.1388 | 335.0902(27)<br>320.0657(38)<br>311.0904(100)<br>296.0670(60)<br>253.0851(36)<br>193.0491(60)<br>190.0585(93) |

[a]The reported values for *m/z* of the $[M+H]^+$ ion are all within 5 ppm of the calculated *m/z* for the molecular formula indicated.
[b] *m/z* values of the fragment ions are measured with a mass error of ≤ 10

**Table S1 (cont.). Mass spectral data for isolated compounds in the positive ion mode (continued).**

| Compound | Molecular Formula | Retention Time | $[M+H]^+$ *m/z*[a] | Fragments[b] and Intensities |
|---|---|---|---|---|
| **18** | $C_{20}H_{18}NO_4$ | 4.74 | 336.1225 | 336.1219(36)<br>321.0982(50)<br>320.0908(100)<br>307.0814(12)<br>306.0752(29)<br>304.0959(22)<br>292.0959(82) |
| **19** | $C_{20}H_{21}NO_4$ | 4.52 | 340.1540 | 340.1535(6)<br>176.0702(100)<br>149.0594(10) |
| **20** | $C_{18}H_{16}O_5$ | 6.15 | 313.1066 | 313.1061(80)<br>298.0826(100)<br>297.0749(38) |
| **21** | $C_{17}H_{14}O_5$ | 5.82 | 299.0911 | 299.0906(100)<br>284.0671(54)<br>256.0722(15) |
| **22** | $C_{17}H_{14}O_5$ | 5.93 | 299.09140 | 299.0906(100)<br>284.0670(26)<br>283.0594(20) |
| **23** | $C_{21}H_{21}NO_6$ | 4.26 | 384.14389 | 323.0905(67)<br>293.0798(76)<br>265.0852(35)<br>190.0859(100) |
| **24** | $C_{20}H_{19}NO_5$ | 5.62 | 354.13287 | 354.1327(26)<br>339.1093(11)<br>176.0703(100)<br>164.0464(42) |
| **25** | $C_{19}H_{17}NO_5$ | 5.38 | 340.11725 | 340.1172(17)<br>325.0936(18)<br>176.0703(100)<br>150.0309(12) |
| **26** | $C_{20}H_{17}NO_5$ | 5.68 | 352.11749 | 352.1170(6)<br>337.0935(39)<br>322.0702(100)<br>308.0910(10)<br>294.0753(23) |

[a]The reported values for *m/z* of the $[M+H]^+$ ion are all within 5 ppm of the calculated *m/z* for the molecular formula indicated.
[b] *m/z* values of the fragment ions are measured with a mass error of ≤ 10

**Table S2. Mass spectral data for isolated compounds in the negative ion mode.**

| Compound | Molecular Formula | Retention Time | $[M-H]^-$ *m/z*[a] | Fragments[b] and Intensities |
|---|---|---|---|---|
| **10** | $C_{11}H_{12}O_6$ | 4.76 | 239.0562 | 163.0401(30)<br>148.0167(100)<br>133.0296(20)<br>123.0453(20)<br>108.0218(28) |
| **13** | $C_{17}H_{16}O_5$ | 5.97 | 299.0923 | 179.035(30)<br>164.0116(18)<br>119.0502(100)<br>93.0346(11)<br>79.019(9) |
| **20** | $C_{18}H_{16}O_5$ | 6.09 | 311.0923 | 311.0926(4)<br>296.0689(100)<br>295.0612(18) |
| **21** | $C_{17}H_{14}O_5$ | 5.92 | 297.0764 | 297.0767(12)<br>283.0567(8)<br>282.0533(100)<br>281.0455(16) |
| **22** | $C_{17}H_{14}O_5$ | 6.03 | 297.0766 | 297.0767(12)<br>283.0567(8)<br>282.0533(100)<br>281.0456(15) |

[a] The reported values for *m/z* of the $[M+H]^+$ ion are all within 5 ppm of the calculated *m/z* for the molecular formula indicated.
[b] *m/z* values of the fragment ions are measured with a mass error of ≤ 10

APPENDIX B

SUPPLEMENTARY FIGURES

**Figure S1. Time dependent reactions that display the relative amount of disaccharides produced as a function of time with a logarithmic fit of $y = 4 \times 10^6 \ln(x) - 6 \times 10^6$ ($R^2 = 0.8946$)**

**Figure S2. Fractionation scheme: *H. canadensis* leaves were percolated in MeOH, subjected to liquid/liquid partitioning. The compounds were isolated using three subsequent stages of chromatography, two rounds of flash chromatography over silica gel and a preparatory scale HPLC**

**Figure S3. $^1$H NMR spectrum (400 MHz, $CDCl_3$) of 3,4-dimethoxy-2-(methoxycarbonyl)benzoic acid (10)**

**Figure S4. $^{13}$C NMR spectrum (100 MHz, $CDCl_3$) of 3,4-dimethoxy-2-(methoxycarbonyl)benzoic acid (10)**

**Figure S5. HSQC spectrum of 3,4-dimethoxy-2-(methoxycarbonyl)benzoic acid (10)**

**Figure S6. HMBC spectrum of 3,4-dimethoxy-2-(methoxycarbonyl)benzoic acid (10)**

**Figure S7. COSY spectrum of 3,4-dimethoxy-2-(methoxycarbonyl)benzoic acid (10)**

**Figure S8. $^1$H NMR spectrum (400 MHz, $CDCl_3$) of 3,5,3´-trihydroxy-7,4´-dimethoxy-6,8-*C*-dimethyl-flavone (11)**

**Figure S9. $^{13}$C NMR spectrum (100 MHz, $CDCl_3$) of 3,5,3´-trihydroxy-7,4´-dimethoxy-6,8-*C*-dimethyl-flavone (11)**

**Figure S10. HSQC spectrum of 3,5,3´-trihydroxy-7,4´-dimethoxy-6,8-*C*-dimethyl-flavone (11)**

**Figure S11. HMBC spectrum of 3,5,3´-trihydroxy-7,4´-dimethoxy-6,8-*C*-dimethyl-flavone (11)**

**Figure S12. COSY spectrum of 3,5,3´-trihydroxy-7,4´-dimethoxy-6,8-*C*-dimethyl-flavone (11)**

**Figure S13. $^1$H NMR spectrum (400 MHz, $CDCl_3$) of chilenine (12)**

**Figure S14. $^{13}$C NMR spectrum (100 MHz, $CDCl_3$) of chilenine (12)**

**Figure S33. HMBC NMR spectra of 38**

**Figure S34. COSY NMR spectra of 38**

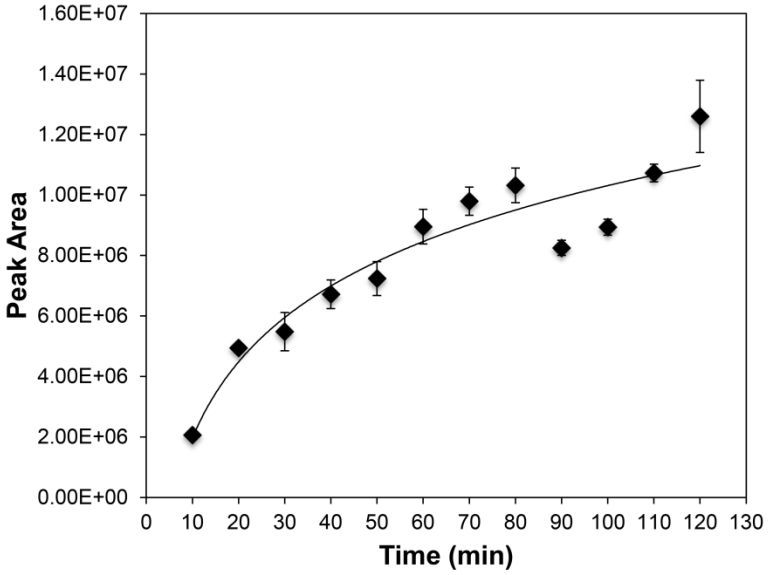


**Figure S1. Time dependent reactions that display the relative amount of disaccharides produced as a function of time with a logarithmic fit of $y = 4 \times 10^6 \ln(x) - 6 \times 10^6$ ($R^2 = 0.8946$).** The reaction time of 15 min was selected for this assay on the basis of these data.

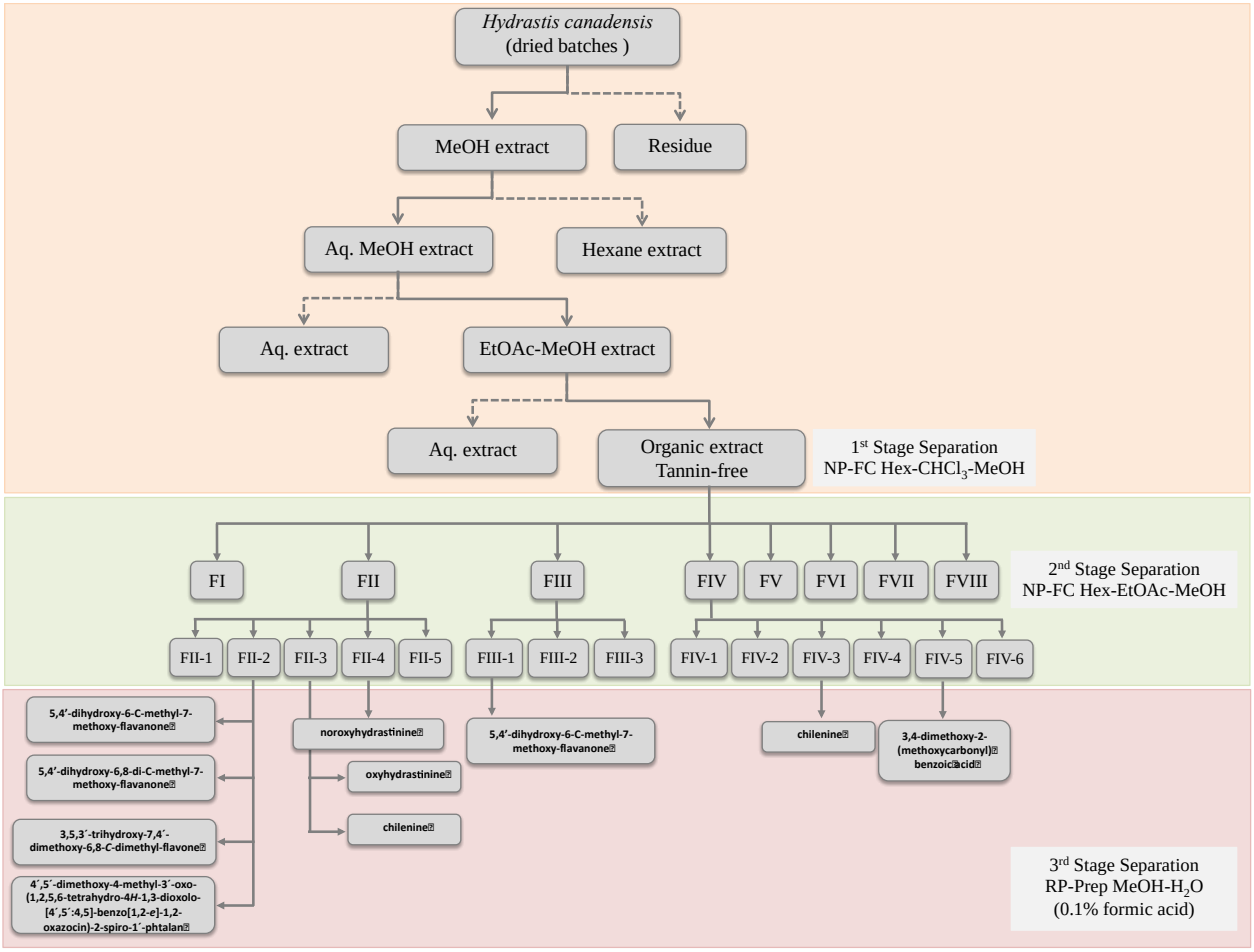


**Figure S2. Fractionation scheme: *H. canadensis* leaves were percolated in MeOH, subjected to liquid/liquid partitioning**. The compounds were isolated using three subsequent stages of chromatography, two rounds of flash chromatography over silica gel and a preparatory scale HPLC.

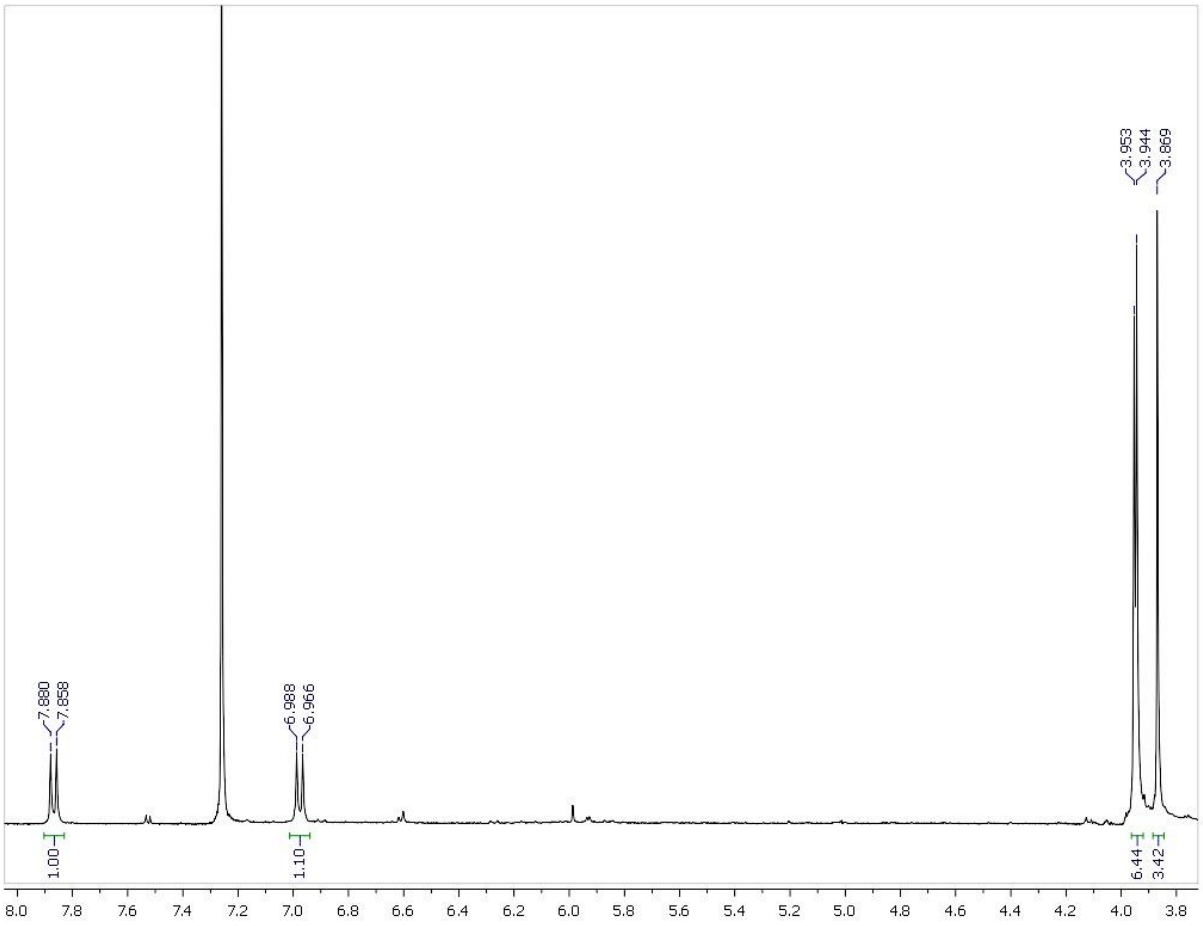


**Figure S3. $^{1}$H NMR spectrum (400 MHz, $CDCl_3$) of 3,4-dimethoxy-2-(methoxycarbonyl)benzoic acid (10).**

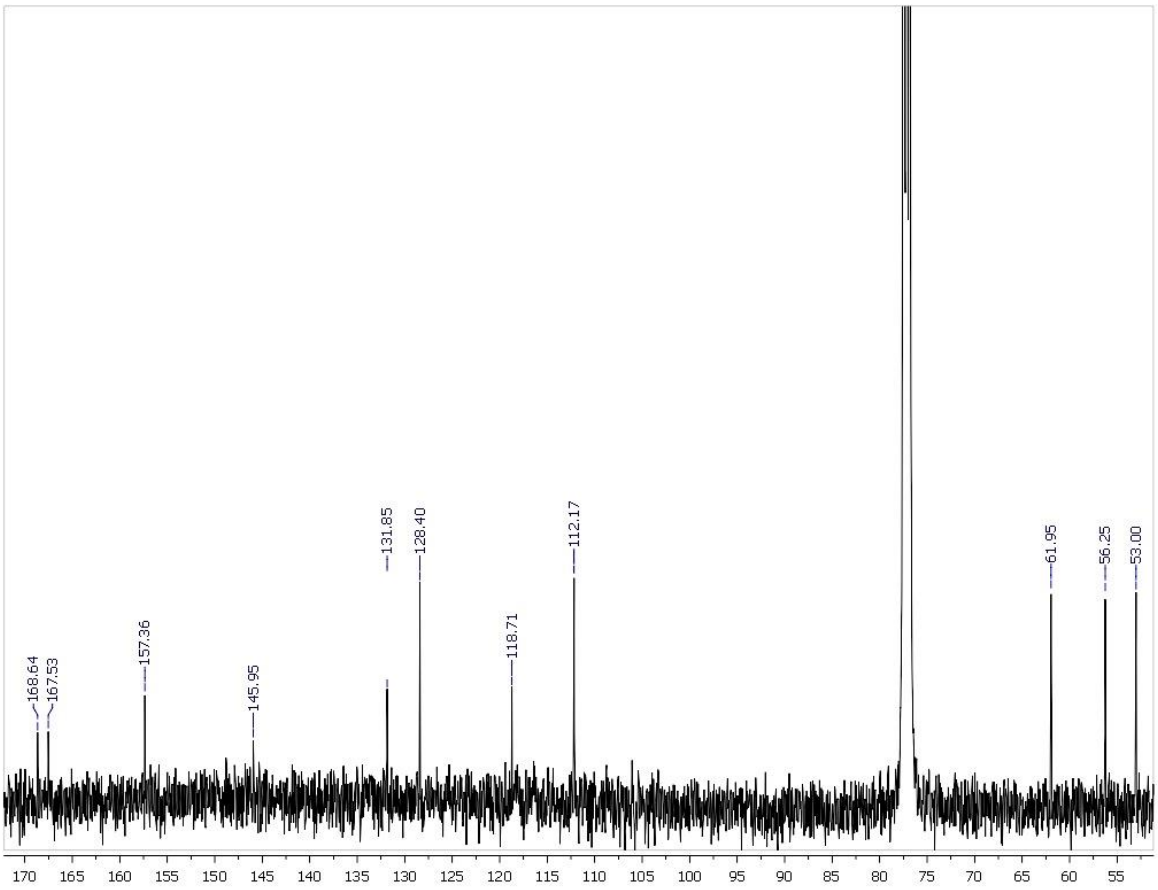


**Figure S4. $^{13}$C NMR spectrum (100 MHz, $CDCl_3$) of 3,4-dimethoxy-2-(methoxycarbonyl)benzoic acid (10).**

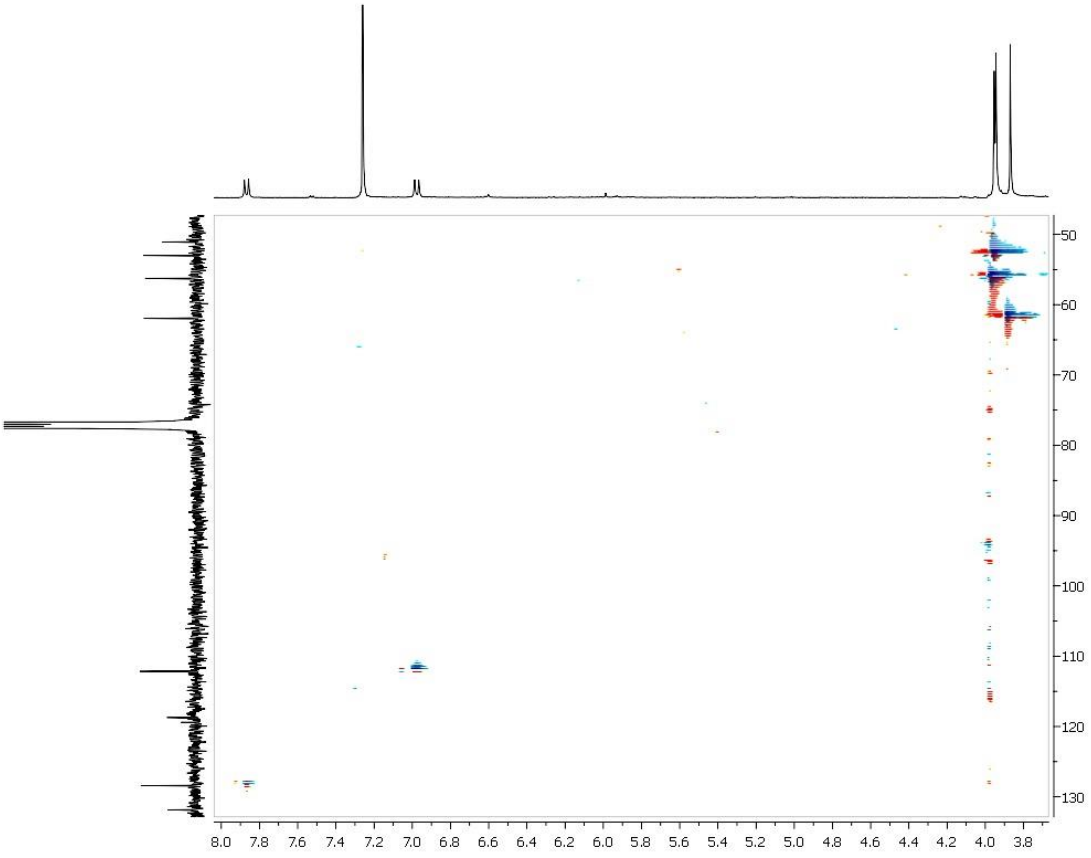


**Figure S5. HSQC spectrum of 3,4-dimethoxy-2-(methoxycarbonyl)benzoic acid (10).**

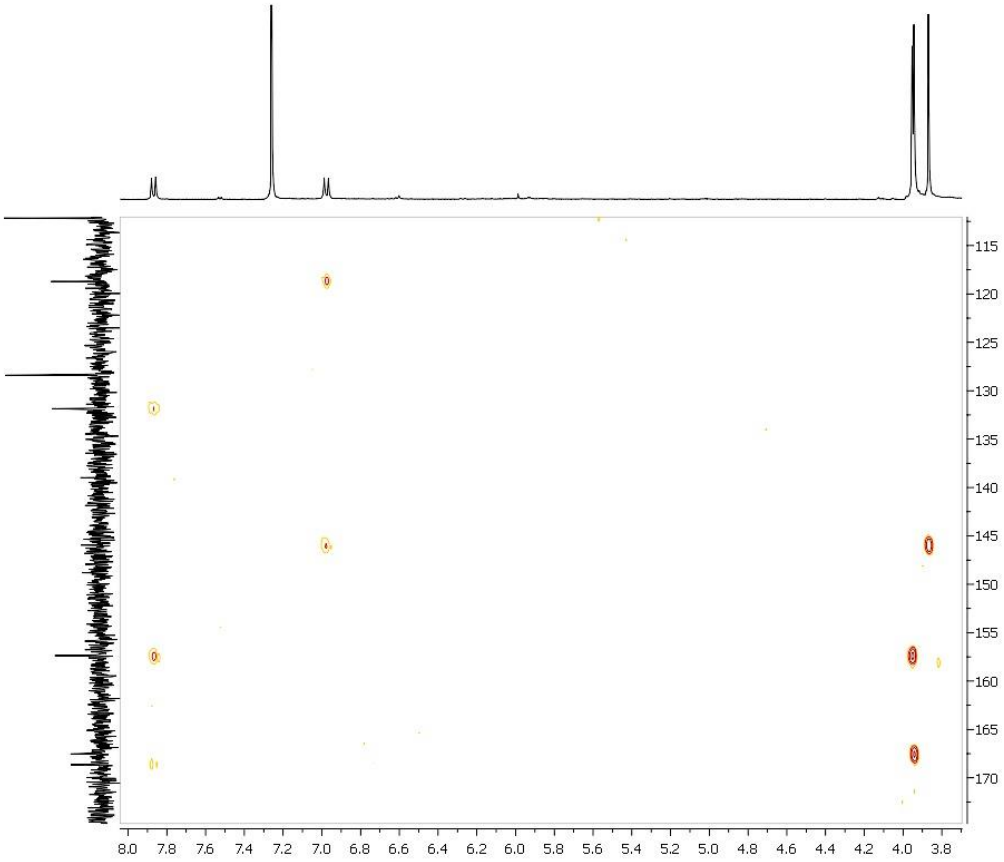


**Figure S6. HMBC spectrum of 3,4-dimethoxy-2-(methoxycarbonyl)benzoic acid (10).**

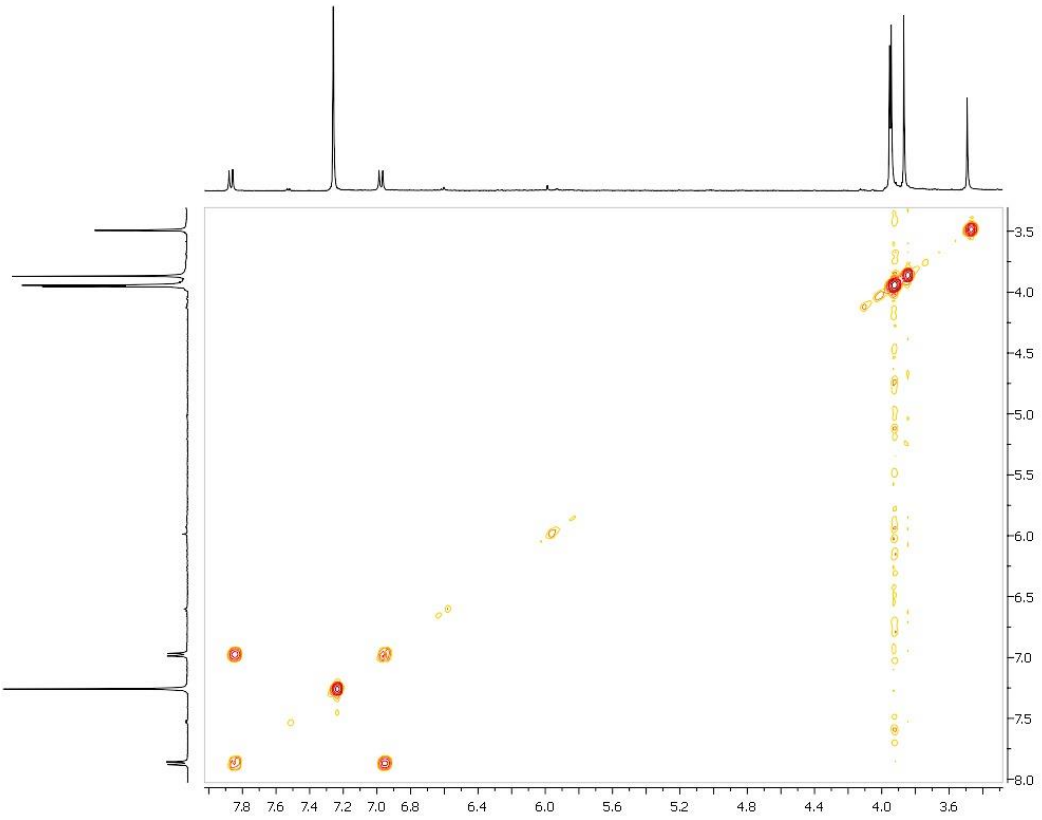


**Figure S7. COSY spectrum of 3,4-dimethoxy-2-(methoxycarbonyl)benzoic acid (10).**

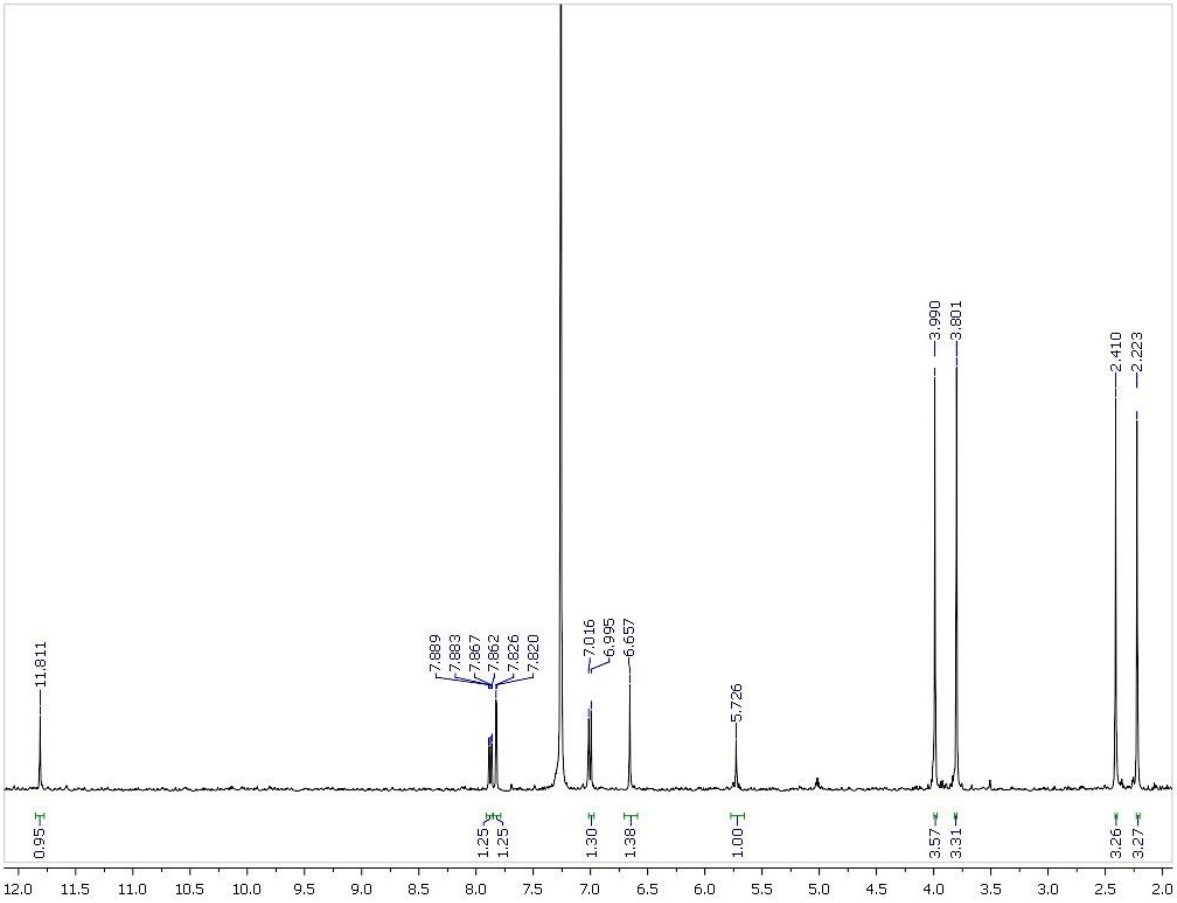


**Figure S8. $^{1}$H NMR spectrum (400 MHz, $CDCl_3$) of 3,5,3´-trihydroxy-7,4´-dimethoxy-6,8-*C*-dimethyl-flavone (11).**

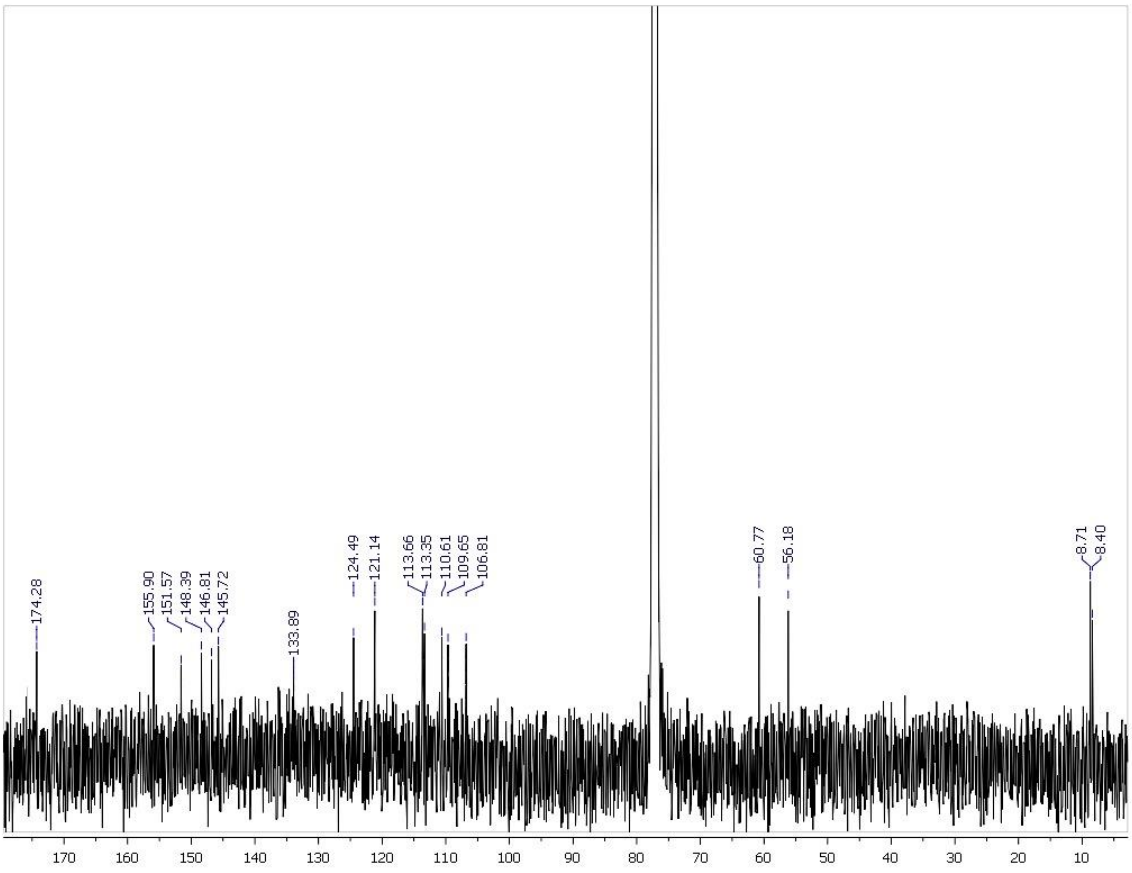


**Figure S9. $^{13}$C NMR spectrum (100 MHz, $CDCl_3$) of 3,5,3´-trihydroxy-7,4´-dimethoxy-6,8-*C*-dimethyl-flavone (11).**

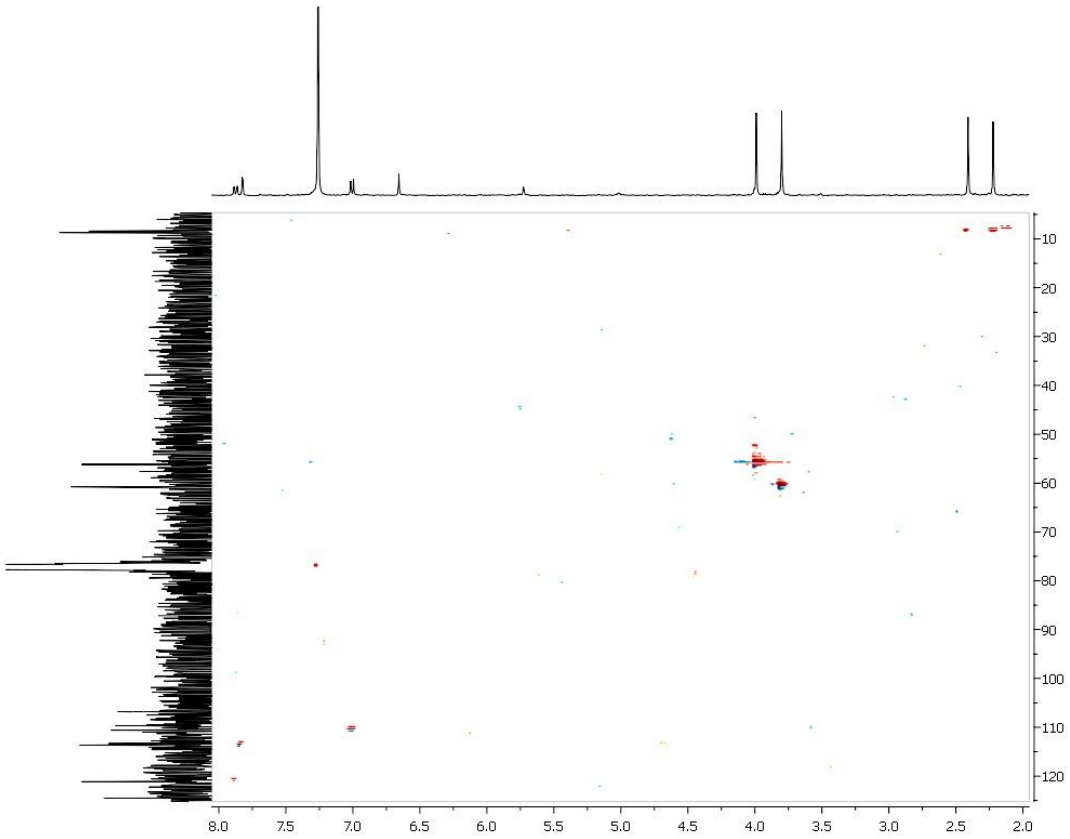


**Figure S10. HSQC spectrum of 3,5,3´-trihydroxy-7,4´-dimethoxy-6,8-*C*-dimethyl-flavone (11).**

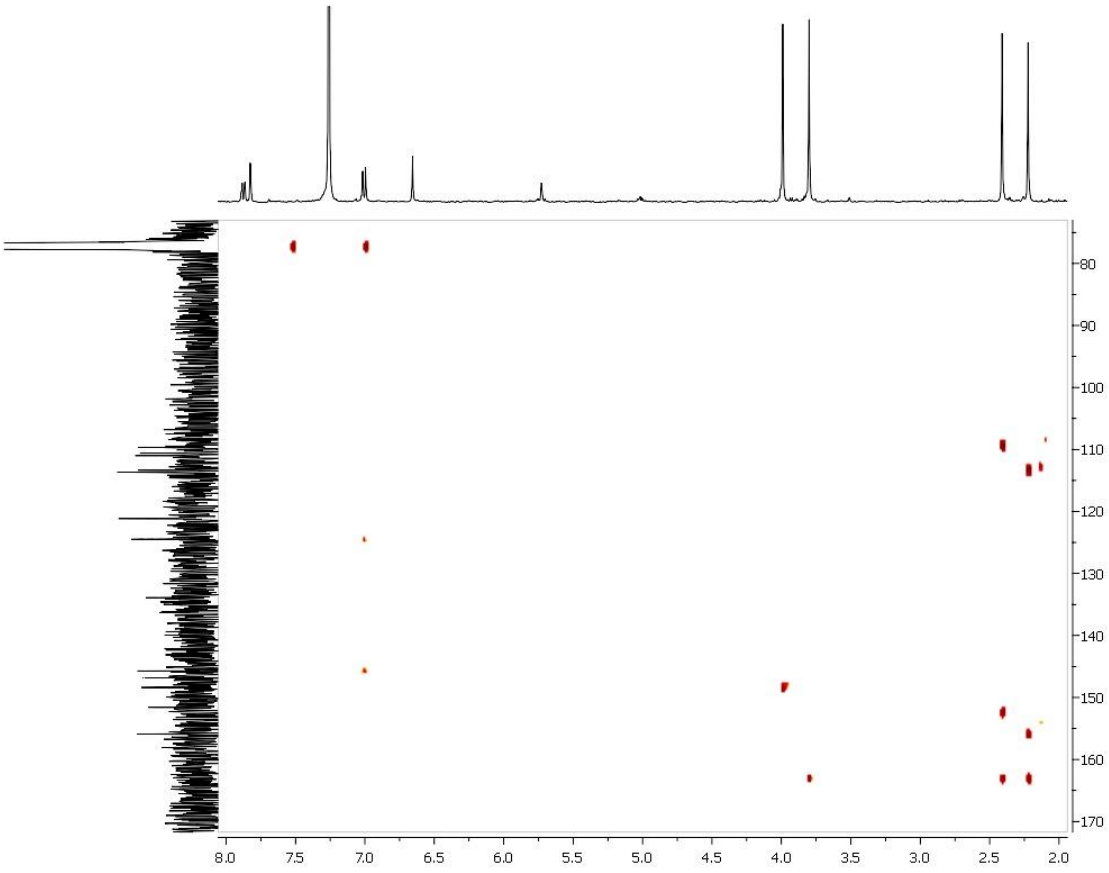


**Figure S11. HMBC spectrum of 3,5,3´-trihydroxy-7,4´-dimethoxy-6,8-*C*-dimethyl-flavone (11).**

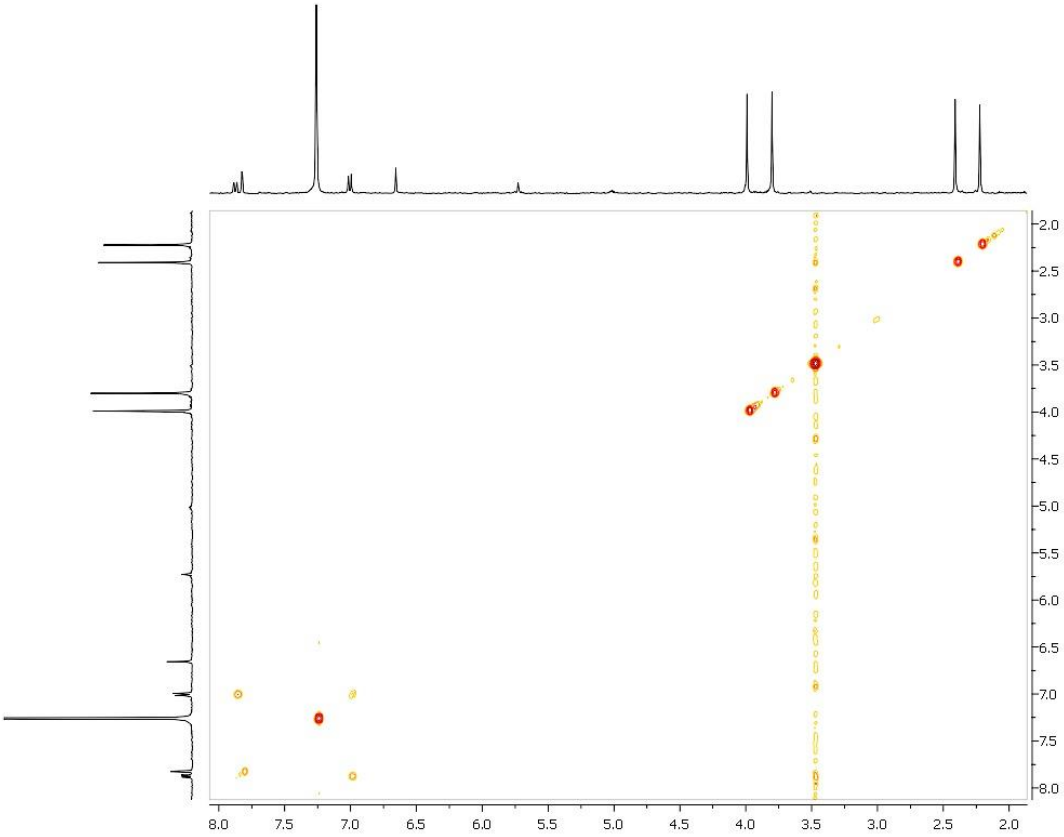


**Figure S12. COSY spectrum of 3,5,3´-trihydroxy-7,4´-dimethoxy-6,8-C-dimethyl-flavone (11).**

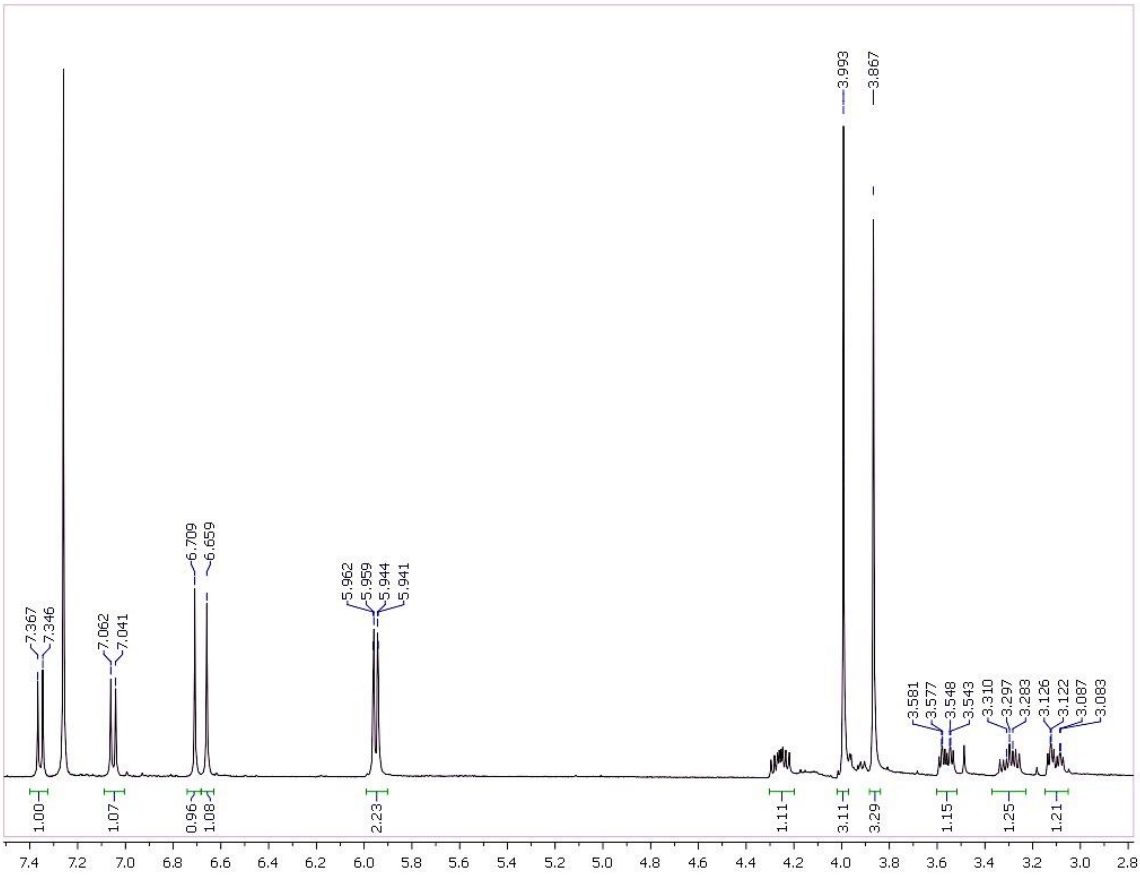


**Figure S13. $^{1}$H NMR spectrum (400 MHz, $CDCl_3$) of chilenine (12).**

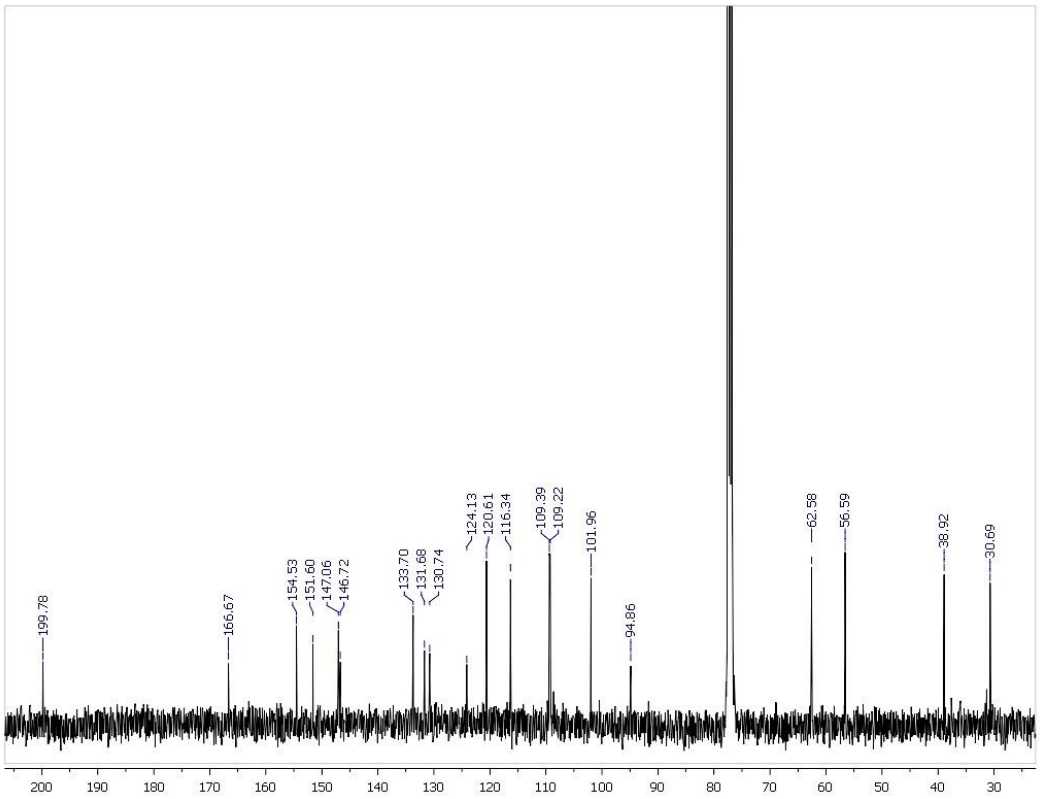


**Figure S14. $^{13}$C NMR spectrum (100 MHz, $CDCl_3$) of chilenine (12).**

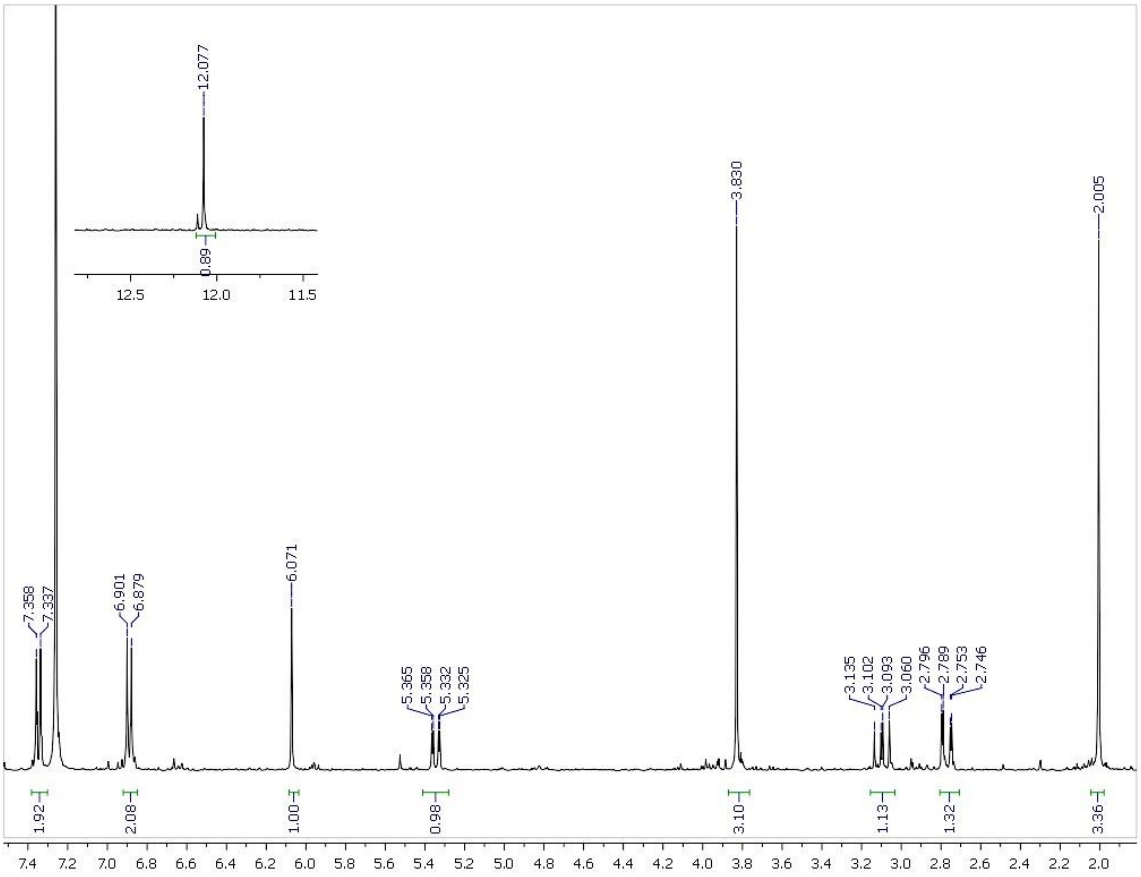


**Figure S15. $^{1}$H NMR spectrum (400 MHz, $CDCl_3$) of (2*R*)-5,4´-dihydroxy-6-*C*-methyl-7-methoxy-flavanone (13).**

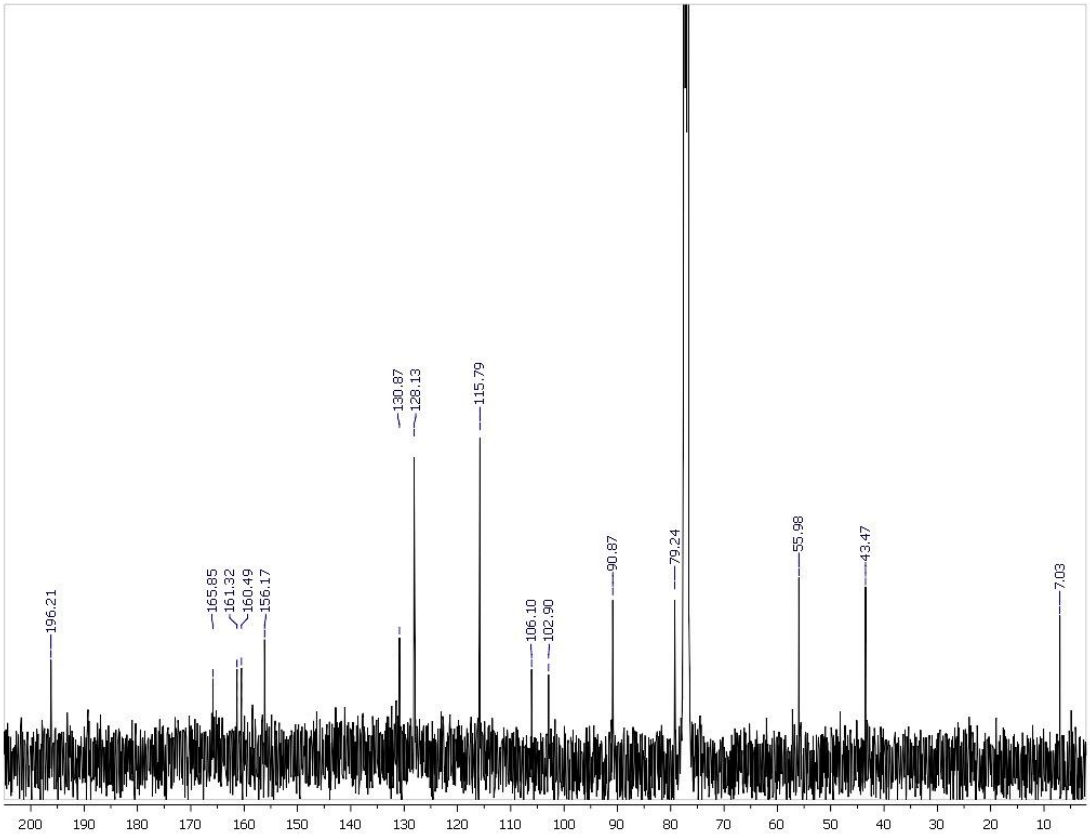


**Figure S16. $^{13}$C NMR spectrum (100 MHz, $CDCl_3$) of (2*R*)-5,4´-dihydroxy-6-*C*-methyl-7-methoxy-flavanone (13).**

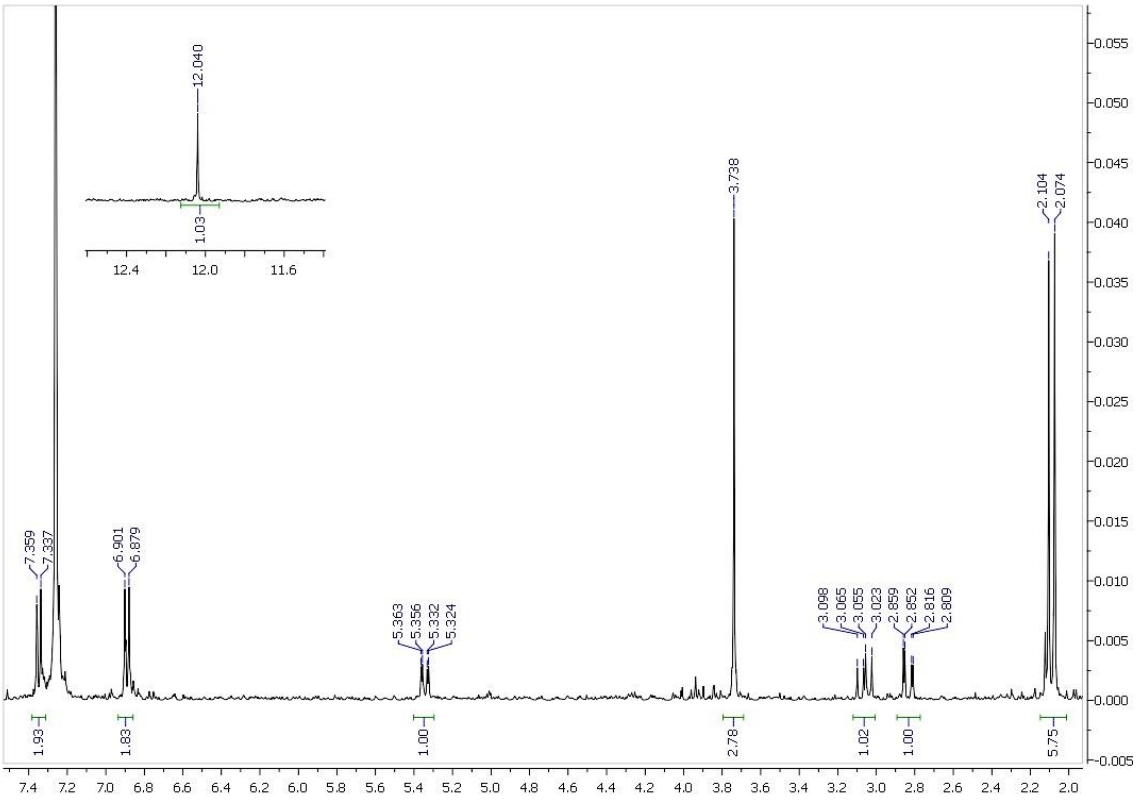


**Figure S17. $^{1}$H NMR spectrum (400 MHz, $CDCl_3$) of 5,4´-dihydroxy-6,8-di-*C*-methyl-7-methoxy-flavanone (14).**

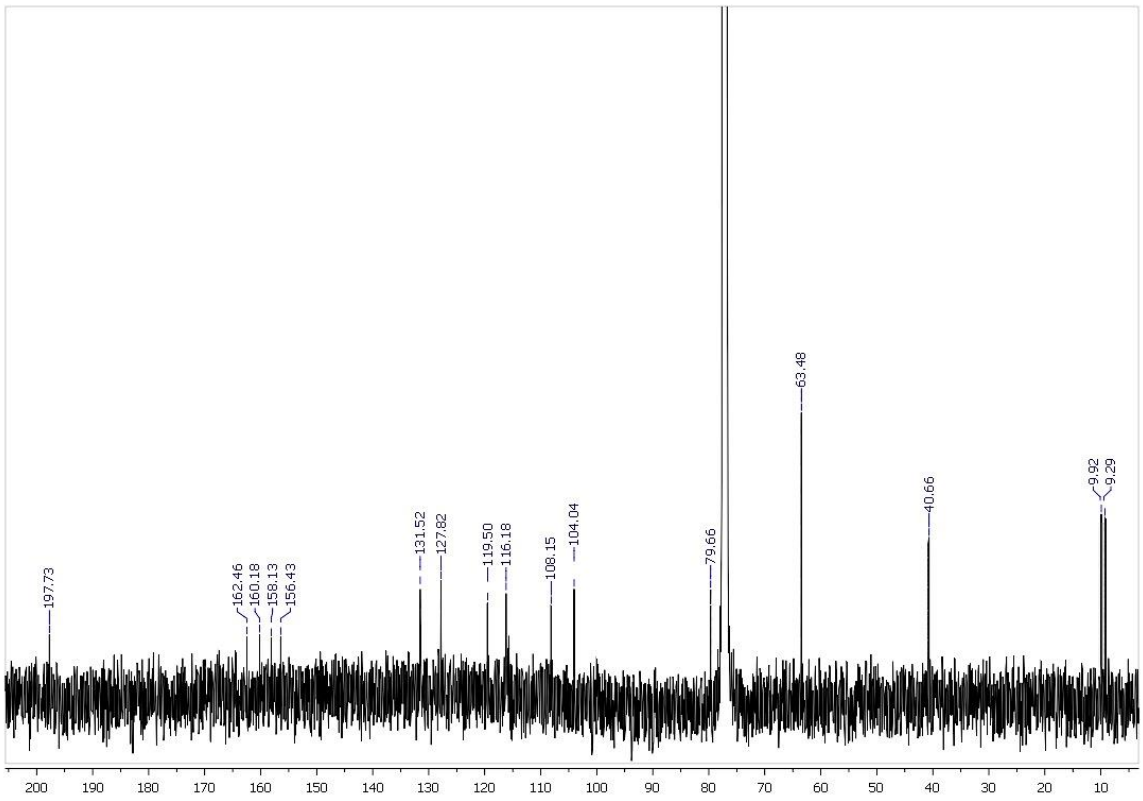


**Figure S18. $^{13}$C NMR spectrum (100 MHz, $CDCl_3$) of 5,4´-dihydroxy-6,8-di-*C*-methyl-7-methoxy-flavanone (14).**

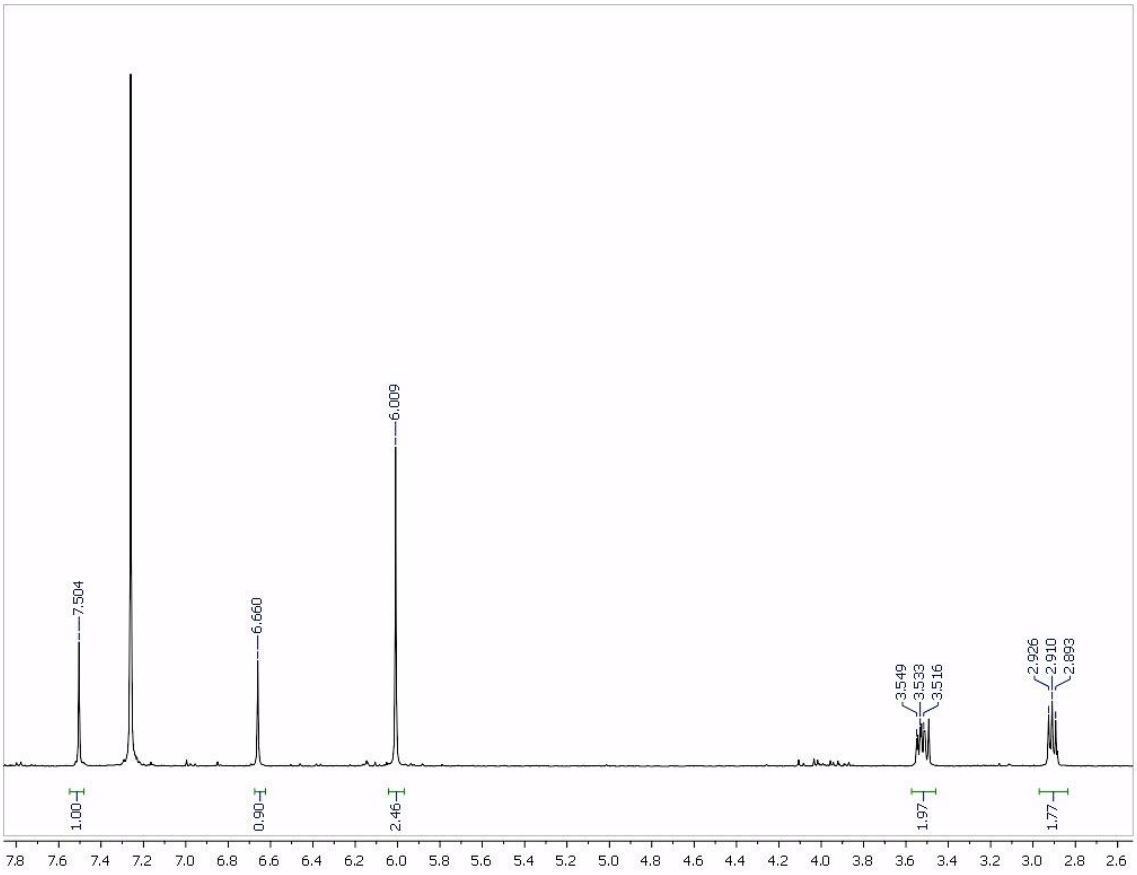


**Figure S19. $^{1}$H NMR spectrum (400 MHz, $CDCl_3$) of noroxyhydrastinine (15).**

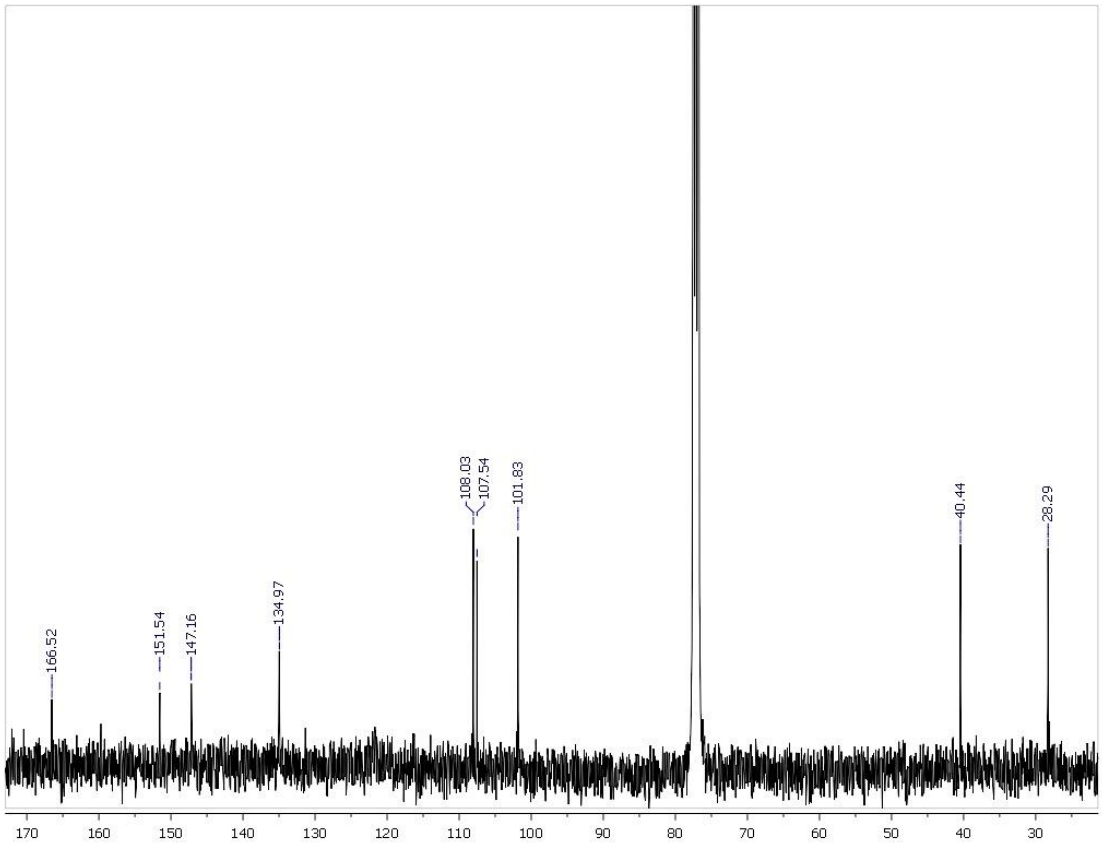


**Figure S20. $^{13}$C NMR spectrum (100 MHz, $CDCl_3$) of noroxyhydrastinine (15).**

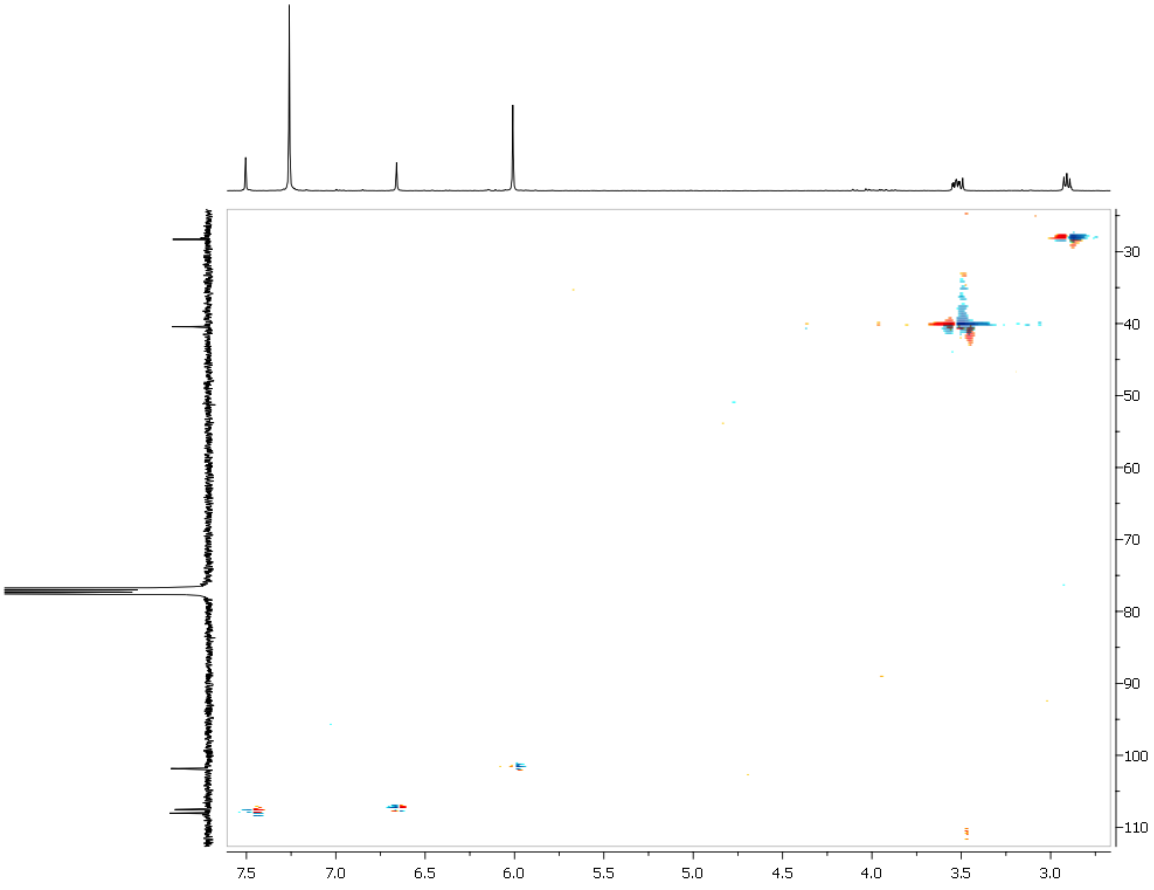


**Figure S21. HSQC spectrum of noroxyhydrastinine (15).**

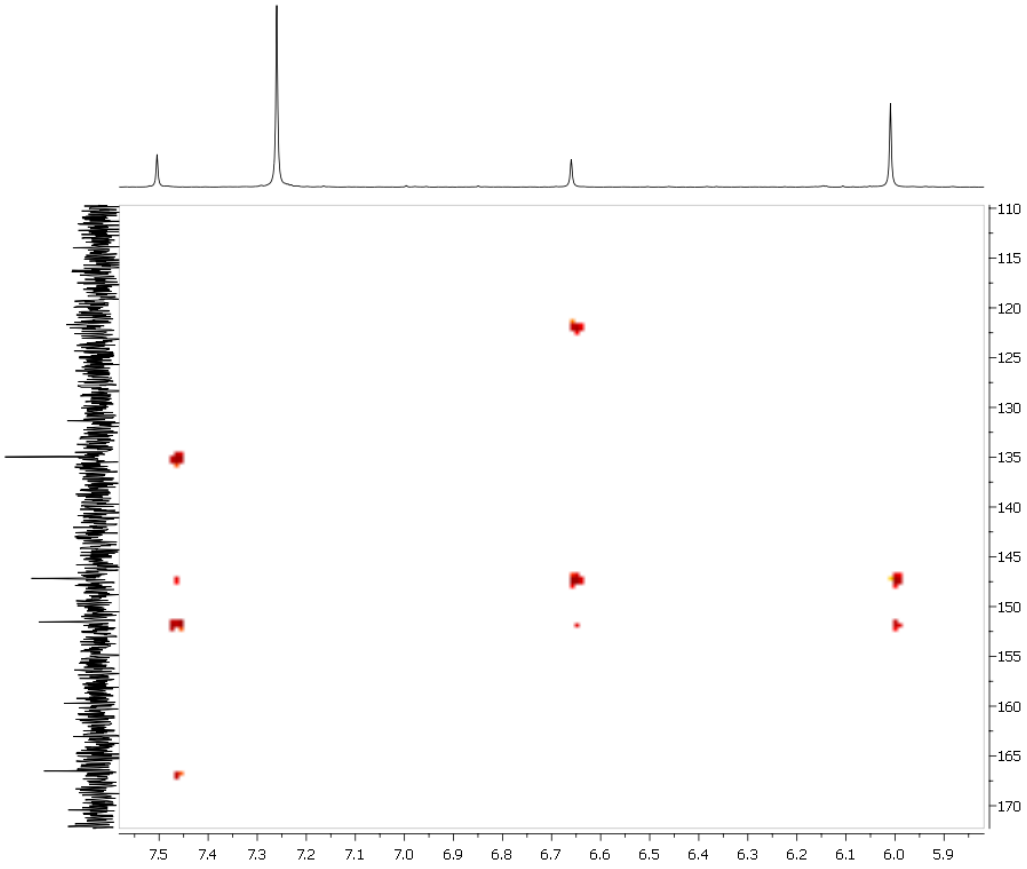


**Figure S22. HMBC spectrum of noroxyhydrastinine (15).**

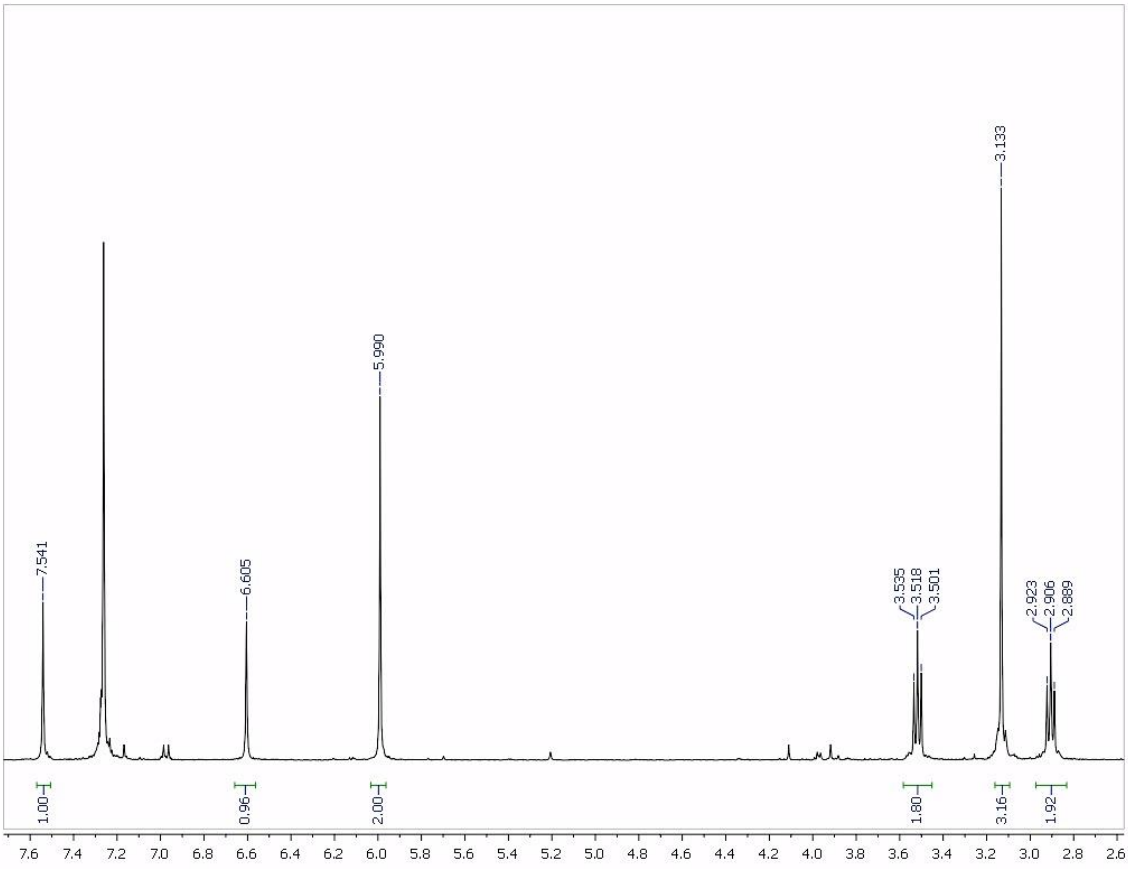


**Figure S23. $^{1}$H NMR spectrum (400 MHz, $CDCl_3$) of oxyhydrastinine (16).**

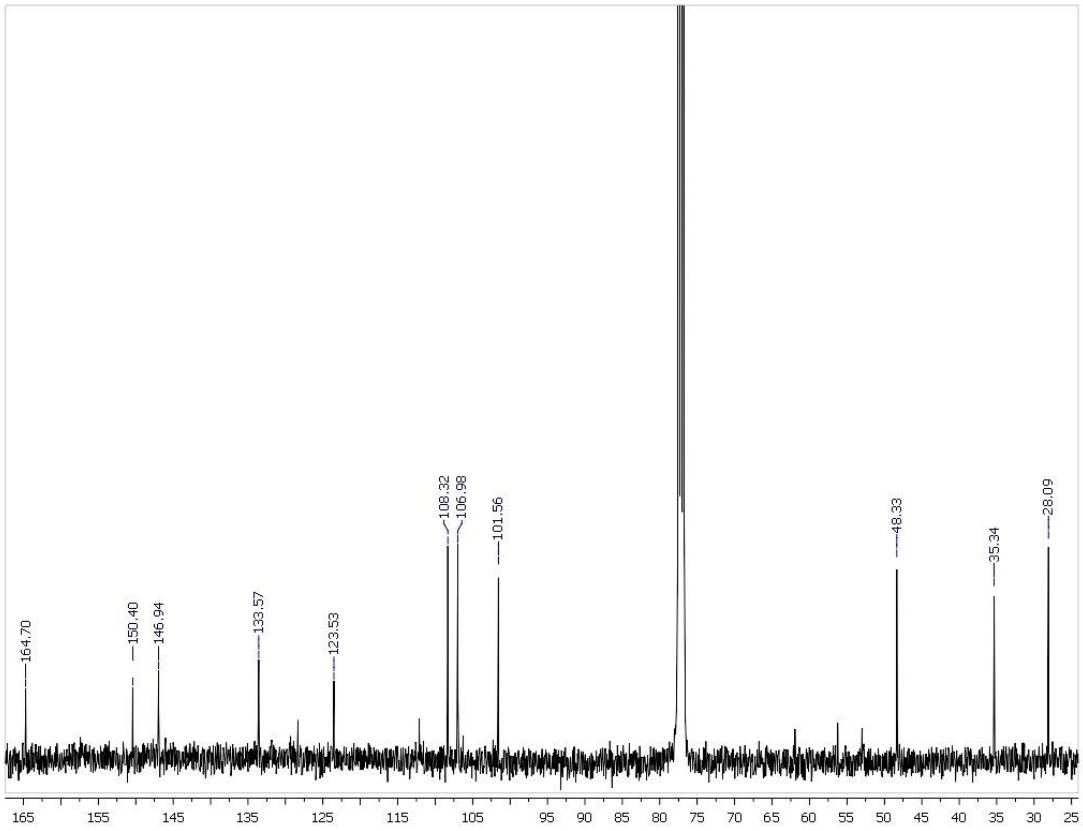


**Figure S24. $^{13}$C NMR spectrum (400 MHz, $CDCl_3$) of oxyhydrastinine (16).**

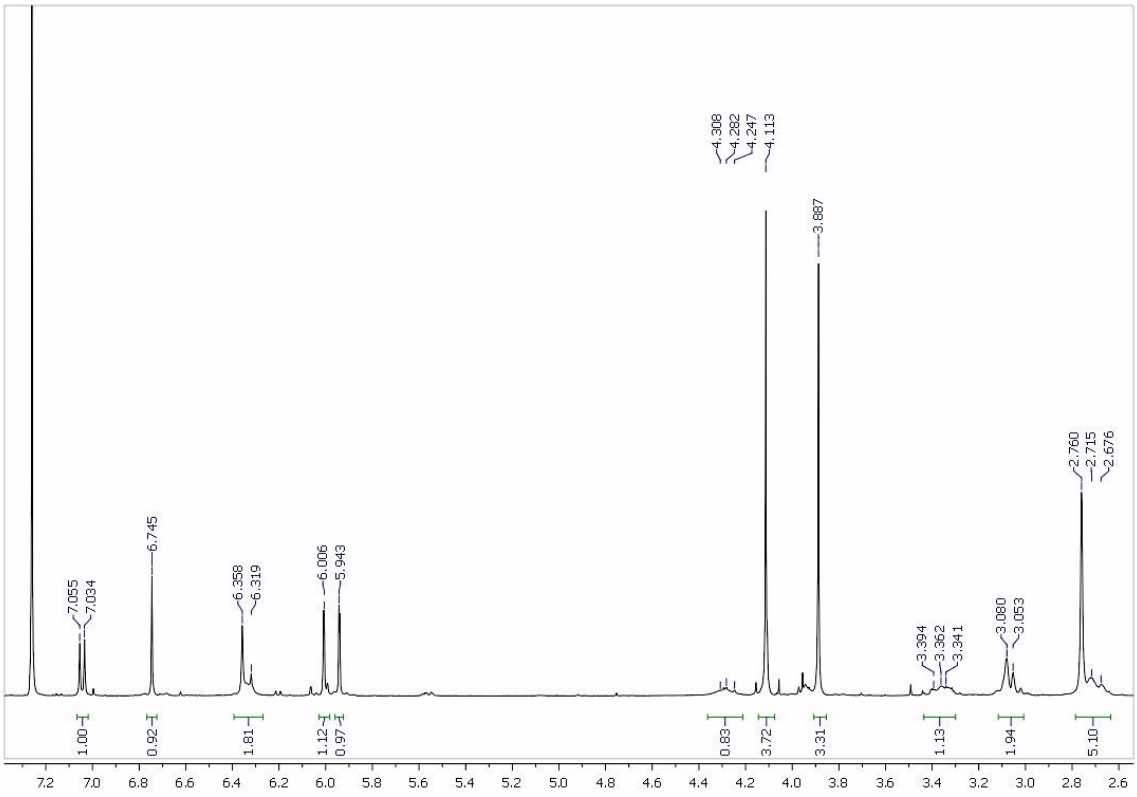


**Figure S25. $^{1}$H NMR spectrum (400 MHz, $CDCl_3$) of 4´,5´-dimethoxy-4-methyl-3´-oxo(1,2,5,6-tetrahydro-4*H*-1,3-dioxolo-[4´,5´:4,5]-benzo[1,2-*e*]-1,2-oxazocin)-2-spiro-1´-phtalan (17).**

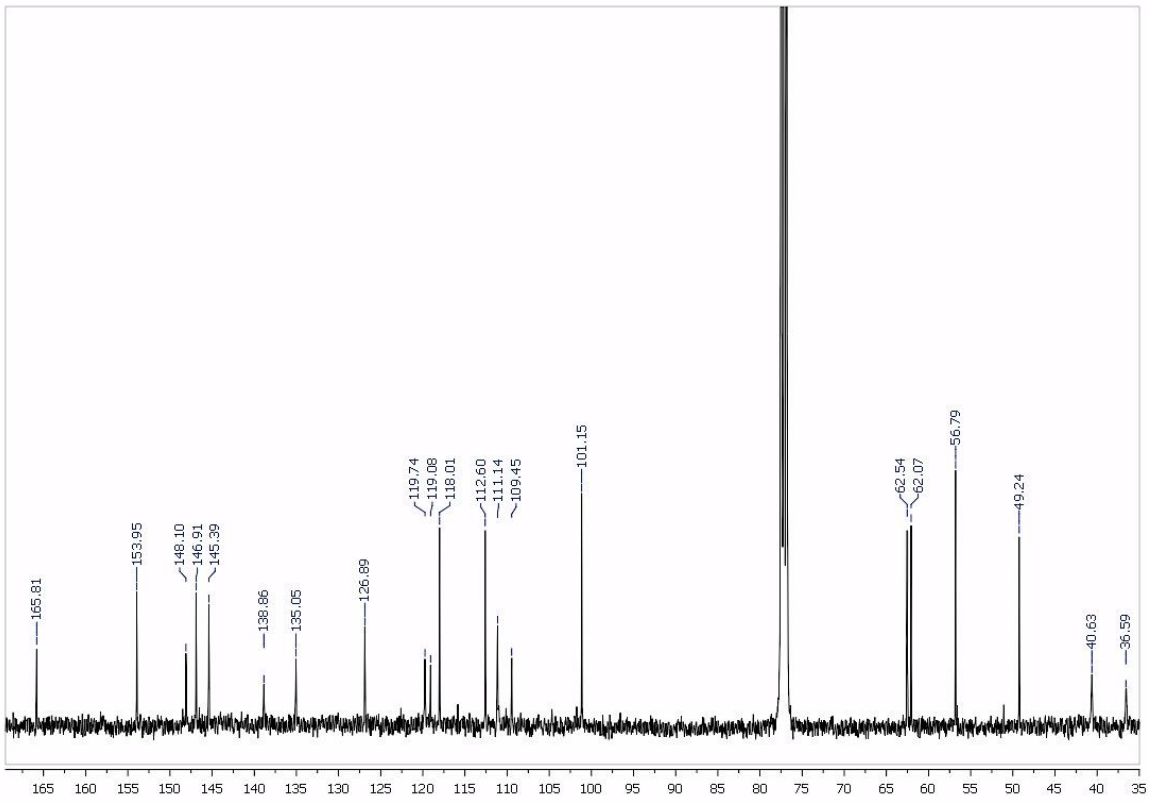


**Figure S26. $^{13}$C NMR spectrum (100 MHz, $CDCl_3$) of 4′,5′-dimethoxy-4-methyl-3′-oxo(1,2,5,6-tetrahydro-4*H*-1,3-dioxolo-[4′,5′:4,5]-benzo[1,2-*e*]-1,2-oxazocin)-2-spiro-1′-phtalan (17).**

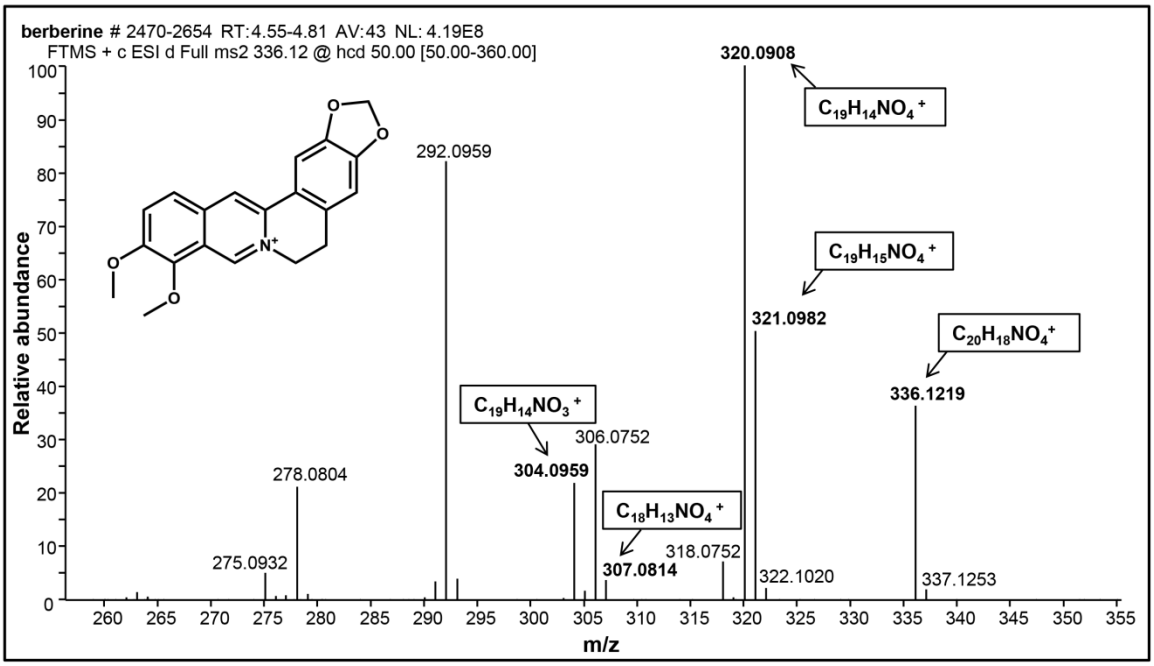


**Figure S27. Accurate mass fragmentation spectrum of berberine (18) in the positive polarity.** Fragments and molecular formulas were predicted using ACD MS fragmenter (Advanced Chemistry Development, Inc. Toronto, Canada) and compared to experimental data. Bold ions had a mass error within 10 ppm of the associated molecular formula.

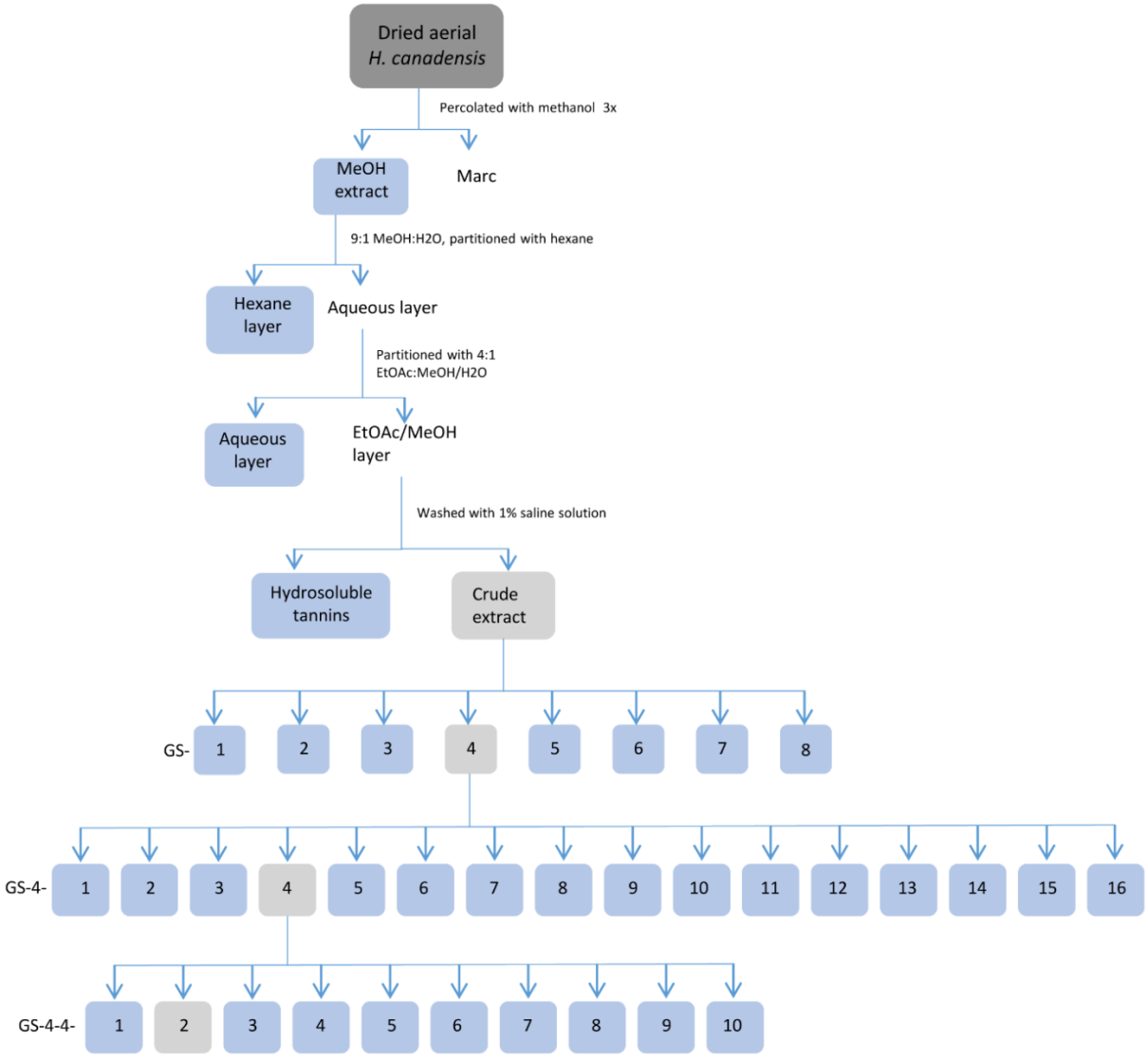


**Figure S28. Fractionation scheme.**

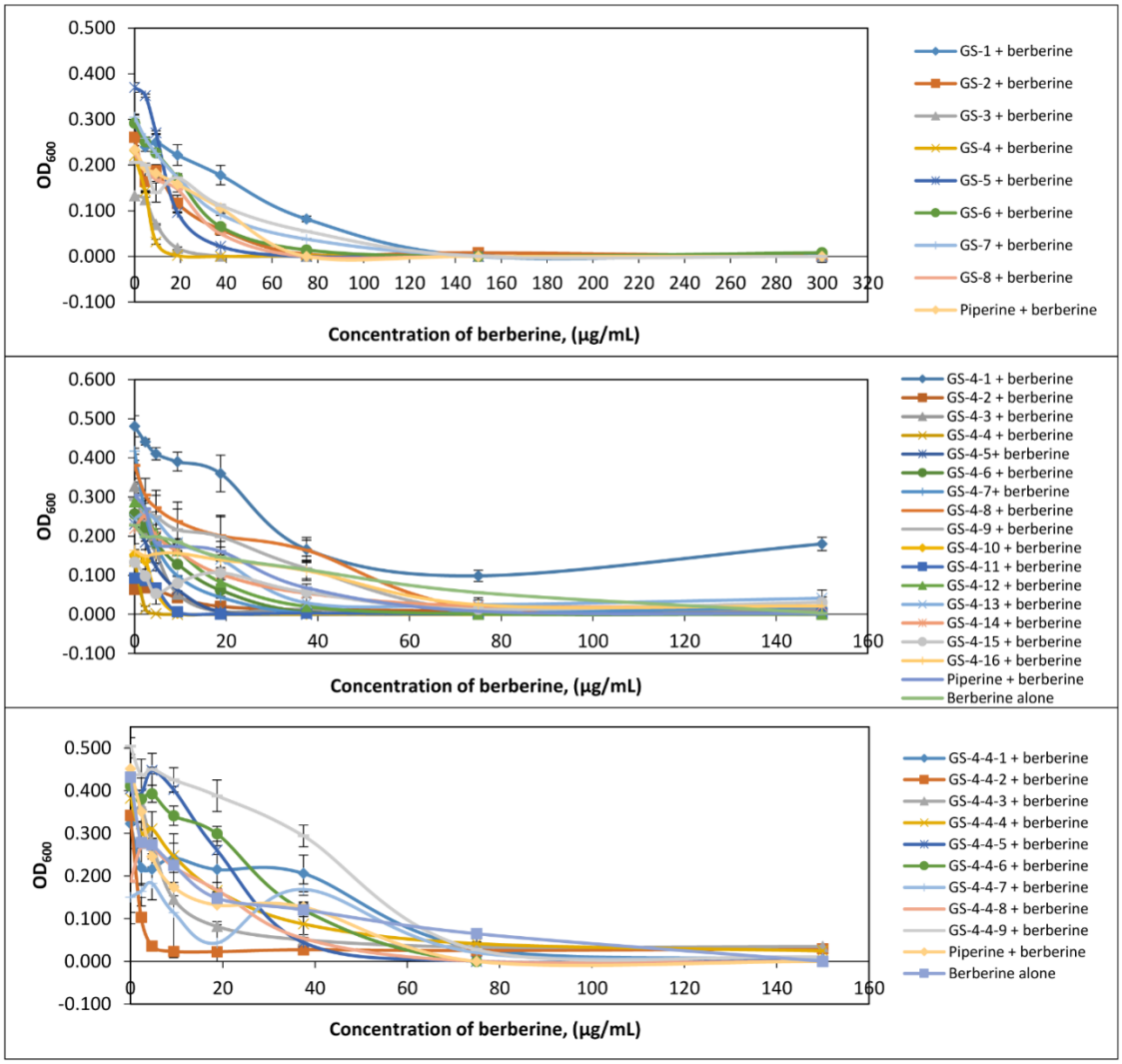


**Figure S29. Minimum inhibitory concentration (MIC) curves for berberine in combination with a constant concentration of fraction (75 µg/mL).** Each point represents the average $OD_{600}$ of three wells with identical treatments, and error bars represent standard error of those measurements.

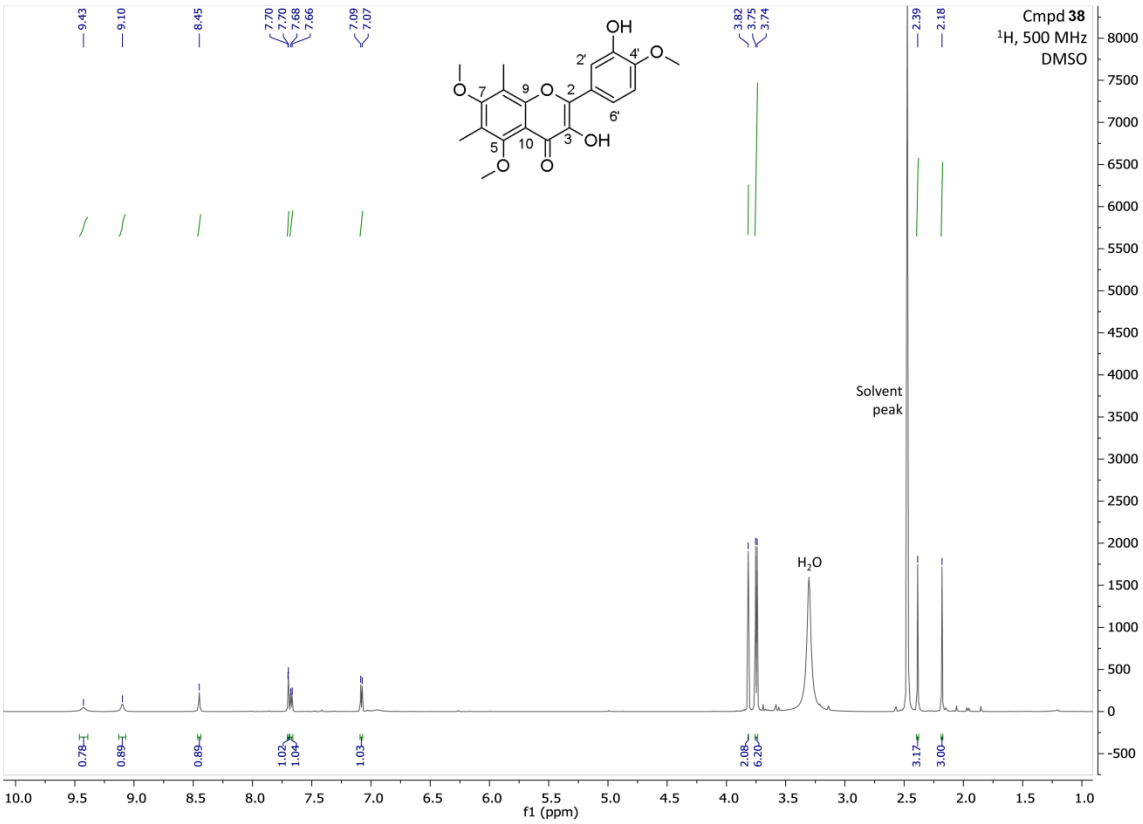


**Figure S30. $^{1}$H NMR spectra of 3,3´-dihydroxy- 5,7,4´ trimethoxy- 6,8-C-dimethyl-flavone (38).**

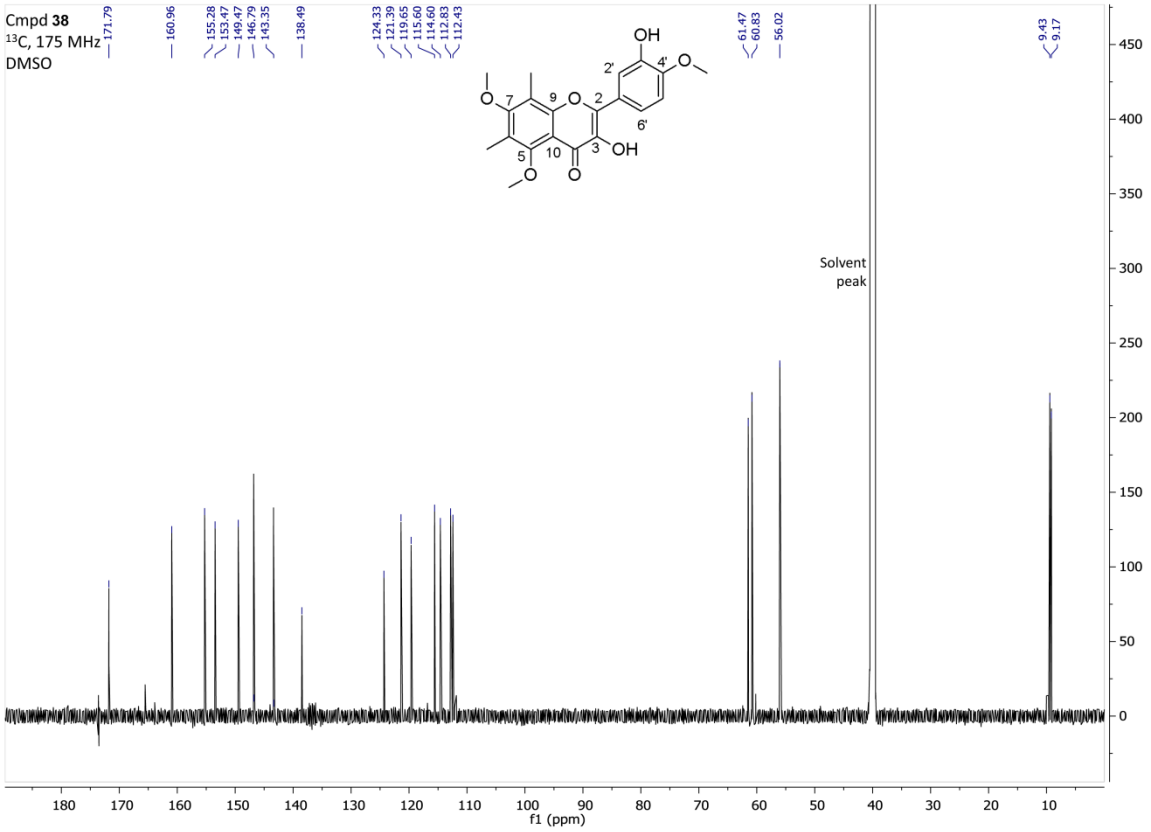


**Figure S31. $^{13}$C NMR spectra of 38.**

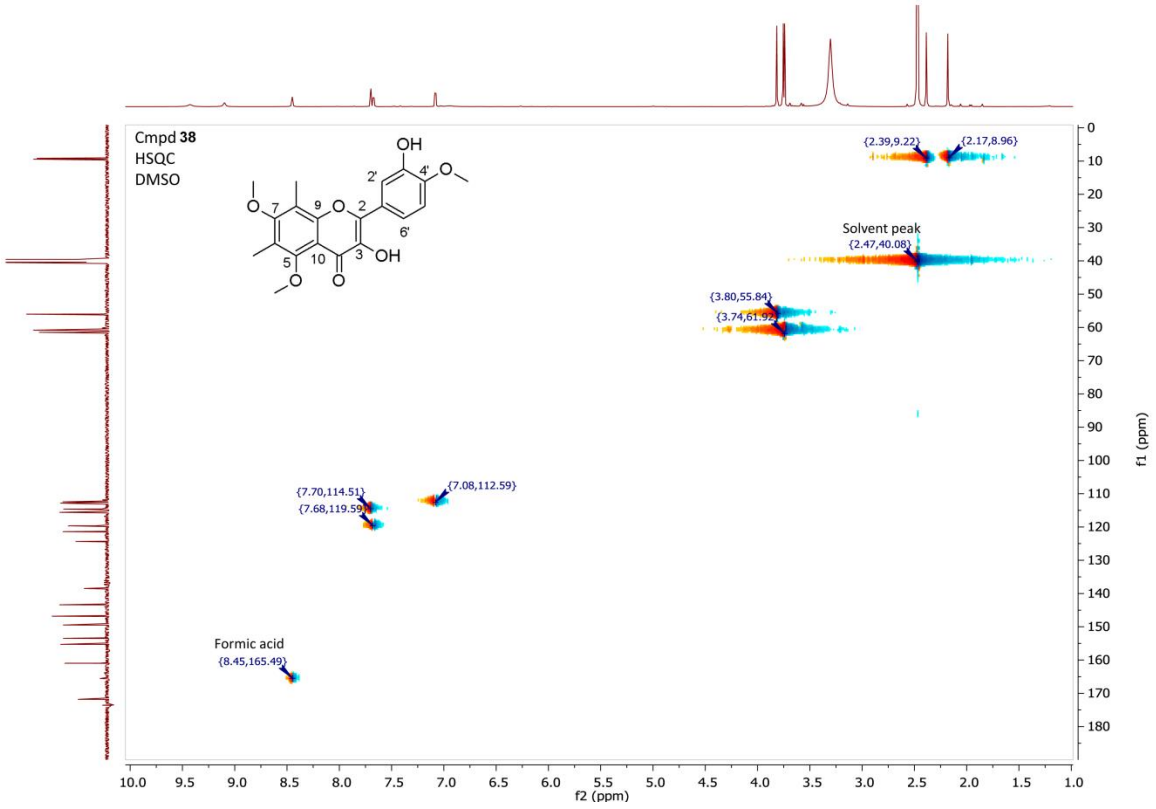


**Figure S32. HSQC NMR spectra of 38.**

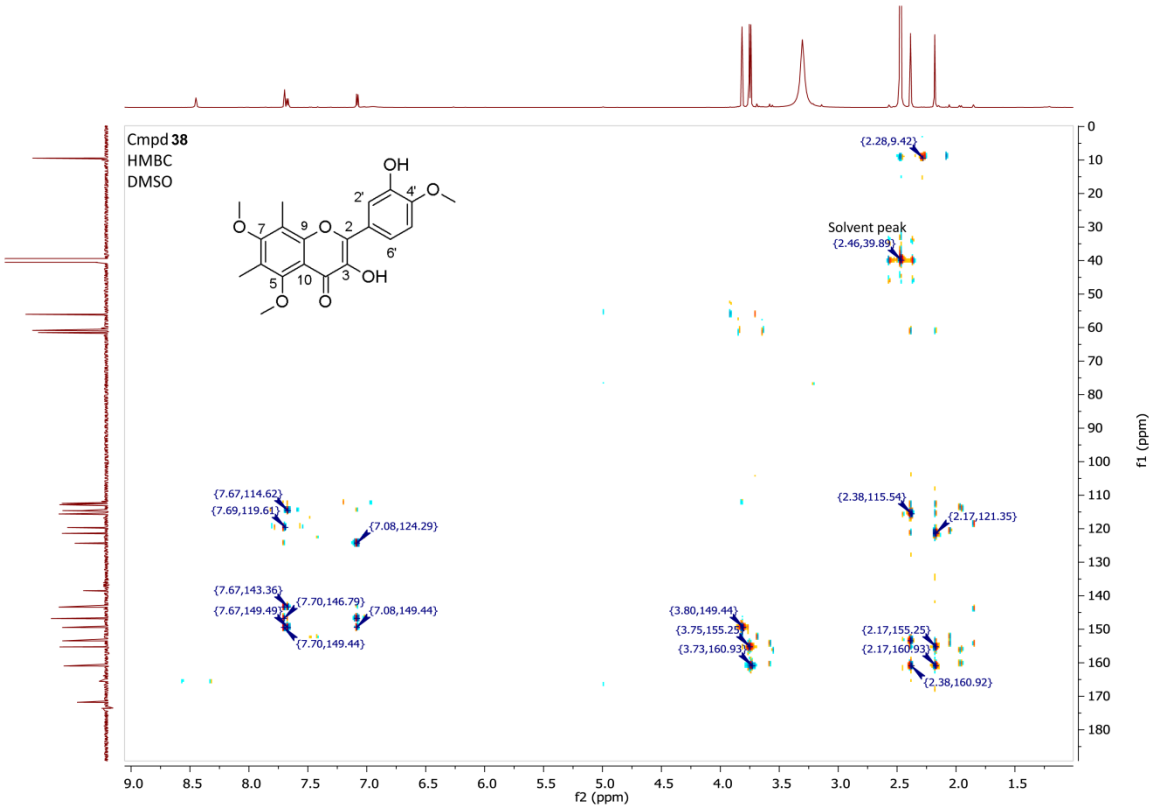


**Figure S33. HMBC NMR spectra of 38.**

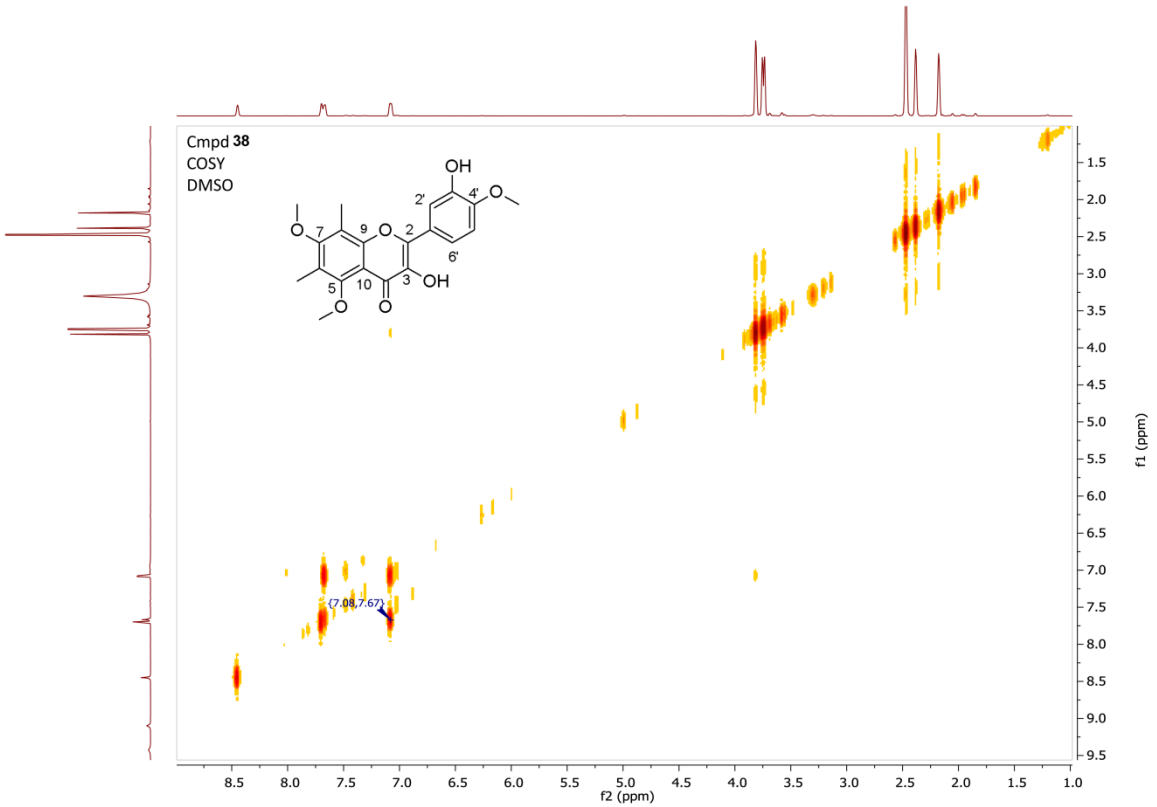


**Figure S34. COSY NMR spectra of 38.**